AD-772 987

AN INVESTIGATION OF THERMAL MECHANICAL FRAGMENTATION OF HARD ROCK

George B. Clark, et al

Missouri University

Prepared for:

Advanced Research Projects Agency
Bureau of Mines

October 1973

DISCLAIMER NOTICE

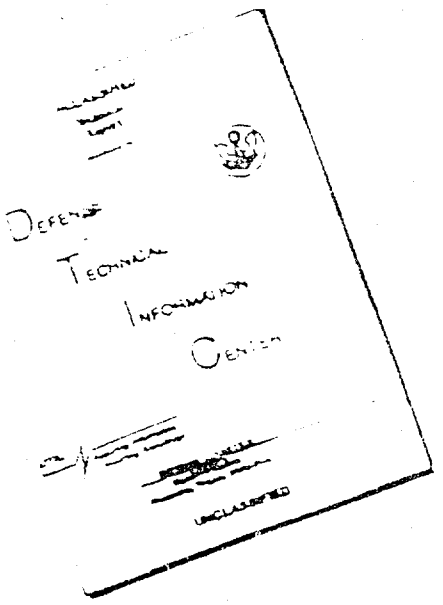

THIS DOCUMENT IS BEST QUALITY AVAILABLE. THE COPY FURNISHED TO DTIC CONTAINED A SIGNIFICANT NUMBER OF PAGES WHICH DO NOT REPRODUCE LEGIBLY.

AD-772 987

AN INVESTIGATION OF THERMAL-MECHANICAL FRAGMENTATION OF HARD ROCK

Final Report
October 1973

by

G.B. Clark, T.F. Lehnhoff, M. Patel and V. Allen

Rock Mechanics & Explosives Research Center
University of Missouri-Rolla
Telephone 314/341-4365

ARPA Order No. 1579, Amendment 3
Program Code No. 2F10
Contract No. H0220068
Contract Period: June 12, 1972 through August 12, 1973
Total Amount of Contract: $65,829.
Sponsored by: ARPA

This research was supported by the Advanced Research Projects Agency of the Department of Defense and was monitored by the Bureau of Mines under Contract No. H0220068

Disclaimer:

The views and conclusions contained in this document are those of the authors and should not be interpreted as necessarily representing the official policies, either expressed or implied, of the Advanced Research Projects Agency or the U.S. Government.

UNCLASSIFIED

SECURITY CLASSIFICATION OF THIS PAGE (When Data Entered)

REPORT DOCUMENTATION PAGE	READ INSTRUCTIONS BEFORE COMPLETING FORM
1. REPORT NUMBER	2. GOVT ACCESSION NO.	3. RECIPIENT'S CATALOG NUMBER AD-772 987
4. TITLE (and Subtitle) AN INVESTIGATION OF THERMAL-MECHANICAL FRAGMENTATION	5. TYPE OF REPORT & PERIOD COVERED Final Report 6/12/72-8/12/73
	6. PERFORMING ORG. REPORT NUMBER
7. AUTHOR(s) George B. Clark, Terry F. Lehnhoff, Mahen Patel, and Vernon Allen	8. CONTRACT OR GRANT NUMBER(s) H-0220068
9. PERFORMING ORGANIZATION NAME AND ADDRESS Rock Mechanics & Explosives Research Center University of Missouri-Rolla Rolla, Missouri 65401	10. PROGRAM ELEMENT, PROJECT, TASK AREA & WORK UNIT NUMBERS ARPA Order No. 1579, Amend 3, Code Number 2F10
11. CONTROLLING OFFICE NAME AND ADDRESS Advanced Research Projects Agency 1400 Wilson Boulevard Arlington, Virginia 22209	12. REPORT DATE October 1973
	13. NUMBER OF PAGES 209
14. MONITORING AGENCY NAME & ADDRESS(if different from Controlling Office)	15. SECURITY CLASS. (of this report) Unclassified
	15a. DECLASSIFICATION/DOWNGRADING SCHEDULE

16. DISTRIBUTION STATEMENT (of this Report)
Distribution of this document is unlimited

17. DISTRIBUTION STATEMENT (of the abstract entered in Block 20, if different from Report)

18. SUPPLEMENTARY NOTES

19. KEY WORDS (Continue on reverse side if necessary and identify by block number)
thermal fragmentation, thermal stresses, fracture, rock, thermal properties, rapid excavation

20. ABSTRACT (Continue on reverse side if necessary and identify by block number)
Based upon research utilizing heat applied to the surface of rock and at the base of slots cut in the rock, it was determined that heat applied internally is markedly more effective in fracturing hard rock. Coiled wire resistance heaters proved effective in fracturing 30 in. cubes of rock in the laboratory. They also were employed to fracture granite in place, but burned out in a short time in bore holes.

Carbon arcs were found to be economical and effective heat sources. These were employed in three and four hole geometries to fracture rock with three faces,

DD FORM 1 JAN 73 1473 EDITION OF 1 NOV 68 IS OBSOLETE

UNCLASSIFIED

SECURITY CLASSIFICATION OF THIS PAGE (When Data Entered)

and a plane of fracture parallel to the working face was consistently formed. Fracture is augmented with rock splitters which also remove blocks from the working face. Finite element studies have been made of temperature and thermal stress distribution in support of field research.

The concept is being developed to drill a tunnel round with pneumatic drills, with heat to fracture the rock in a manner analogous to an explosive round. Slot, V, and pyramid cuts are being tested. Projected rates of advance and costs per foot are favorable.

ACKNOWLEDGMENT

The last five of the field experiments described in this report and final calculations of temperature distribution and stress analysis were performed with support from National Science Foundation Grant No. NSF-GI-38984. These results are included herein for the sake of completeness.

TABLE OF CONTENTS

Table of Contents (continued)

Table of Contents (continued) Page

Table of Contents (continued) Page

LIST OF FIGURES

List of Figures (continued) Page

List of Figures (continued) Page

List of Figures (continued) Page

LIST OF TABLES

THERMAL MECHANICAL FRAGMENTATION OF HARD ROCK

Chapter 1

INTRODUCTION

General

The problems related to underground rapid excavation and their societal relevance are described in NAS Report 1690, "Rapid Excavation: Significance, Needs, Opportunities," 1968. The research described herein is part of an ongoing program in disintegration of hard rock for the rapid excavation of tunnels, power stations, mines, and underground military installations. The rate of productivity in hard rock in 1968 was increasing only about 3 to 3-1/2 percent per year, which is insufficient to keep hard rock excavation costs constant, and projected rates of excavation are still minimal in 1973 for the methods now in use.

The NAS Report 1690 gave first priority to: "Development of processes and equipment for boring tunnels and shafts in hard abrasive rock and for reducing down time experienced with current mining and tunneling machines in soft or medium rock masses". It was further noted that of the several novel rock disintegration techniques then being studied only a few showed promise for application within two decades. There is a good indication that the method described in this report may be developed for practical application within a period of five years.

Any means of excavation that can contribute to the reduction of costs of mining minerals or to increasing their production rate directly contributes to the improvement of the standard of living, the increase of mineral reserves, etc. The availability of underground

high speed transportation of people, e.g., in the Northeast Corridor (Washington, New York, Boston), with the incident requirement for rapid, acceptably ecological methods of excavation of hard rock, is an essential factor in the functioning of society in highly populated areas. Excavation of openings in rock under populated areas will require rapid, quiet methods of rock disintegration.

Achievement of the required improvements in rapid excavation of hard rock will contribute to the projected improvement of effective mass transportation in heavily populated areas, will extend our mineral resources and make their production more economical, and will improve methods of excavation of underground civil and military installations. The latter two factors directly affect the whole of our society.

The successful development of a new method of fragmentation will lead to the design of the basic elements of a new, rapid excavation system for hard rock. It will advance the knowledge of rock disintegration, thermal response of earth materials, energy transfer to rock, and the relationship of those factors to rock and mineral properties. This will in turn lead to the design and construction of a prototype system for pilot studies and the later development of full scale equipment and excavation systems.

The excavation industry as a whole is basically interested in the improvement of methods of mining of earth materials as indicated by representatives of government and industry in NAS Report 1690, at the OECD Tunneling Conference (Washington 1971) and the Conference on Rapid Excavation and Tunneling (Chicago 1972), by the Interagency Committee on Rock Mechanics, and the committees sponsored by the National Academy of Science.

Thermal stresses (fire setting) have been employed since antiquity in the fragmentation of rock. The most active use of heat in recent and current operations has been that of the flame jet for drilling hard rock and cutting and facing of spallable monument stone. Its successful employment led to the investigation of the feasibility of a flame jet tunneling machine, i.e., the utilization of flame jets for weakening rock to make it more susceptible to roller cone cutting. Slot cutting by flame jets and wedging of ridges between kerfs were also suggested as a possible excavation process. Large amounts of excess heat and combustion generated gas, inefficiency of heat transfer from a flame jet to rock and other factors appeared to mitigate against its use, as well as the resulting limited increase of rock removal efficiency by roller cones.

The advantages of the use of tunnel boring machines in soft to medium hard rock, which they can excavate economically, and the disadvantages of drill and blast methods (cyclic character, overbreak into walls, and vibration and noise problems) in hard rock have led to an intensive search for novel method(s) which will increase tunneling capabilities primarily in hard rock. Of the several methods recently investigated, the use of heat has been the subject of considerable research, some fourteen techniques having been proposed and investigated for drilling and breaking rock. Flame jets have been in use for a long time, but are limited to application in drilling and quarrying. Various types of heat drills have not been applied to date because of non-adaptability of equipment to underground conditions, environmental problems created by the excavation device, high energy consumption, or because results obtained in the laboratory could not be applied to rock in place.

It should be noted that, while recent technical literature has emphasized the specific energy of drilling, breakage and other types of rock removal, the absolute value of this factor for a given rock and process combination is seldom a deciding factor by itself unless a critical value for specific energy is exceeded. The most critical operational factor, assuming specific energy requirements are not near or above maximum permissible values, is the rate of advance, for both drilling and excavation.

While some novel methods of rock drilling and excavation have been found to be technically feasible, equipment, energy or other operational costs prohibit their use. Hence, this investigation is designed to evaluate both the technical and the economic feasibility of the application of the method of excavation by use of thermal rounds.

Future research is designed to evaluate further the factors of importance in the development of a thermal round (of the same concept as a high explosive blasting round) for fragmentation of hard rock in such a manner that the process can be employed in operating excavation systems. This includes a study of heat sources, hole placement and geometry, pertinent mineral and rock properties, heat transfer, temperature distribution, thermal stress distribution, fracture initiation and propagation, required strain relief, methods of slot cutting, and related factors. Based upon these findings appropriate existing equipment will be modified or new equipment designed to accomplish the operation of the fragmentation process. Three years of research (as of June 1973) have been completed on this problem.

A reasonable assessment of a method of thermal fragmentation and excavation can be made by investigation of the following factors:

(1) Current status of: a) theory, b) research, and c) development.

(2) Energy and fracture characteristics: a) specific energy requirements, b) efficiency of energy transfer, c) availability of energy, and d) control of energy source.

(3) Application characteristics: a) control of energy within the rock, b) preservation or strengthening walls and roof, c) smoothness of opening excavated, d) efficiency of energy utilization, e) environmental factors, f) adaptability to variable rock properties and conditions, g) feasibility of equipment design and construction, h) continuity of method - down time, i) research and development required, j) time to develop and apply new method, and k) rate of advance.

(4) Cost factors: a) research and development, b) capital equipment, c) operating: labor, materials, etc., and d) overhead.

The above factors have been studied in relation to the research project under this project (Contract No. USDI-H0220068 [ARPA]). Theoretical and experimental studies are in advanced stages on heat transfer, thermal stress analysis, and thermal properties of minerals and rocks. Field tests of thermal fragmentation of granite have reached a stage which indicates a high probability of successful application. Rate of advance and cost analysis studies are in progress.

Scientific and Engineering Background

While there have been specialized studies made of some of the thermal properties of rocks, mostly in relation to flame jet drilling, only a limited number of investigations have been made of the specific scientific and engineering factors which are directly related to the problems posed by this investigation. There is a large fund of information from ceramics studies of heating and melting of synthetic silicates and selected clays, studies of the calcination of carbonates in their sintering for manufacture of Portland cement, and the physical chemistry of some types of rock in geologic studies of igneous action and metamorphic processes. There is little information on the thermal, physical, or electrical properties of molten rock.

Thermal Rock Drilling and Fracture

Twelve methods of drilling or breaking rock by thermal means were reviewed by Maurer in 1968 (1). These included flame jet (jet piercing), electric disintegration by low frequency current, cyclic heating and cooling with superheated steam and liquid nitrogen, high frequency currents, microwaves, induction, fusion and vaporization (LASL), nuclear heat (penetration), electric arc (drill), plasma drill, electron beam, and lasers. Carstens (2) reviewed several of these methods again in 1972, and described an additional method of forming an internal thermal inclusion and fracturing rock (3). Considerable research has been accomplished in the past four years, particularly on electron beams (4), lasers (5 and 6), with flame jets (7, 8 and 9), high temperature penetrators (10), plasma jets (11), resistance wire and electric arc heaters (12).

Several other approaches have been suggested in the last decade for the possible use of heat application within the rock to cause fragmentation. The fracture of rock has been the subject of several patents by Sarapu (13) starting in 1965. In a study of laser effects on rock Zar (5) proposed that a heated annulus of the surface of a hard rock face would cause the rupture of a section of the rock face. However, this assumes that the rock is free from fractures, joints, etc.

Thirumalai (14) was the first to report (1970) on a method of formation of an internal thermal inclusion by dielectric heating. Laboratory test blocks of granite and basalt, somewhat larger than 1 foot cubes were fragmented without melting by localized heating below 600°C, the heated volume being less than 2 percent of the total rock volume. As a first approximation, a thermal inclusion was considered to exert a pressure on the inside of a cylindrical hole in an infinitely thick cylinder. However, quartzite blocks could not be fragmented by dielectric heating. The total electrical energy required to fracture Dresser basalt blocks varied from 0.067 to 0.100 kwhr, and the volume of the thermal inclusion from 105 to 206 cc.

Coiled wire resistance heaters of Kanthal wire at 1000°C were found, during the investigation described herein, to fracture hard granite when they were placed in pneumatically drilled holes, but the heaters failed after short term usage. Electric arcs between carbon electrodes generate an effective thermal inclusion in multiple holes in solid granite and create thermal stress fields which will cause fractures over distances of 2 feet or more at reasonable energy levels. Tests to date have yielded promising results for possible application.

For granite the electrical energy was 0.10 kwhr and the volume of the thermal inclusion was 206 to 350 cc. Time for fracture was less than 2 minutes. In tests 2 foot cubes of Missouri red granite were easily fractured by means of a rock (partially fused) melt created in a drill hole in the center of the rock with carbon electrodes. The total electrical energy was approximately 1 kwhr and the volume of the melt about 380 cc, the total heated volume of rock being larger. This represents about 0.2 percent of the total volume of the block. Similar results were obtained in granite in situ.

The amounts of electrical energy per unit volume of rock are in the ratio of 1.6:1 for Missouri red granite as compared to the basalt and granite tested by Thirumalai. The time for fracture and the total energy applied vary approximately as the volume of the block, indicating that the cube root law for energy usage may apply for similar rocks and geometries.

In each of the above tests, as in investigations reported by Nixon (4) with electron beams, radial cracks as well as cracks normal to the axis of the hole or inclusion were formed. Nixon (4) reports that temperature distributions were calculated by empirical formulas, with the assumption of a 1700°C melting temperature at the boundary of a finite element program utilizing values of Young's modulus, Poisson's ratio and thermal coefficient of expansion as functions of temperature. Both tangential and radial stresses near the cavity were found to be compressive, while in the cold zone the stresses were tensile.

Nixon also came to the conclusion that for electron beam penetration and heating the compressive stresses and gradients are typically

larger by an order of magnitude than the tensile stresses and gradients. The expansion of the cavity along its axis and the radial growth of the heated region cause tensile stresses in the axis-radius plane and in the tangential direction. At depths equal to the melt cavity and below, the tensile stresses in the r-axis plane are larger than the tangential stresses creating favorable conditions for a crack normal to the axis. The calculations were confirmed only by the behavior of blocks of quartzite, however, and not with other types of rock.

Thirumalai proposed that dielectric internal heating to form a thermal inclusion be applied to ore and rock in stopes where two free faces exist for displacement. However, the feasibility of breakage by this means was not tested. He (15) also suggested two types of tunnel rounds using thermal inclusions, one with a cut at the bottom of the face, and a V-cut type round with no strain relief other than the tunnel face. The feasibility of such tunnel rounds also was not investigated.

Most of the novel methods which have been proposed for the rapid excavation of hard rock are being considered in terms of several years for possible development and application. Some have inherent disadvantages which may not be easy to overcome. For example, the x-rays created by electron beams are difficult to shield. Current laser equipment is not adaptable for use underground. Plasma jets are inefficient for breaking rock.

On the other hand, many of the principles of the thermal fragmentation method proposed herein have been investigated in sufficient detail to indicate a strong probability of successful application within a relatively short period of time.

The principles of breakage employed are similar to those which have been successfully applied in blasting. A large part of the equipment to be used in further research and development is available for purchase, i.e., air compressors, drills, power sources, carbon electrodes, etc. Some adaptation of equipment will be required, and only a few of the components will require new design and development. All of the components envisioned are adaptable to use in underground environments. Environmental problems will be minimal, i.e., less ventilation will be required than with explosives. Some of the problem areas are to be found in the development of rugged carbon electrodes, working in very wet tunnels, investigation of other high temperature heaters, etc.

Several methods utilizing rock melting combined with fracture processes have been proposed by Los Alamos Scientific Laboratory (10, 16 and 17) for the excavation of tunnels. These include (a) full face melting (Subterrene 2), (b) partial face melting and solid core excavation (Subterrene 1), and (c) a multiple hot prong melting and fracturing head. Experimentation has been performed on penetration of rocks and soils with 2 in. models which form a glass lined hole in porous rock and soil, and eject melted material from the hole in non-porous rocks.

Maurer (1) notes that in early tests (17) a 5 kw heater drilled a hole 5.1 cm diam in basalt at a rate of 1.2 cm/min, which he further reports corresponds to a specific energy of 12,300 joules/cm^3. However, the basalt used at Los Alamos is porous, some of it having a density of 1.43 whose heat of fusion would be 2720 joules/cc of hole created. This ratio of heat required of over 4 to 1 should be expected

because some of the rock around the hole is melted. If the work required to force the drill into the rock is taken into account, the ratio would be greater.

Such a device has two disadvantages. The minimum energy required to melt holes in granite, assuming all of the energy goes into the melted rock, is in the neighborhood of 5000 joules/cc, while that for a pneumatic drill is 250 to 400 joules/cc. The drilling (melting) rate for electric heaters is (1) 1 to 3 cm/sec while that for pneumatic drills is 50 to 75 cm/sec.

The feasibility of molten rock penetration into the rock mass around a tunnel has been shown for porous earth materials and a granite. The stability of unreinforced, brittle ceramic glass tunnel liners has not been investigated, nor the effects of heat upon surrounding rock and soil.

The multiple hot prong drilling heater suggested by LASL (16) appears to have two disadvantages. The first is the amount of energy required to make holes in the rock face by melting. The second concerns the mode of fracture from internal thermal inclusions. For effective fracturing lateral displacement relief is required, which cannot be provided by the drilling head. In principle, a "no cut" round is proposed, which has been found to be feasible for explosives in some types of rock. However, experimentation has shown that more displacement relief is required for crack propagation caused by thermal stress than for stress waves produced by explosives.

Because of the high heat of fusion of rock, the energy requirements and costs for melting of any significant portion of the rock are critical factors. For example, for the 7 meter diameter tunnel excavation proposed by LASL (10) 50 Mw of power are required for melting (of one-fourth of the face) alone, but heat absorption and losses may increase

this by as much as three times. Thus, at 3 cents per kwhr the power cost would be from $750 to $2250 per foot of tunnel. Ventilation costs, also, would be very high.

The required heat flux of 500 w/cm^2 to accomplish necessary rates of advance are well beyond the state-of-the-art, e.g., 30 w/cm^2 for lithium heat pipes and 200 w/cm^2 for electrical heaters.

Recent investigations (18, 19) have also shown that complex reactions take place in radiant heaters with carbon heating elements, molybdenum shells, and boron nitride insulation. The average lifetime of such a penetrator is about six hours, while those without boron nitride have been tested to approximately 45 hours.

Chapter II

ROCK CHARACTERISTICS

The response of rocks to the application of heat depends upon their composition, structure, density, thermal properties, and mechanical properties. The percentage of SiO_2 in a rock affects the thermal behavior markedly as well as the strength, brittleness, and other factors.

While the research program described herein is concerned primarily with hard igneous and metamorphic rocks, the applicability of thermal fragmentation to sedimentary rocks is also of interest.

Igneous Rocks

Johannsen (20) proposed a classification for igneous rocks which will be particularly useful in the present study. It is based on a double tetrahedron (Fig. 1) with quartz at the apex at the top and K, Na and Ca feldspars at the common base corners and feldspathoids at the bottom apex. Thus, rocks containing free quartz (or without) may be classified by their composition and their position in the double tetrahedron according to their composition and class name.

In a consideration of the physical chemistry of rock melts, the phase rule of mineralogy may be useful as a guide. This rule states that (21) the number of different minerals in a rock should not exceed but may be equal to the number of components in the magma from which the rock is formed. It is noted that over 90 percent of the earth's crust consists of silicate minerals, including quartz. Hence, the behavior of these minerals, which has been studied extensively by ceramists and geologists, is of basic interest in this investigation. Eitel (22) has compiled a useful comprehensive treatment of the thermal behavior of silicate minerals (to 1965). However, most of the silicate

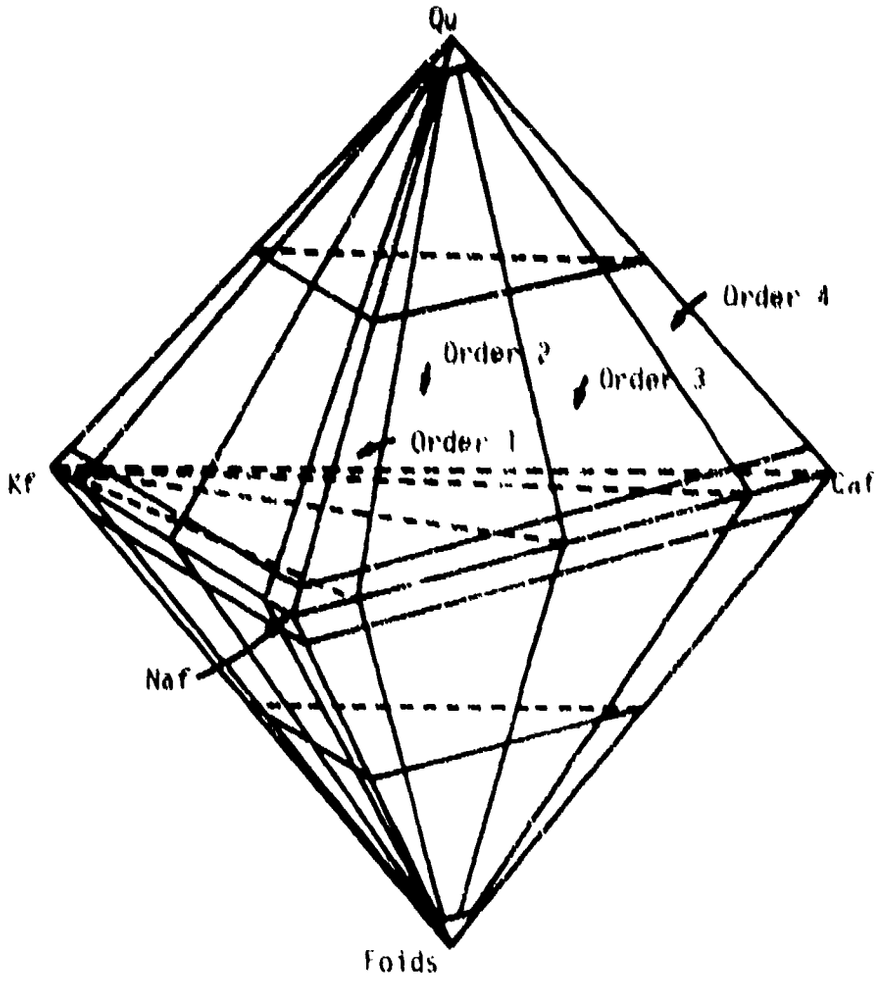

Figure 1. Double Tetrahedron for Classification of Igneous Rocks

systems studied do not correspond to the compositions of igneous rocks. Principal constituents may be in the same proportions, but small amounts of accessory minerals or compounds may grossly affect the properties of rocks, sinters, melts, and glasses produced.

The principal types of plutonic igneous rocks vary in average composition from 25 percent to no quartz, and may contain feldspars or other silicate minerals in varying amounts (Table 1). The volcanic compositional equivalents of granites include the rhyolites, dacites and porphyries. That is, types of plutonic rocks may have approximate volcanic equivalents in chemical composition. Volcanics may be hard and dense, or soft and porous, e.g., tuffs and pyroclasts.

The composition, density and related physical properties determine melting temperature and general response to application of heat. Melting temperatures of noneutectic compositions are higher than those at or near the eutectic condition, and other thermal properties are closely related to rock type, texture and origin.

Sedimentary Rocks

Sedimentary rocks are easily fractured by heat in small test blocks and it may be desirable to apply the proposed method to them in the future. They vary in composition more than igneous types. An average chemical composition (Table 2) shows that they contain many of the same combinations of elements as igneous rocks. However, the minerals and rock structure are the result of large scale chemical and mechanical fractionation processes. Their thermal and mechanical properties are different from igneous rocks, and tunnels can be excavated in most of them with boring machines. The most common sedimentary rocks are sandstone, limestone, and shale.

TABLE 1

Approximate Mineral Composition of Principal Types of Plutonic Igneous Rocks (21)

Mineral	Granite	Syenite	Granodiorite	Quartz diorite	Diorite	Gabbro	Olivine diabase	Diabase	Dunite
Quartz	25	--	21	20	2	--	--	--	--
Orthoclase and microperthite	40	72	15	6	3	--	--	--	--
Oligoclase	26	12	--	--	--	--	--	--	--
Andesine	--	--	46	56	64	--	--	--	--
Labradorite	--	--	--	--	--	65	63	62	--
Biotite	5	3	3	4	5	1	--	1	--
Amphibole	1	7	13	8	12	3	--	1	--
Orthopyroxene	--	--	--	1	3	6	--	--	2
Clinopyroxene	--	4	--	3	8	14	21	29	--
Olivine	--	--	--	--	--	7	12	3	95
Magnetite	2	2	1	2	2	2	2	2	3
Ilmenite	1	1	--	--	--	2	2	2	--
Apatite	tr	tr	tr	tr	tr	--	--	--	--
Sphene	tr	tr	1	tr	tr	--	--	--	--

TABLE 2

Average Chemical Composition of Rocks (21)

Constituent	Igneous	Shale	Sandstone	Limestone	Sediment[a]	Sediment[b]
SiO_2	59.14	58.10	78.33	5.19	57.95	44.5
TiO_2	1.05	0.65	0.25	0.06	0.57	0.6
Al_2O_3	15.34	15.40	4.77	0.81	13.39	10.9
Fe_2O_3	3.08	4.02	1.07	0.54	3.47	4.0
FeO	3.80	2.45	0.30	-	2.08	0.9
MgO	3.49	2.44	1.16	7.89	2.65	2.6
CaO	5.08	3.11	5.50	42.57	5.89	19.7
Na_2O	3.84	1.30	0.45	0.05	1.13	1.1
K_2O	3.13	3.24	1.31	0.33	2.86	1.9
H_2O	1.15	5.00	1.63	0.77	3.23	-
P_2O_5	0.30	0.17	0.08	0.04	0.13	0.1
CO_2	0.10	2.63	5.03	41.54	5.38	13.4
SO_3	-	0.64	0.07	0.05	0.54	-
BaO	0.06	0.05	0.05	-	-	-
C	-	0.80	-	-	0.66	-
MnO	-	-	-	-	-	0.3
Total....	99.56	100.00	100.00	99.84	99.93	100.0

[a]Shale 82, sandstone 12, limestone 6; after Leith and Mead.

[b]Poldervaart, *Geol. Soc. Amer. Spec. Paper* 62, 132, 1955.

Sandstone may be composed largely of particles or grains of quartz, of quartz and feldspar, or they may be graywackes (basalt, slate, felsite, rhyolite, schist, quartz and feldspaths), or tuffaceous sandstones. Shales are clastic rocks containing silt and clay. The carbonate rocks (general term limestone) include dolomites and limestone, whose primary constituents are calcium carbonate, calcium magnesium carbonate, and other carbonates. They may also contain fragments of many other types of minerals. Perhaps the most important reaction of these rocks to application of heat is their loss of water and CO_2.

Metamorphic Rocks

The mineral content of metamorphic rocks is somewhat similar to that of igneous rocks. They include schists, gneisses, quartzite, slate, marble, hornfels and many others. Many of them are hard, strong, and difficult to excavate. The conceptual tunnel system for the NE Corridor plans for considerable excavation through metamorphic rocks. Their response to the application of heat is generally similar to that of igneous rocks, with notable exceptions. One is a quartzite which may be 90+ percent quartz. Sioux quartzite, for example, has been found to be difficult to melt in tests at UMR, but fractures readily when heat is applied because of the high coefficient of thermal expansion of quartz and its crystallographic phase change at 573°C. Other metamorphic rocks have their own individual characteristic response to high temperatures depending upon composition, grain size, structure, etc.

Thermal Properties of Molten Rocks and Glasses*

Solidus and liquidus temperatures of representative rock types. Sufficient information about chemical compositions of rocks and phase equilibria in rock-forming systems is available to provide, on completion of a thorough synthesis, a reliable estimate of the temperatures of initial liquid formation and of complete melting. Ternary systems involving SiO_2, $A\ell_2O_3$, Na_2O, K_2O, CaO, MgO, "FeO", and Fe_2O_3 have been rather well investigated and quaternary relationships of importance are understood. Reasonable extrapolation to higher order systems should be possible, though some direct experimental work will be necessary to fill the gaps.

Nonequilibrium assemblages. Because the process of rapid, localized melting of rocks involves a considerable thermal gradient, the phase assemblages will necessarily vary from equilibrium or near-equilibrium, through all stages of thermal equilibria, outward to unaltered rock. Nonequilibrium assemblages formed during the rapid heating and cooling processes are expected, however, and will be sensitive to secondary rock properties such as particle size, porosity, presence of accessory nucleating agents, and the nature of the transitory environment of melting, particularly water and carbon dioxide pressures. Though a good general picture of equilibrium phase assemblages can be obtained from available phase equilibria data, direct investigation of real rock will be necessary to determine the importance of nonequilibrium assemblages.

---

* Section written by Dr. Charles A. Sorrell, Dept. of Ceramic Engineering, University of Missouri-Rolla

Glass transition temperatures. Experimental determinations of glass transition temperatures have been largely restricted to commercial glass compositions, none of which approximate major rock types. Because the rate of melting and heat transfer will be affected by the manner in which a glass inclusion is formed, it may be necessary to obtain glass transition temperatures of rock compositions. Of equal importance are temperature-viscosity relationships in liquid-crystal assemblages likely to be encountered because of incomplete melting or partial crystallization during cooling of the inclusion.

Devitrification. Strengths of glasses are strongly dependent not only on crystals present because of partial melting but also on very small crystals formed by devitrification below glass transition temperatures. In many cases, as in commercial glass-ceramics (Pyroceram), considerable devitrification, induced by nucleation of primary phases on precipitates of a minor component (TiO_2), strengthens the material appreciably and improves thermal shock resistance. The effects of devitrification on strength and other properties of glasses should be studied in real rocks and some consideration given to addition of nucleating agents during the melting operation in order to promote beneficial devitrification. This is important in relation to the LASL studies.

Volume changes associated with melting. Though some DV_{Fusion} data are available, the bulk volume changes which occur on melting are complicated by variable porosity and by loss of volatile components. Bulk densities of rocks and densities of glasses formed from them should be measured. Johannsen (20) has indicated that glasses occupy from 5 to 20 percent greater volume than their crystalline rocks.

Alteration of rock composition by additives. Nonsilicate rocks, such as limestone, and some silicate rocks, notably those rich in SiO_2, will not form glasses or will do so only at very high temperatures. In general, addition of other oxide components will lower eutectic and liquidus temperatures considerably. Deliberate introduction of Na_2O and SiO_2 to the area of melting may be expected to result in glass formation in a limestone in the 500-700°C range.

Transitory Environments

Oxidation-reduction reactions. Some elements, notably iron, are readily reduced or oxidized, with associated structural changes, dissociation and recrystallization, which affect the physical strength of the rock. Though the iron oxides are well understood, the oxidation-reduction relationships in iron-bearing silicates have not been studied thoroughly. Provision of a transitory environment during melting, moreover, complicates the situation even more, with the nature of the environment in large part determined by the composition of the heating element. All experiments with materials likely to undergo oxidation or reduction should be done in at least two ways, one with a locally reducing environment, as in graphite crucible, and the other in an oxidizing environment, as in a platinum crucible.

Effects of volatile components. Melting and glass formation in some materials will be preceded or accompanied by formation of volatile components which, in addition to changing the amount of condensed material, will provide a transitory environment. Unfortunately, only meager information regarding phase equilibria in complex systems containing water and CO_2 is available and even less information on partial pressures or vaporization rates of volatile components of the silicates.

Attempts to predict the magnitudes of the effects of volatile components on melting and glass formation must be secondary to experimental measurements.

Heating element-melt compatibility. In general, silicate melts do not react with metals or carbon unless the metals are permitted to oxidize. Use of metallic heating elements in contact with melts should cause no problem unless the stability of the element is dependent on formation of an oxide layer. The same generalizations are appropriate to the refractory carbides. Experimental evaluations of different heating element materials in contact with different melt compositions should be made.

Experimental Studies of Melts and Glasses

A reasonably thorough understanding of the chemical processes which occur during rapid, localized melting of major rock types, with or without additional components, should be obtainable through a detailed synthesis of available physical chemical data. A limited, carefully selected set of experiments is planned in the future, utilizing natural rock and soil samples, to determine the following:

1. temperatures of initial and complete liquid formation in reducing and oxidizing environments,
2. phase assemblages developed as functions of temperature and distance from the heating element - rock interface,
3. volume changes associated with the melting process,
4. compatibility of heating element materials with silicate melts,
5. glass transition temperatures of common rock compositions, viscosity, dissociation, electrical properties,
6. physical changes in unmelted or partially melted rocks resulting from decrepitation, volume changes, thermal fracturing.

Closely related to these are studies of the electrical characteristics of natural rock melts in arc created environments.

Heated and melted rocks. The heat capacities, melting points, heats of fusion, and thermal coefficients of expansion of hard rock forming minerals are of primary importance in the present study and some have been tabulated (23). The thermal coefficient of expansion of the silicate minerals varies with temperature, crystallographic direction and composition (24). The coefficient for quartz (plus its crystallographic change at 573°C) is larger than that for most silicates (Table 3) which is one of the primary causes of thermal spallation of rocks containing a relatively high percentage of free silica (25). However, experiments performed at UMR under the current program show that rocks composed of minerals with low coefficients of expansion, such as basalts and dolomites, will fracture readily under the influence of internal thermal stress fields.

Data on the melting temperatures of silicate systems have been acquired in studies of ceramic glasses, and have been compiled because of geological interest (26). Although the melting point of some of the constituents in the Al_2O_3--K_2O--SiO_2 system, as with other systems, are quite high, eutectic mixtures may have lower melting points (Fig. 2). Certain combinations of glass systems are possible (27). It is reasonable to assume that systems which result from glass formation from some kinds of rock will be more corrosive than others on heaters to be employed for heating and melting, e.g., if iron sulphide is present.

Carbonaceous rocks which are heated under pressure are decarbonated (Table 4) and are a source of volatiles which may cause problems.

TABLE 3

Coefficients Of Volume Expansion, $\alpha_V = \frac{1}{V}\left(\frac{dV}{dT}\right)$,

Of Selected Silicates At Atmospheric Pressure (23)

Compositions, where stated, are in mole per cent. The coefficients were derived by analytically differentiating polynomial functions fitted to the volume-temperature data by the method of least squares. Most sets of measurements commence at room temperature giving poor control of the derived functions at 20°C, compared to the control at higher temperatures, and leading to an uncertain estimate of α_V at 20°C. The values enclosed in parentheses were derived by extrapolating from temperatures where adequate control on the functions could be established. Less credence should be given the values at 20°C than those at 400°C or 800°C.

Compound	$\alpha_V \times 10^6$ °C^{-1} 20°C	400°C	800°C	Ref.
Akermanite	(26)	30	33	11
Andalusite	16	29	43	19
Coesite	8	11	14	18
Cordierite (synthesized at 1420°C)	(14)	18	22	11
Feldspars				
Adularia $Or_{88}{\cdot}_3Ab_9{\cdot}_3An_2{\cdot}_4$	14	20	24	3
Microcline $Or_{83}{\cdot}_5Ab_{16}{\cdot}_5$	(7)	17	23	15
Plagioclase $Ab_{99}An_1$	18	27	33	6
Plagioclase $Ab_{77}An_{23}$	12	19	24	6
Plagioclase $Ab_{56}An_{44}$	13	17	20	6
Plagioclase Ab_5An_{95}	12	12	20	6
Garnets				
Almandine	15	25	30	17
Andradite	21	25	29	17
Grossularite	18	23	28	17
Pyrope	19	26	30	17
Spessartite	15	28	34	17
Gehlenite	(23)	25	26	11
Hornblende	23	28	33	8
Kyanite	11	28	30	19
Merwinite	(29)	38	42	11
Mullite	9.5	15	17	1
Nepheline				
$Ne_{78}Ks_{22}$	(31)	53	72	16
$Ne_{59}Ks_{41}$	(66)	51	49	16

TABLE 3 - continued

Compound	$\alpha_V \times 10^6 °C^{-1}$ 20°C	400°C	800°C	Ref.
Olivine				
Fa_{100}	(27)	30	31	12
$Fa_{80}Fo_{20}$	(26)	32	34	13
$Fa_{41}Fo_{59}$	(27)	32	35	13
$Fa_{15}Fo_{85}$	(25)	32	39	13
$Fa_{10\cdot1}Fo_{89\cdot9}$	(23)	31	39	10
Fo_{100}	24	38	44	18
Monticellite	(32)	36	39	11
Fe-Monticellite	(25)	32	38	12
Pseudo-wollastonite	(30)	32	36	11
Pyroxenes				
Augite	18	25	32	9
Clinoenstatite	(25)	29	33	11
Diopside	24	28	32	7
Jadeite	(20)	29	(38)	20
Quartz	34	69	- 3	2,4,14
Sillimanite	10	18	26	19
Topaz	14	20	25	5
Zircon	9.3	13.7	17.7	1

TABLE 4

Reactions Involving Decarbonation (23)

	Temperatures (°C)				
	Pressure (kb)	.25	.5	1.0	2.0	Ref.
Calcite - lime + CO_2 $CaCO_3 = CaO + CO_2$						
Magnesite - periclase + CO_2 $MgCO_3 = MgO + CO_2$		650	710	775	850	4
Rhodochrosite - manganosite + CO_2 $MnCO_3 = MnO + CO_2$		615	660	710	775	1
Smithsonite - zincite + CO_2 $ZnCO_3 = ZnO + CO_2$		..	285	340	410	3
Dolomite - calcite + periclase + CO_2 $CaMg(CO_3)_2 = CaCO_3 + MgO + CO_2$		710	765	825	900	4
Calcite + quartz - wollastonite + CO_2 $CaCiO_3 + SiO_2 = CaSiO_3 + CO_2$		..	630	680	745	5
Wollastonite + calcite - spurrite + CO_2 $2CaSiO_3 + 3CaCO_3 = Ca_5Si_2O_8(CO_3) + 2CO_2$		960	..	..	..	8
Calcite + diopside + forsterite - monticellite + CO_2 $2CaCO_3 + CaMgSi_2O_6 + Mg_2SiO_4 = 3CaMgSiO_4 + 2\ CO_2$		780	865	965	..	6
Calcite + diopside - akermanite + CO_2 $CaCO_3 + CaMgSi_2O_6 = Ca_2MgSi_2O_7 + CO_2$		845	890	965	..	6
Calcite + wollastonite - Tilleyite + CO_2* $3CaCO_3 + 2CaSiO_3 = Ca_5Si_2O_7(CO_3)_2 + CO_2$		890	..	..	..	2
Tilleyite - spurrite + CO_2* $Ca_5Si_2O_7(CO_3)_2 = Ca_5Si_2O_8(CO_3) + CO_2$		935	..	..	..	2

* Tilleyite could be synthesized only in the presence of small amounts of Al_2O_3 and fluorine, although the latter may have acted merely as a flux.

X=$K_2O.Al_2O_3.4SiO_2$
(leucite)

W=$K_2O.Al_2O_3.6SiO_2$
(potash feldspar)

E'=$K_2O.Al_2O_3.2SiO_2$
(hexagonal and orthorhombic K Al SiO_4)

G'=$K_2O.Al_2O_3.SiO_2$

N=867±3° T=918±5°
I=990±20° U=905±10°
J=1470±10° V=923±5°
L=1470±10° X=1686±5°
M=985±20° A'=1316±10°
N=1140±20° B'=1588±5°
O=1150±20° C'=1553±5°
P=710±20° D'=1615±10°
Q=725±5° F'=1680±10°
R=810±5° H'1540°±
S=695±5° I'=1540°±

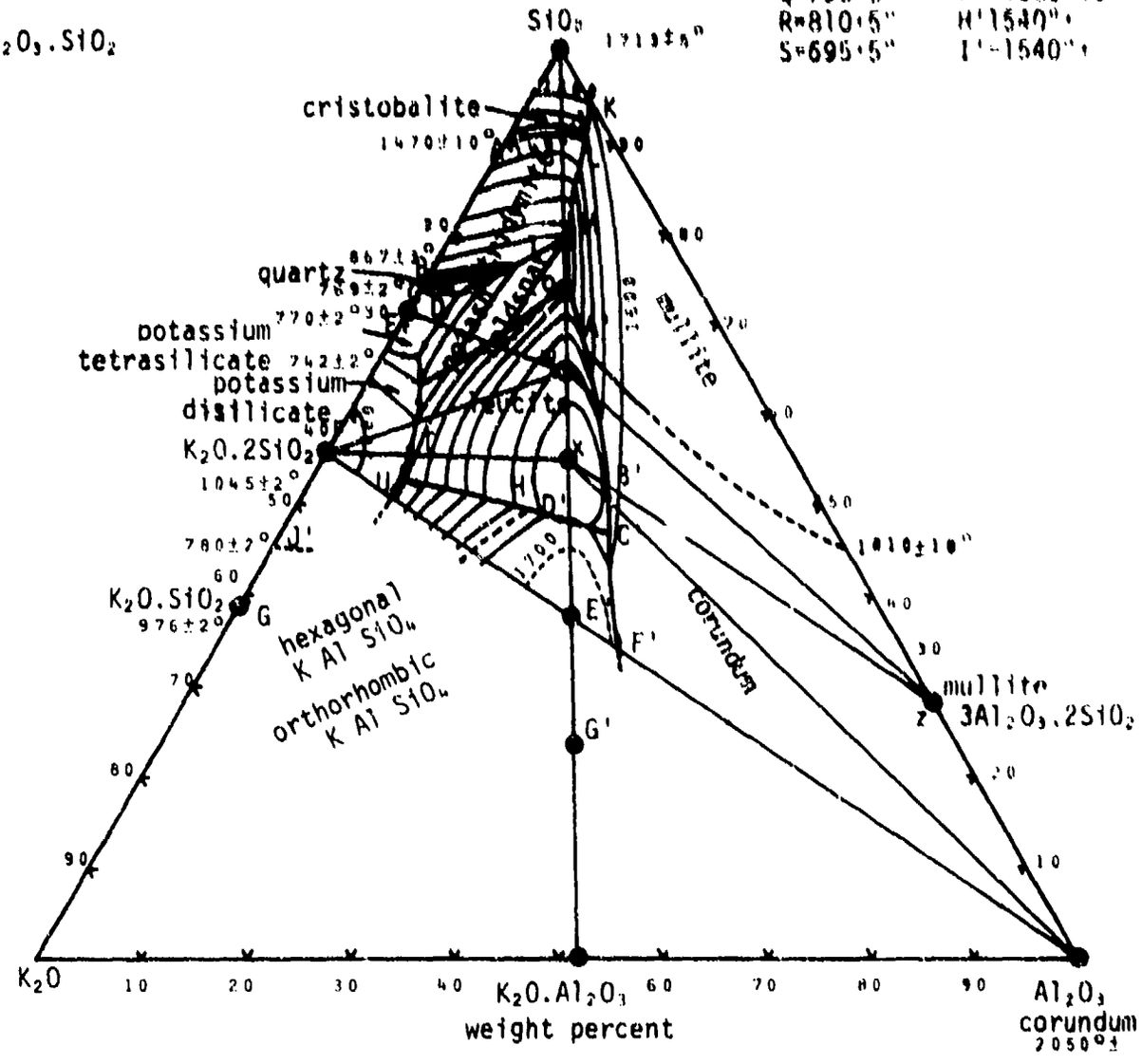

Figure 2. The system Al_2O_3-K_2O-SiO_2.. (23)

Although most carbonate rocks are soft enough to be excavated with tunnel boring machines, some may be of interest in this project. Also, when bare carbon electrodes are employed in a drill hole in a rock, CO and CO_2 may be formed as the electrodes are involved in chemical relations.

As indicated above, other important behavioral factors of silica or silicate melts are concerned with the volatiles which are produced, and corrosivity of the melt. Water content has a marked effect on melting points, and when minerals have combined water their (hydrothermal) behavior is different from that of the dry silicates.

Viscosity of molten rock (23). Molten silicates are believed to fall in the category of being Newtonian fluids, whose viscosity is independent of shear rate. Viscosity is a simple activated process which may be represented by the function $\eta = \eta_0 \exp(E_\eta/RT)$ (where η_0 is the limiting viscosity at high temperatures and E_η is the activation energy). This law is obeyed by silica, and more complex silicate liquids may be represented by a sum of terms.

The viscosities of SiO_2, obsidian, granite and andesite, are higher than those of less siliceous rocks (Table 5), while those of basalts and lava are quite low at 1400°C. This has been found to be true of the rocks melted with carbon arcs in research at UMR. It was difficult to form a melt from nearly pure quartzite, and the melt from granite containing about 20 percent free quartz was very viscous. Under the same test conditions the melt formed from a basalt flowed easily.

The amount of SiO_2 present in silicate system (Table [5]) has a marked effect on its viscosity, the viscosity increasing with the percentage of SiO_2. Thus, more siliceous rocks would require higher

TABLE 6

Viscosity of Minerals & Rocks (23)

Mineral or rock	Temperature, °C	Viscosity, poises
SiO_2	1100	4.7×10^{13}
	1400	4.62×10^{10}
	1800	5.74×10^{8}
	2000	2.82×10^{6}
Olivine basalt	1200	3,180
	1400	137
Andesitic basalt	1200	31,200
	1400	140
Nepheline basalt	1200	190
	1400	80
Lava, Mt. Vesuvius	1200	2,760
	1400	256
Obsidian	1400	1×10^{6} to 4.4×10^{6}
Hornblende granite	1400	2×10^{6}
Hornblende mica andesite	1400	1.6×10^{5}
Andesites	1400	150 to 1500
Diabases	1400	15 to 400

temperatures and more heat to cause them to flow, or artificially introduced fluxes would be required to reduce the viscosity.

Chapter III

ELECTRIC ARCS

Arcs - Rock Drilling

A review of the important characteristics of electric arcs was made by McMaster, et al (28) in relation to an investigation of the feasibility of their use in drilling oil wells. Their performance in air and water was of direct interest in these studies, and much of this information is of basic interest in the rock fragmentation research with which this project is concerned.

The low voltage required for arcs may be advantageous for rock breakage, i.e., it is generally easier and safer to use in underground environments. McMaster (28) reported that the voltage drop (dc) at the cathode is of the order of the least ionization potential of the gas or vapor in which it burns. The arcs employed in drilling experiments were subject to severe transients and rapid fluctuations in length, position, current and voltage so that the average characteristics might not correspond to a steady state operating condition. The temperature of the arc column in air was reported (28) to vary from 4330°C to 7330°C at atmospheric pressure, and as high as 10,760°C in the center of the arc column for high current arcs. It is noted that the temperature of the surrounding gas just a few hundredths of an inch from the boundary of the arc may be nearly ambient. Also, the temperature of the electrodes cannot exceed their boiling temperature, and hence, very large temperature gradients exist at the ends of the arc and at its boundaries. Conduction, convection, and ionization potential affect the voltage gradient and arc-column diameter. If the ionization potential is lowered by the presence of easily ionized substances, the voltage gradient and temperature are reduced.

Heat is lost from the arc-column by conduction, convection, and diffusion through the surrounding gas. It is estimated that about 15 percent of the heat is given off by radiation. Most chemical compounds, particularly gases, are completely dissociated at arc temperatures, and contribute significantly to transfer of heat. That is, dissociated atoms, ions, and electrons diffuse from the arc column, and when they recombine in the cold surroundings they give up their energy of dissociation.

In a survey of literature on electric arcs made by Cooper, et al (29) in 1950, they report that Filkelnberg showed that burn-off of carbon electrodes is due almost entirely to evaporation, i.e., it occurs only when the boiling point of the carbon is reached in the cathode spot.

One equation relates the voltage gradient of the arc to the current by

$$E = B/i^n \qquad (3.1)$$

where

E = voltage gradient

i = current

n and B = constants

For nitrogen and air, n = 0.60, and for steam n = 0.59. The equivalent value for the material in the arc-column in molten or vaporized rock is not known, but for basalt, granite, and quartzite the arc becomes stable after a melt is formed. The above mathematical law is an opposite effect than that described by Ohm's law. This negative characteristic requires a series resistance to maintain a stable arc.

The current densities in high current arcs reported to 1949 were as high as 20,000 amps/in^2. An amount of heat, approximately equal to the voltage drop at the electrode times the arc current, is produced at each electrode, and an additional amount from the recombination of dissociated molecules.

• Arc stability, or its ability to reignite after short circuit, or after each reversal of alternating current, is determined by the arc characteristics and the recovery-voltage capabilities of the power source. It has been found that superposition of high frequency voltages may add to the stability of arcs. An arc is usually started by bringing the electrodes in contact, or by "striking the arc", preferred voltages for dc being 60 to 150 volts and for ac, 80 to 200 volts.

The kinetics of an arc formed in a molten rock environment and the associated heat transfer processes are very complex. Hence, experiments will be designed primarily to measure gross phenomena. Unless the physical and chemical processes which take place in the rock near the arc are of such a character that much of the generated heat cannot be recovered, the high temperature of the arc provides such a large temperature difference that heat flow is rapid. This factor plus the heat transfer by recombination of atoms, etc., at the surface of the cavity makes for efficient flow of heat energy into the rock. Carbon arcs need not be cooled, a process which often represents a large heat loss. Pertinent information from an abundant literature on arcs will be obtained and utilized in support of further research effort.

The only problems encountered to date in the use of carbon arcs are (a) the electrodes fracture easily, and (b) it is difficult to maintain stable arcs without high frequency, high voltage current similar to that employed in TIG welding.

Arcs-Characteristics

It has been found (30) that arcs may be initiated (1) by transition from a low current discharge such as a glow, (2) by means of a transient non-steady spark discharge, or (3) by separating two current-carrying electrodes initially in contact, usually called striking an arc. Molecules of gases and other substances are electrically neutral, and will conduct electricity only if charged particles are introduced or created in them. In most common gases the carriers are electrons and ions, while in the complex environment created by an arc inside of a rock additional types of carriers may be involved.

An arc channel in mercury vapor has been shown to be at 5900°K and contains approximately equal densities of positive and negative charge. Several other conditions are shown (30) to hold in arc behavior including types of equilibria, number of collisions, etc. Under extreme conditions the temperature of the central arc column may exceed 50,000°K.

Energy is transferred out of the arc column to a surrounding wall in several ways:

1) By impact of molecules, ions, or electrons, at high pressures by thermal conduction.

2) By ions and electrons diffusing to the wall, recombining and giving up their energy of ionization.

3) By excited atoms giving up energy of excitation.

4) By dissociated atoms re-associating and giving up energy of dissociation.

There are also several types of radiation occurring, including those of atomic and molecular spectra, and radiation involved in

volume recombination. The distribution of energy transfer is known for mercury vapor and other gases as a function of pressure, but no results of such studies for vaporized minerals could be found in the literature.

In an arc between carbon electrodes in a drill hole in granite the arc must be initiated in an atmosphere of air. As the temperature of the rock increases it is melted and vaporized and the arc environment becomes a combination of melt and vapors from the rock.

It is pointed out by Somerville that electrode-column junctions have sharp discontinuities, electrically, thermally, and other ways. Electrically, a transition is made from a conductor (electrode) in which current is carried by electrons to one (gas) in which both electrons and ions carry current. At the anode electrons may enter the metal, but ions do not move from the metal to the gas, while at the cathode gaseous ions move to the metal, but electrons must overcome a potential barrier. Thermally, the arc column is very hot and the electrode relatively cool. These and associated problems are of fundamental interest in heater design.

Arc Experimentation - Recent

In 1965 the Bureau of Mines (31) published a comprehensive review of the literature and some experimental results of tests on high current metallic arcs. Much of this information is pertinent to the current project including the Glossary of terms.

GLOSSARY

Anode Fall: A very thin space-charge region in front of an anode surface, characterized by a steep potential gradient through the region.

Arc Plasma: The space between arc terminals in which gaseous conduction of electricity takes place. Approximately equal numbers of electrons and ions virtually neutralize the space charge, but ionization and excitation are generally intense. The potential gradient is low.

Cathode Fall: A very thin space-charge region in front of a cathode surface, characterized by a steep potential gradient through the region.

Cathode Spot: A bright candescent spot on the surface on a cathode, apparently an active area through which current flows from the plasma.

Cathode-Spot Mode: A particular mode of arc operation as observed in laboratories of the Linde Company. The cathode spot is unusually bright and the arc is abnormally constricted at the cathode terminus. The same behavior has been called the "contracted mode."

Cold-Cathode Arc: An indefinite term descriptive of any arc with a cathode that is not candescent.

Electrode Burn-Off Rate: The rate at which an electrode is consumed by an arc in units of mass per time per arc power.

Electrode Consumption Rate: The rate at which an electrode is consumed by an arc in units of mass per time per arc current.

Electrode Melting Rate: The rate at which an electrode is consumed by an arc in units of mass per time.

Globular Transfer: Also known as "drop transfer" or more specifically as "large-drop transfer." The term describes the transfer of metal as relatively large drops or globules during consumable-electrode arc welding.

High-Current Metallic Arc: An electric arc between metal terminals and at a high enough current to cause appreciable melting of at least one terminal.

High-Intensity Arc: Similar to a high-current metallic arc, except not necessarily between metal terminals. The term originally was used to describe arcs of several hundred amperes between carbon electrodes in air.

N-Mode: A corruption of "normal mode", a term that contrasts with "cathode-spot mode"; a particular mode of arc operation as observed in laboratories of the Linde Company. The normal mode has a normally diffuse cathode spot and no unusual constriction at the cathode.

Normal Arc: A term specifically intended to differentiate between the arcs that are commonly observed and the low-pressure "skittering arcs."

Positional Stability: A basis employed at the Westinghouse Research Laboratories to describe the behavior of vacuum arcs. The cathode spot(s) of positionally stable arcs operate at the tips of cathodic electrodes. The cathode spot(s) of positionally unstable arcs operate up and down the sides of cathodic electrodes.

GLOSSARY (continued)

Skittering Arc: An anomalous low-pressure arc form characterized by multiple cathode spots of small size and in rapid motion. Skittering arcs are further described as "stable" if the cathode spots operate at the tips of cathodic electrodes, and as "displaced" if the cathode spots operate up and down the sides of cathodic electrodes.

Spray Transfer: Also known as "small-drop transfer." The term describes the transfer of metal as a spray of droplets during consumable-electrode arc welding. Spray transfer is further described as "axial" when the stream of droplets is along the arc axis, and as "rotating" if it rotates at an oblique angle to the arc axis thus generating a conical surface.

Experimental equipment utilized by the Bureau of Mines consisted of a small scale arc furnace with appropriate auxiliary instrumentation and controls. Arc potential was found to vary with material of the cathode and anode, gas pressure, type of gas, arc gap, current, and some other factors, for a configuration utilizing a button anode and a consumable metallic electrode.

The following trends were noted: 1) current densities may be in the order of 10^3 amp/cm^2 for normal arcs, and 10^5 to 10^6 amp/cm^2 for skittering arcs, 2) increase of arc current results in an increase of cathode-spot area, which decreases before it increases in size, 3) cathode-spots for normal arcs diffuse at lower pressures, 4) cathode-spot densities are different for different gases, 5) the arc gap affects the cathode-spot area.

The electrode consumption (melting) rate of zirconium in argon gas at 250 torr, 520 to 540 amps, varied from 4.19 to 4.42 grams/sec or about 0.48 gm/min per amp. The cathode-spot temperature for thoriated tungsten varied from 2322°C to 2867°C, the latter for 500 amps at 32 volts. No data are given for carbon electrodes.

In early research the cathode-spot temperature for carbon arcs, measured by optical pyrometry, was near 3600°K. Most of the equations developed for relationships between potential, are gap, and current are for low currents with electrodes other than carbon. However, they offer only approximations. The arc potential includes the cathode fall, the anode fall, and the plasma potential component. There is little direct experimental data on these parameters for any types of electrodes.

For studies of current densities made with water-cooled copper electrodes and total arc currents of 100 amperes, the current density ranged from about 2 by 10^2 to 2.5 by 10^3 amp/cm^2 at the center of the anode area, with an approximate Gaussian distribution about the center.

The temperatures of arc plasmas are determined by measurements of the electron density from which the temperature may be calculated. Ionization temperatures are measured by observation of line spectra, the intensity of which is related to the temperature. All such measurements usually are accepted with qualification because of several uncertain measurement and calculation factors.

Maximum arc temperatures are a function of arc current (Fig. 3) and range from about 4000°K to 2 by 10^5°K. It is reported that some toroidal-discharge plasma temperatures continue to increase at higher current reaching about 2 by 10^6 to 4 by 10^6°K at 150,000 amperes, although arc plasmas may not follow the same path. Also, if proper nuclei are present nuclear interactions may begin to occur at 80,000 amperes in the toroidal discharges, yielding neutrons.

Axial temperatures of the arc are lower near the anode, differences ranging from a few hundred degrees to several thousand degrees. Molecular gases appear to be related to higher temperature differentials than atomic gases. Although pressure has an effect on arc performance, other research in the thermal fragmentation project is being conducted largely at or near atmospheric pressure.

The arc plasma is largely electrons and ions of non-uniform distribution, and may be classified as a normal or skittering arc according to mode.

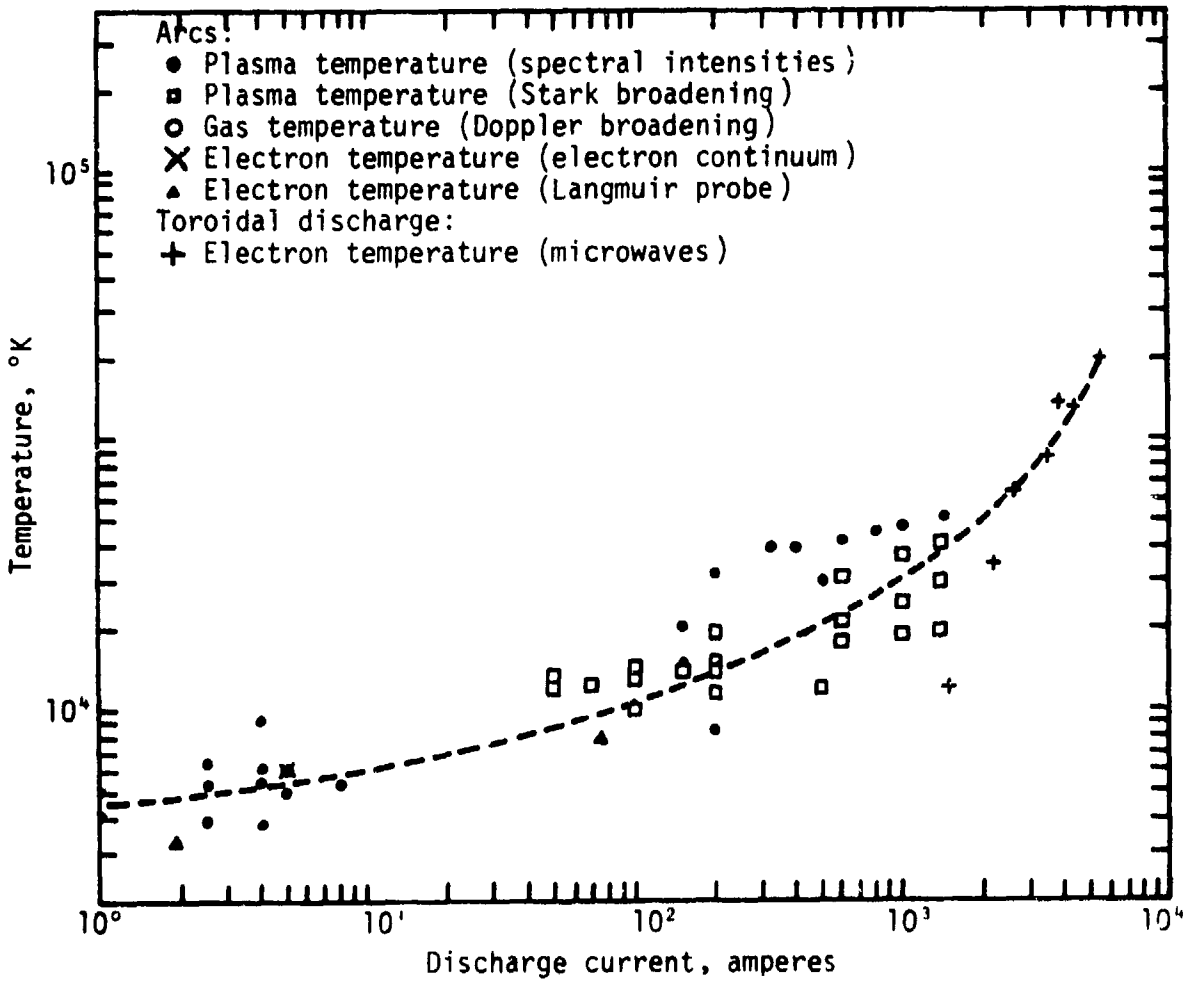

Figure 3. Maximum Temperatures in Arcs and Toroidal Discharges as a Function of Current (31).

Electrode consumption rates for metal are affected by the composition of the electrodes, the arc current, the pressure and composition of arc environmental gas, the electrical conductance of the electrodes, the arc gap, the anode size, and other dimensional factors. The first three appear to be the most dominant.

The characteristics of the cathode, plasma, and anode regions of the arc are discussed in some detail by Wood and Beal (31) and this information will be of importance in projected research studies of the behavior of arcs in environments composed of the vapors created by an arc in a closed hole in rock. It is noted that even though the power input into an arc can be estimated, the expenditure of power is determined by the properties of the system, which include thermal conductivity, emissivity, vapor pressure, electron work function, enthalpy, heats of fusion and vaporization, the melting and boiling points of the electrode, and the transmittance and thermal conductance of the gas surrounding the electrode.

Chapter IV

THEORY - INTRODUCTION

The cost of experimentally studying the various parameters of most engineering systems justifies simplified theoretical studies which provide guidance for the optimal design of such systems. It is often of value to be able to confirm theoretically certain unusual phenomena which have been observed experimentally. The mechanics of the thermal mechanical rock fragmentation system considered here are typical in that full scale tests are difficult and expensive.

The actual fragmentation system is three-dimensional. Figure 4 shows a semi-infinite region with equally spaced holes. The holes are drilled to a constant depth over the area where rock is to be removed. Heat sources are placed at the bottoms of the drilled holes. The resulting thermal inclusions (heated zones) cause two types of fractures, one of which is along planes containing the axes for the rows of holes. A more important fracture occurs parallel to the working face (perpendicular to the hole axes) at approximately the depth of the inclusions. This fracture pattern makes possible the removal of rectangular blocks of rock, the block dimensions being determined by the hole spacing and the depth of the thermal inclusions. To facilitate fracture and removal of the rock, free surfaces in the form of slots (Figure 5) or as would be provided by a spiral round are required. The slots can possibly be cut by several different means. Drilling tangent holes is one method which has been explored. Other possible methods include water jets, electron beams, plasma

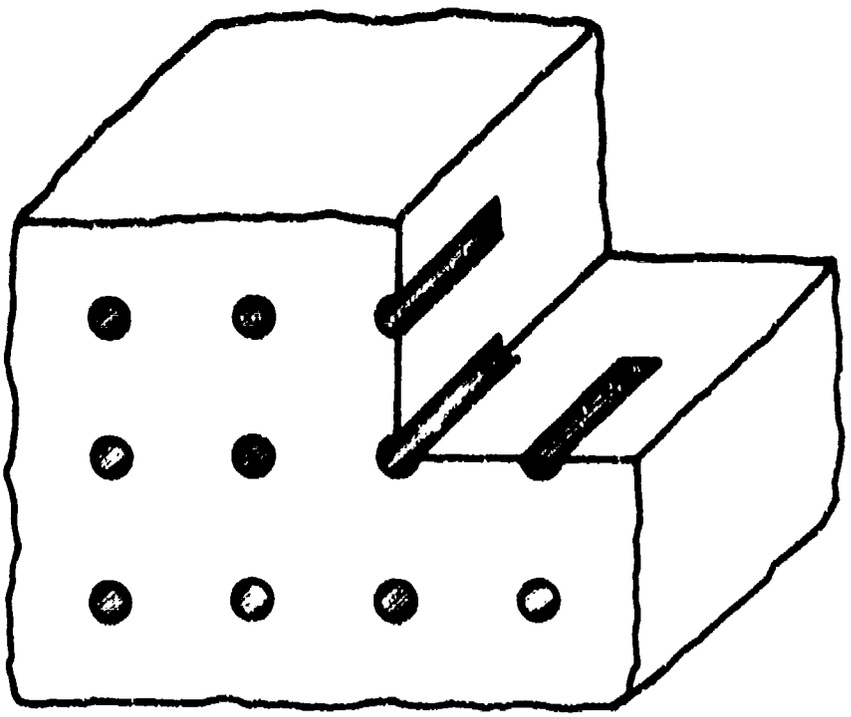

Figure 4. Three Dimensional Configuration for Thermal Rock Fragmentation

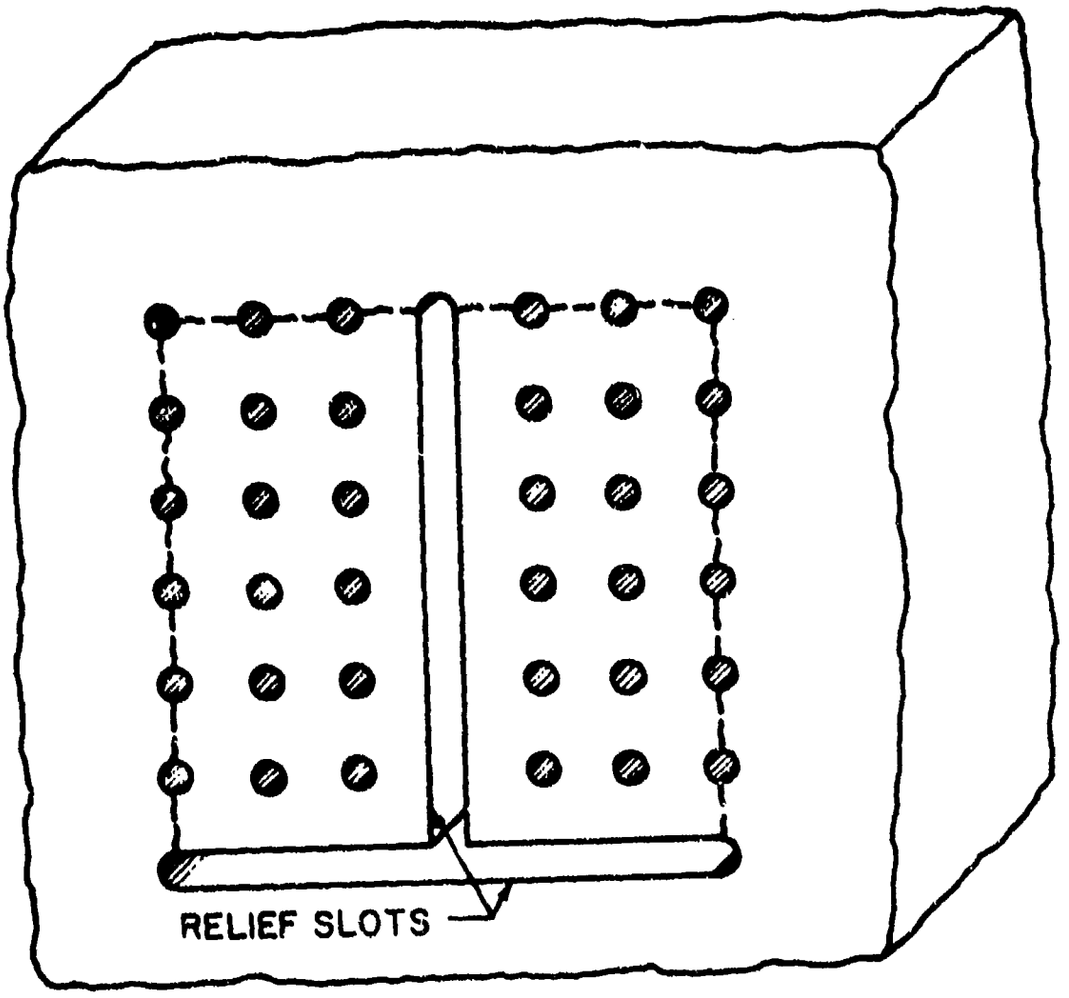

Figure 5. Slot Configuration for Displacement Relief

jets, lasers and other novel techniques. Employing heaters for pyramid cuts or in a spiral round similar to the way explosives are used is possible. However, the theoretical studies assume no displacement relief.

A complete theoretical analysis of the mechanics of the process required a transient temperature, thermal stress and fracture study of the three-dimensional geometry shown in Figure 4. The problem is nonlinear in the sense that the thermal and elastic properties of most rocks are highly dependent on temperature.

To study the fracture or fragmentation problem two alternatives to the method selected have been considered. The first and best alternative from the viewpoint of accuracy would have been to study the actual three-dimensional geometry with anisotropic properties and temperature dependent boundary conditions. From the three-dimensional geometry the finite element method can be used to study most of the parameters which affect fracture. Three-dimensional codes capable of performing the calculations would have had to be developed at much greater cost. The second alternative would have been to treat a single hole and heater in a semi or half space. If the interactions between the individual stress fields can be neglected, the stress at any point in the rock can be found by adding the contributions to the total stress at that point of each of the surrounding holes.

The approach used allows the displacement boundary conditions to supply the interaction between the stress fields. Isotropic material properties are used and the effect of temperature on the thermal properties has been considered only in the one-dimensional studies.

For the two-dimensional studies a particular rock (Dresser basalt) was selected whose thermal properties are relatively independent of temperature. Consider the hole pattern shown in Figure 6. This pattern can be assumed to extend indefinitely in all directions. The dashed lines indicate the intersections with the working face of the planes of symmetry. Over each of these planes of symmetry, material displacements do not take place perpendicular to the plane. Thus, considering the location of these planes the three models shown in Figure 7 can be used to study the significant process parameters. Figures 8-10 show one one-dimensional and three two-dimensional models which have been used in this study. The influence of hole diameter, depth and spacing has been explored using the two-dimensional models. In these studies the elastic properties have been treated as functions of temperature. The temperature distributions were obtained assuming constant thermal properties. The one-dimensional models have been used to study appropriate types of boundary conditions as well as the effect of temperature dependent thermal properties.

The slot model has been used to study the fracture that occurs parallel to the working face of the tunnel or excavation. In the slot model such a fracture passes generally along the bottom of the slots. This fracture depends on the nature of the thermal inclusions. The model is a good indicator of the effect of hole spacing as well as the effect of variations in the heated length.

The hole model has been used to study the fracture that occurs between holes on a plane containing the hole axes. The model provides information about the effect of different hole diameters and spacings.

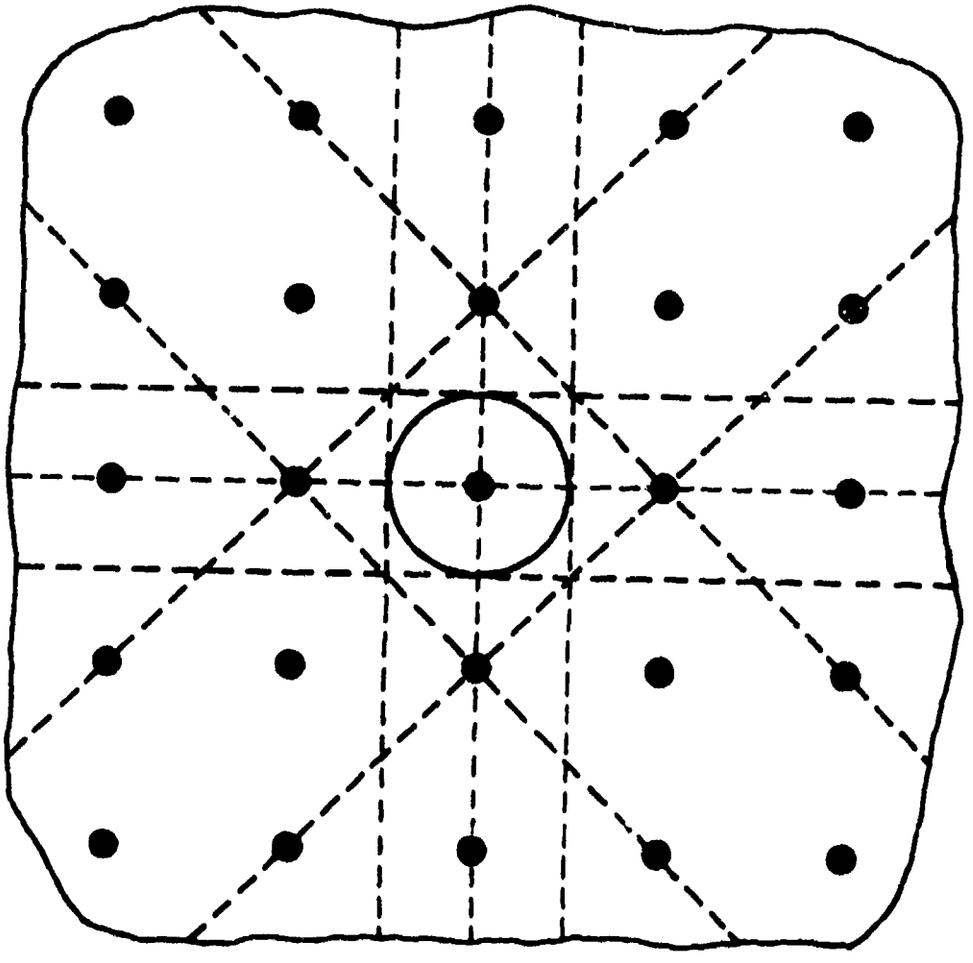

Figure 6. Typical Planes of Symmetry for Mathematical Models

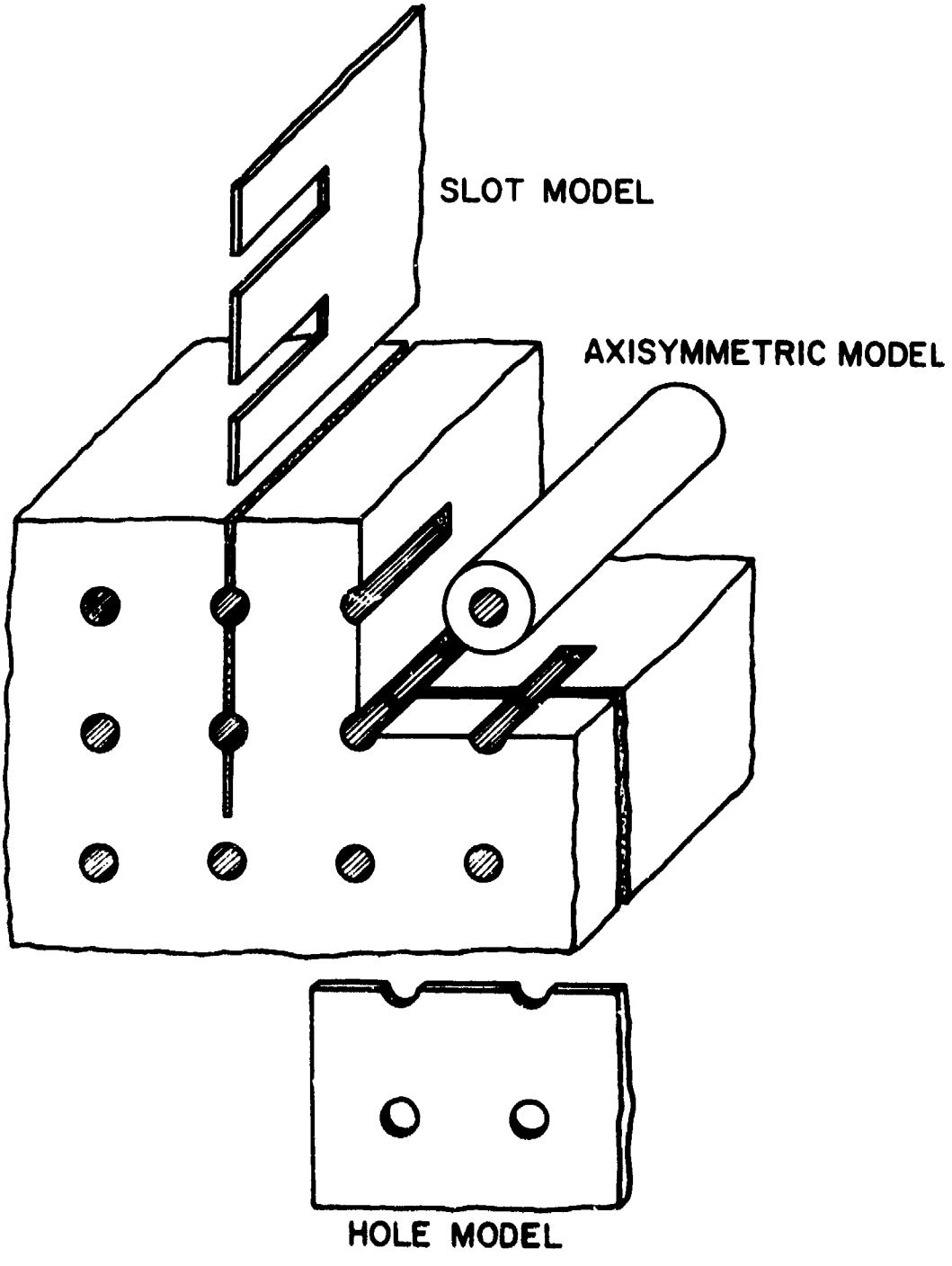

Figure 7. Two Dimensional Models

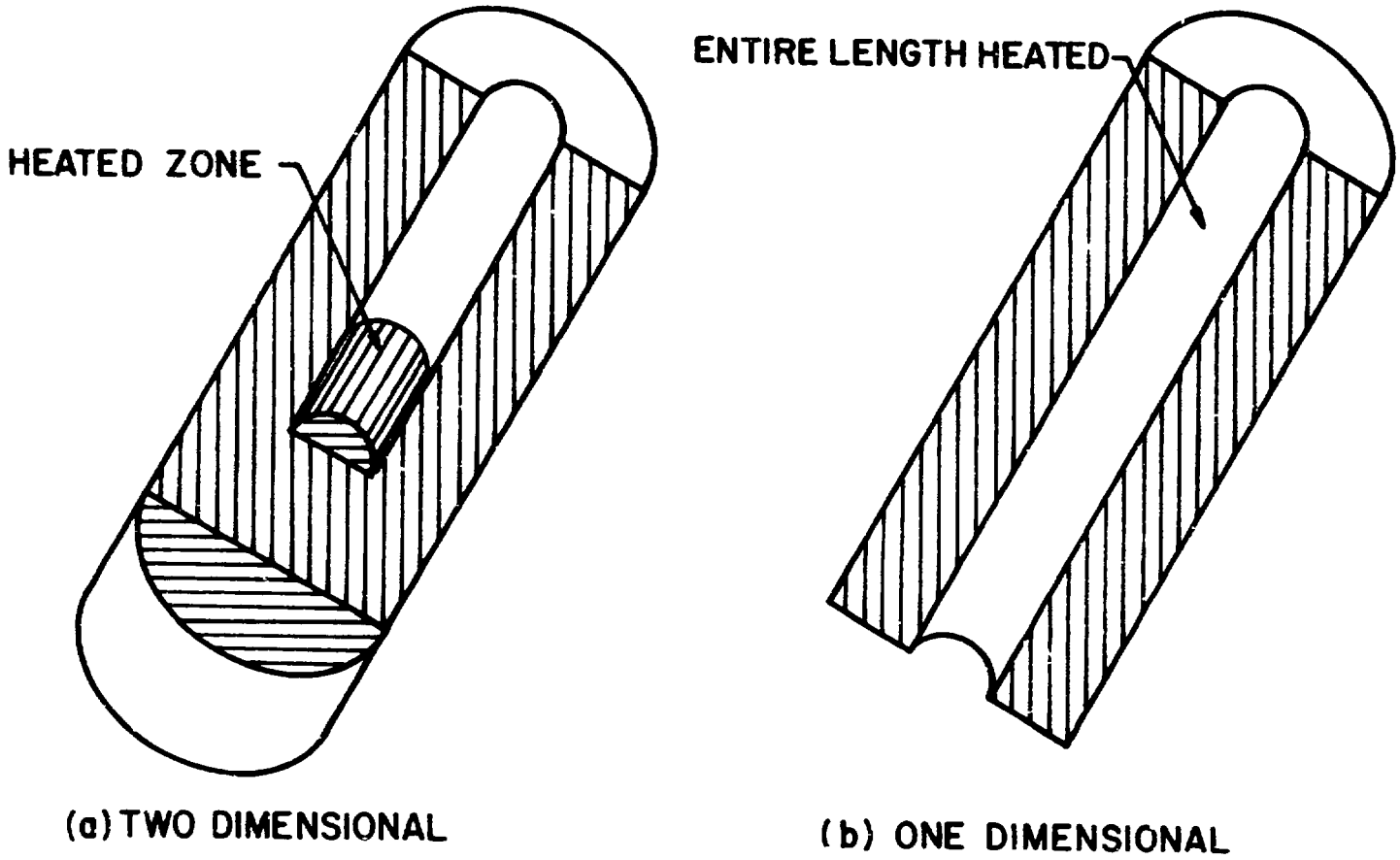

Figure 8. Axisymmetric Cylinder Models

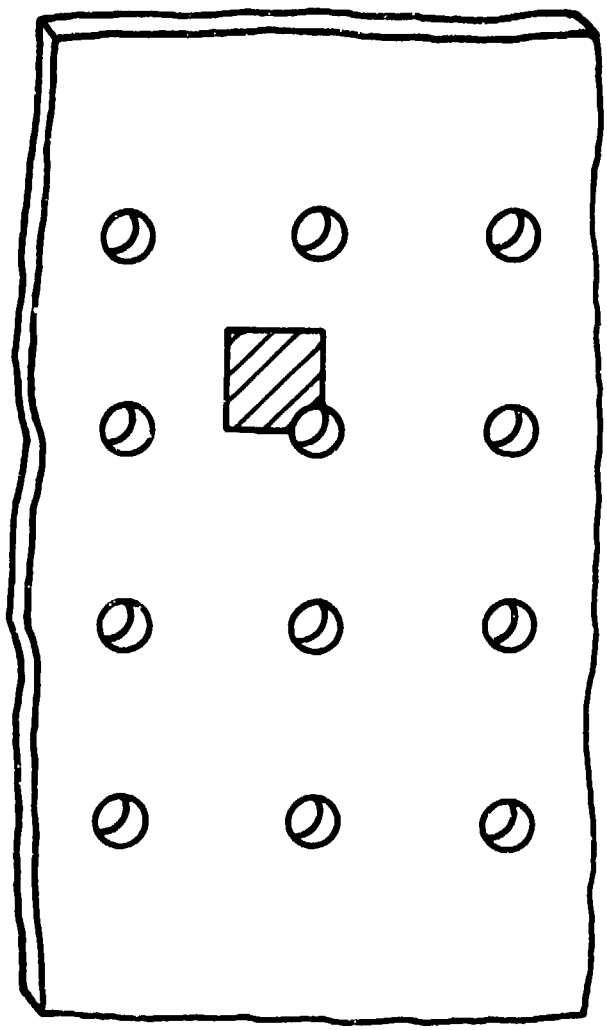

Figure 9. Typical Section for Hole Model Analysis

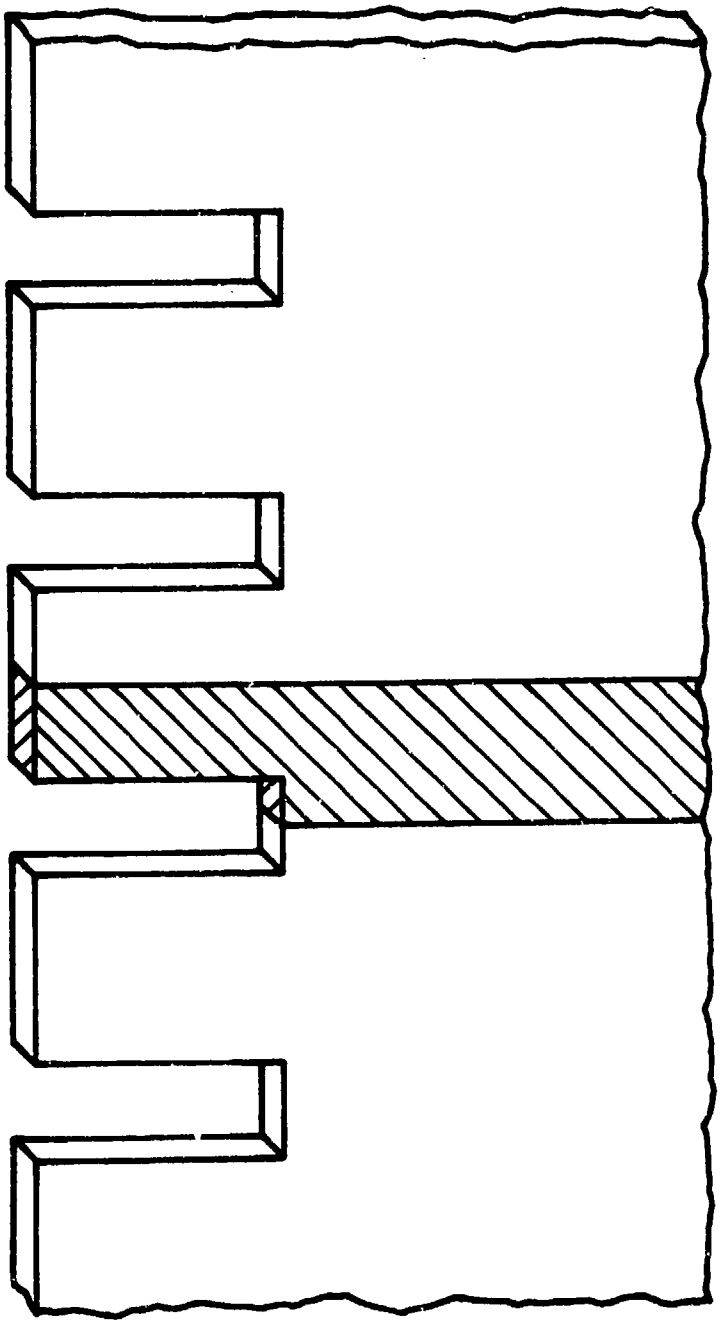

Figure 10. Typical Section for Slot Model Analysis

The cylinder model has been treated both as one and two-dimensional. The one-dimensional cylinder model was selected to obtain more basic information such as the effect of nonlinear properties and the proper type boundary conditions for different types of heaters. The two-dimensional cylinder model in this study was used to verify some of the conclusions obtained from the slot and hole models.

Chapter V

ROCK CHARACTERISTICS AND APPROXIMATIONS

Rocks are, in general, complex materials with inherent inhomogeneity and anisotropy as well as temperature-dependent material properties. For rock related studies one must also consider, among other factors, effects of porosity, moisture content, microcracks, bedding and joints, stress relief and stress absorption. An exact thermal stress analysis with all of these factors will be extremely difficult even for the simplest one-dimensional geometry. Simplifying assumptions are, therefore, necessary in order to obtain a workable solution. A description of general characteristics of different kinds of rock is, thus, in order.

A. General Classification (32)

The most general rock classification system is based on the mode of origin. Rocks are divided into three main groups: igneous rocks, sedimentary rocks, and metamorphic rocks.

Igneous rocks originate from solidification of hot, molten material below the earth's crust. These are very hard, massive rocks with granular nonporous structure and exhibit very high compressive strength. Their tensile strength is many times smaller than their compressive strength, yet their tensile strength is higher than the tensile strength of most other rocks.

The most predominant characteristic of sedimentary rocks is stratification or bedding. As a result, they possess strong transversely isotropic properties, and have much less compressive strength than the igneous rocks.

The term "metamorphism" denotes an aging process which brings about a complete change in the original rock characteristics as a result of very long, continuous action of pressure, temperature, and moisture and chemical reactions of atmospheric gases. Most metamorphic rocks possess the highly crystalline texture of igneous rocks with a parallel structure which closely resembles the stratification of sedimentary rocks. Fracture generally occurs due to cleavage along these planes. Metamorphic rocks that do not possess the cleavage planes usually have hard, massive structure with compressive strength on the same order as granite. Most hard metamorphic rocks exhibit some characteristics resembling closely those of igneous rocks. Quartzite is a well known example of this type.

Since this investigation is concerned with thermal fragmentation of hard rocks, mathematical models will be based on properties characteristic of igneous rocks.

B. Nonlinearity Considerations

As mentioned in the beginning of this chapter, approximations are necessary in order to obtain workable solutions for the two-dimensional analytical models. These approximations will be based on the following three major factors:

i. influence on fracture stresses,

ii. complications involved in theoretical studies, and

iii. accuracy of available property data.

Fracture stresses are influenced differently by different nonlinearity related factors. Material nonhomogeneity, for example, will cause internal loading whereas a work-hardening stress-strain

condition will lead to stress absorption. A similar situation is true regarding the degree of complexity of theoretical analysis. Thus, for example, using finite element methods, material nonhomogeneity and anisotropy can be handled rather easily, whereas the study of crack effects or the influence of rock porosity will require a prohibitively large amount of work. This is true regardless of the fact that, for a particular kind of nonlinearity, certain methods are better than others.

Availability and accuracy of rock properties are perhaps two of the most important factors in the consideration of theoretical analysis. Review of laboratory techniques for measuring rock properti s indicates that there are no general specified standards except for a very few mechanical property measurements (33-34). Besides, rocks are known to exhibit slightly different properties in situ (35). Also, the characteristics of a given rock type from different geological locations vary considerably. Most measured properties, as a result, show about $\pm 5\%$ deviation from the average value. This deviation, however, is considered to be rather small for engineering purposes, and is usually neglected.

The above considerations are used in approximating the following nonlinear rock characteristics:

1. Stress-strain Behavior

For most hard, crystalline rocks, the stress-strain curve is approximately linear and ends abruptly indicating a brittle failure (36). Some of the rocks do exhibit a nonlinear behavior. However, this nonlinearity is attributed to the presence of microcracks which close under confinement (37-40). The stress-strain behavior of in situ rock can, therefore, be assumed to be linearly elastic.

Griggs, Turner, and Heard (41) conducted an extensive study on the effect of temperature on stress-strain relationships of a variety of rocks. According to their results, most rocks show a steady decrease in yield point with increase in temperature. This effect, however, is not important in the study of rock failure resulting from thermal inclusion. This is due to a number of reasons. First, the stress-strain curves for rocks are usually obtained under uniaxial compression, whereas fracture initiates from tensile stresses that are many times smaller than the yield strength in compression. Also, during the preliminary field tests conducted in this investigation, only a small percent of the fractured rock volume was observed to have experienced any appreciable change in temperature. Thus, the effect of the lowered yield strength is localized in nature, in the close vicinity of the inclusion. However, very high temperatures in this region drastically reduce the elastic resistance of the material.

2. Homogeneity and Isotropy

Hard, crystalline rocks consist mainly of quartz, feldspar, augite, magnetite, and mica. For a given rock type, each constituent, in general, differs from others in both texture and grain size. At the same time, average grain size of a constituent varies with rock types. Most hard, crystalline nonporous rocks possess fine-to-medium grained texture and the normal range of grain size is usually from 0.03 mm to 1.0 mm. Individual crystals are chemically heterogeneous and, in general, possess different physical properties. However, the grain distribution is very random. As a result, on a macroscopic scale, hard rocks usually have homogeneous properties. Any slight

heterogeneity will, of course, be quite insignificant for the in situ rock investigations (35).

Anisotropic behavior is pronounced only for sedimentary, stratified rocks and metamorphic rocks which have well defined cleavage planes. These rocks are generally soft to medium hard, and are not included in this analysis. For hard rocks, properties are assumed to be isotropic. As a matter of fact, laboratory measurements are generally obtained in random directions and the properties are then averaged, without recording the variations in individual directions.

3. Crack Effects

Cracks are created in the form of voids as a result of removal of gases and water vapor which are entrapped at high pressure and temperature during rock formation. These voids are extremely small compared to faults and joints and are usually in the form of microcracks in nonporous, hard, dense rocks. Nevertheless, they have very definite effects on rock properties, due mainly to material discontinuity and the pressure of accumulated moisture in the cracks. For example, the initial nonlinearity in the elastic behavior of rock has been shown to be due to the existing microcracks (38-40).

Compressive strength of rocks is observed to decrease with increasing moisture content. Although not completely understood, this weakening effect is believed to result from the internal loading caused by pore pressure. Apart from this weakening effect, cracks act as stress raisers and have a very significant effect on fracture propagation.

As the equations of thermoelasticity are based on the theory of continuum, crack effects are probably the most difficult to study. However, for comparatively nonporous, hard rocks, cracks occupy less

than 1% of total volume as compared to 10-20% for highly porous rocks like sandstone and limestone (42). Hence, for hard rocks which possess a very low apparent porosity, the microcrack effects can be neglected.

4. Temperature Effects

Even though application of heat as a technique to fracture rocks has been used since antiquity, little was known about the mechanisms involved. However, in recent years, a large amount of effort has been put forth on the part of numerous researchers to investigate the mechanisms responsible for thermal fragmentation of rock (4, 14, 43-47). Heating devices being considered include such modern techniques as high frequency electric heating, induction and microwave heating, electric arcs, infra-red rays, electron beam, lasers, and plasma jets. Although parameters such as the heat transfer efficiency, energy input rate, and fracture time vary considerably with the mode of heating, the fracture mechanism involved remains unchanged.

As opposed to the mechanical fragmentation mode, the thermal fragmentation mechanism depends on the following:

i. Variation of physical properties with temperature,

ii. Thermal weakening effects as a result of spallation, intergranular crack growth, chemical changes, and expansion of entrapped gases and moisture.

a. Thermoelastic Properties

Properties of importance in the thermal fragmentation analysis of rocks include thermal conductivity, diffusivity, coefficient of thermal expansion, modulus of elasticity, and Poisson's ratio. For

most rocks, these properties are highly temperature dependent. This is to be expected since the properties of different rock constituting minerals exhibit varying degrees of temperature dependency. Formulating the closed form thermoelasticity equations and their solution for materials with temperature dependent properties is an extremely difficult task. However, using numerical finite element methods, these effects can be studied without a great amount of difficulty.

Thermal conductivity of most igneous rocks decreases with increasing temperature. Figure 11 shows the variation of thermal conductivity for some typical igneous rocks as obtained by Birch and Clark (48).

Diffusivity, in general, is obtained mathematically from the values of conductivity, specific heat, and density. Most hard, non-porous igneous rocks show little variation in density with temperature.

Mean value of specific heat over the temperature range from $25^{o}C$ to $625^{o}C$ was obtained by Geller, et al, (25). Only a small variation was observed among the specific heats of fourteen rock types tested and the values ranged from approximately 0.23 to 0.25 cal/gm-^{o}C. However, no investigations were made to study the variations in specific heat with temperature.

Temperature dependency of specific heats for six hard rock types was later investigated by Lindroth and Krawza (49). Tests were conducted at temperatures up to $1000^{o}C$. According to this study, temperature dependence of specific heat is strongly influenced by the percentage of quartz content. Results of this study are shown in

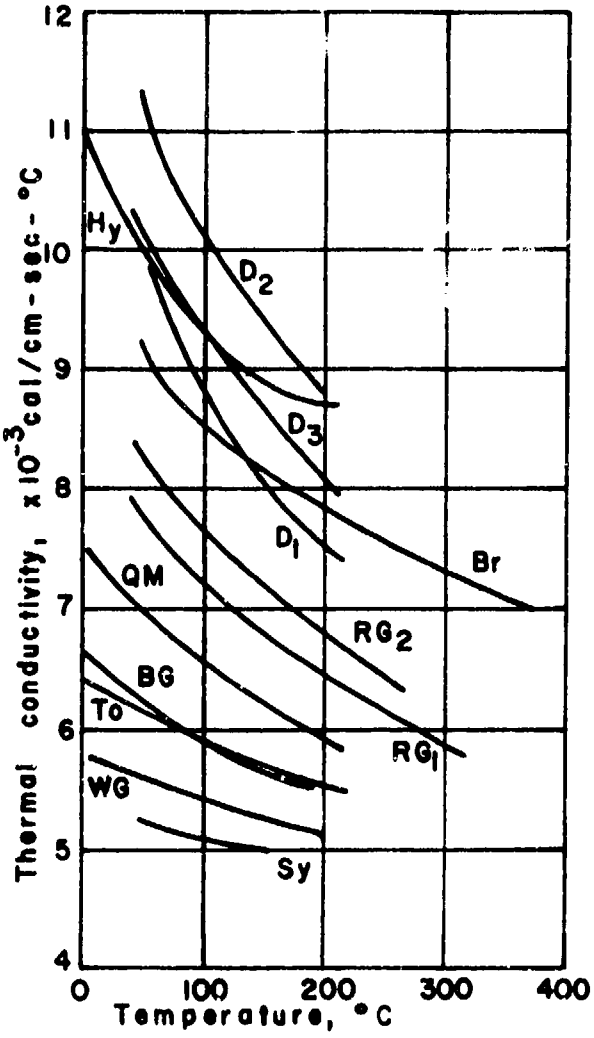

Sy	Syenite, Ontario	RG	Rockport Granite
WG	Westerly Granite	Br	Bronzitite
To	Tonalite, Calif.	Hy	Hypersthenite
BG	Barre Granite	D	Dunite
QM	Quartz Monzonite, Calif.		

Figure 11. Thermal Conductivity of Holocrystalline Rocks (48)

Figure 12 . The break in these curves occurs as a result of a phase change of quartz at approximately 573°C. For rocks containing less than 5% quartz, this break occurs at higher temperatures.

Similar discontinuities can be observed in curves shown in Figure 13, which shows the plot of coefficient of thermal expansion for hard crystalline bodies as a function of temperature. These are part of the results obtained by the Canadian Mines Branch of the Department of Mines and Mineral Surveys which conducted experiments on 37 rock types to determine the variation of linear thermal expansion with temperature (25). Studies on fusion were also performed. Fusion temperatures of 45 rock types were obtained; fusion temperatures for hard crystalline rocks were observed to lie in the range from 1150°C to 1300°C.

Studies conducted on the effect of temperature on elastic properties of rocks indicate that for hard, nonspallable rocks, both Young's modulus and Poisson's ratio show a marked decrease in the vicinity of the fusion temperature. For spallable rocks, however, the upper temperature limit is restricted by the alpha to beta phase transition of quartz, and above this temperature range, only small variations in elastic properties are observed (50-52).

b. Fracture Mechanisms

As opposed to the well defined properties involved in both the temperature and stress analyses, the fracture phenomenon depends on a number of mechanisms for which the variations with temperature have not been described in tabular or graphic form. Little is known about the interactions of various mechanisms involved. Nevertheless, it is

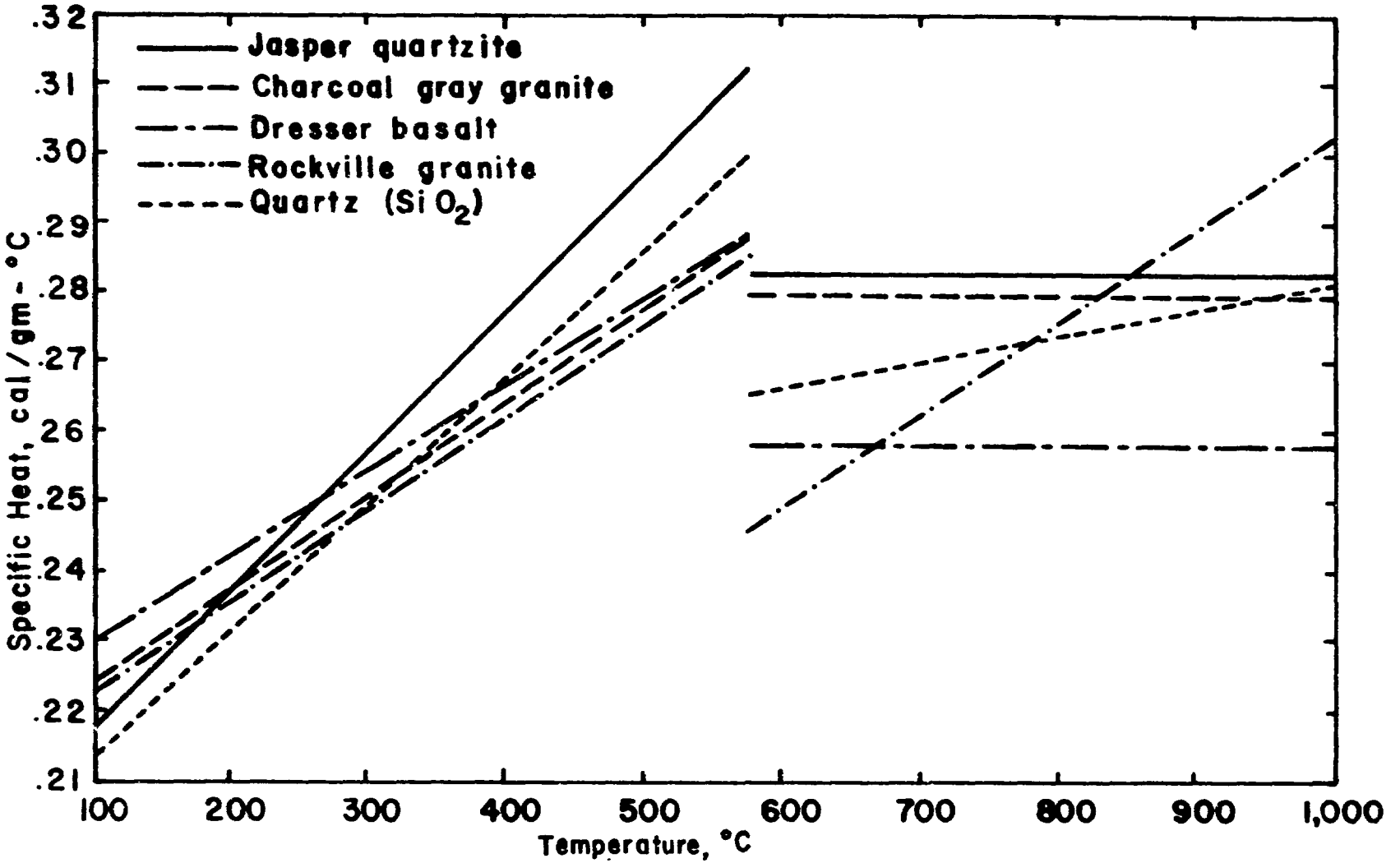

Figure 12. Specific Heat Values of High - Si O_2 Rock Types (49)

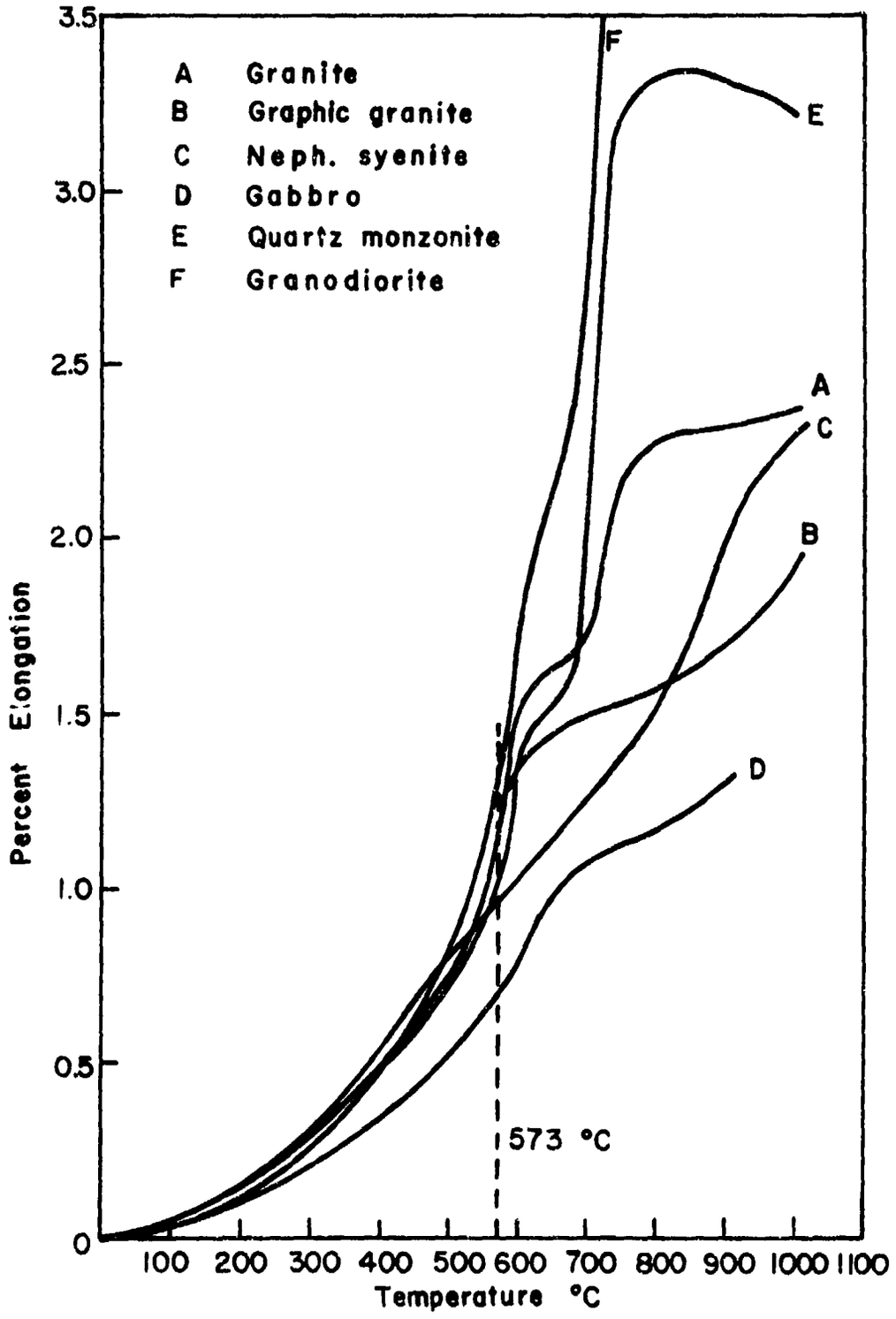

Figure 13. Average Linear Expansion of Igneous Rocks (25)

well established that temperature has definite weakening effects on rock strength, and the mechanisms responsible include, primarily, spallation, intergranular crack growth, chemical changes, and gas and water pocket expansion.

The relative importance of each of these weakening factors depends mainly on the nature of rock; porosity, average grain size, microcracks, and mineral constituents. Except for spallation, relatively little information is available on temperature effects on other mechanisms involved in fracture, mainly due to their inseparation.

The term "spallation" refers to a progressive failure of rock in the form of chips caused by thermal stress. The basic mechanism involved in formation of a spall depends on a sudden increase in the thermal expansion of quartz due to its phase transformation at approximately $573^{o}C$. Although it is well established that a certain percentage of quartz and its phase transition are essential to the inducement of spalling, review of various research efforts on thermal spalling reveals that little agreement exists as to the exact cause of the phenomenon (25, 33, 47, 53-55).

According to Gray (56), spalling can be controlled by proper choice of heating rate. For high heating rates which induce surface melting, spalling effects become trivial. Studies performed by Moavenzadeh, et al, (46) indicate that for igneous rocks complicated crack growth mechanisms have little or no effect on fracture compared to those due to the thermal stress field. Thus, the fracture of rock can be predicted with reasonable accuracy from the knowledge of the stress field alone.

C. Fracture Theories

As discussed above, in thermally induced rock fragmentation studies, the thermal stress field can be regarded as the single major factor responsible for rock failure. Numerous theories have been proposed over the years to relate the stress field to the brittle failure of materials. Of the various theories, the Griffith theory, in its different modified forms, has been the most widely accepted in the field of rock mechanics.

1. Griffith Theory

Griffith's theory evolved through his study of the problem of the tensile strength of glass being much lower than theoretically expected (57). He suggested that the low tensile strength was due to failure caused by stress concentrations at the tips of minute internal and surface flaws which have come to be known as Griffith cracks. In formulating this theory, Griffith assumed the material to be isotropic, homogeneous continuum containing randomly oriented sharp ended elliptical cracks. The mathematical condition for the initiation of a macro-crack was derived based on the energy approach which states that the work done by externally applied forces is equal to the sum of internal strain energy and the surface energy associated with the rupturing of atomic bonds when cracks are formed.

Specific energy is a difficult quantity to evaluate through direct measurements. Hence, the fracture criterion is expressed mathematically in terms of principal stress values. If compressive stresses are taken as negative, the conditions of fracture initiation are given by the following equations.

If

$$3\sigma_1 + \sigma_3 > 0 \tag{5.1a}$$

fracture initiation occurs when

$$\sigma_1 = \sigma_t \quad ; \tag{5.1b}$$

if

$$3\sigma_1 + \sigma_3 < 0, \tag{5.2a}$$

the condition of fracture initiation is given by

$$(\sigma_1 - \sigma_3)^2 + 8\sigma_t(\sigma_1 + \sigma_3) = 0 \ . \tag{5.2b}$$

In these equations

σ_1 = major principal stress,

σ_3 = minor principal stress, and

σ_t = uniaxial tensile strength of the material.

For failure governed by Equation 5.1a , the microscopic crack begins to propagate in its own plane in a direction perpendicular to that of the major principal stress. For failure conditions given by Equation 5.2a , however, the crack begins to extend in a plane at an angle θ from the minor principal stress axis, given by

$$\cos 2\theta = -1/2 \, \frac{\sigma_1 - \sigma_3}{\sigma_1 + \sigma_3} \tag{5.3}$$

It should be noted that the fracture criterion given by Equations 5.1a and 5.2a was developed for a biaxial stress state.

Sack (58) extended Griffith's theory to three dimensions by considering a penny-shaped crack under a triaxial stress state, and concluded that the fracture initiates as a result of growth of cracks that are parallel to the intermediate principal stress direction. Thus, the intermediate principal direction is the most critical crack orientation. However, the magnitude of this principal stress component has no appreciable influence on the crack growth and the Griffith biaxial fracture criterion given by Equations 5.1a 5.3 can be applied to triaxial stress conditions as well. This result has experimentally been verified by Brace (59) for igneous rocks such as granite.

2. McClintock-Walsh Modification

Experimental verification of Griffith's criterion, however, brought to attention some serious flaws in Equations 5.2a and 5.3. Under uniaxial compression ($\sigma_1=0$, $\sigma_3 < 0$), the formula loses its meaning as it implies that the compressive strength of the material is equal to eight times its tensile strength. For most rocks, however, this is not true as the compressive strength is much higher than eight times that in uniaxial tension. Also, under uniaxial compression, according to Equation 5.3 , the most critical cracks would be those at 45^{o} to the stress direction. However, experimental studies by Brace (59) and Bieniawski (60) show that under a compressive stress state, cracks propagate out of their plane in the direction of the major principal compressive stress. These discrepancies required some modification of the Griffith theory for rock failure when one or two of the principal stress components are compressive.

Experimental studies by Brace (59) and Bieniawski (60) served to give an insight into the more complex mechanism involved in rock failure. Based on their experiments, they concluded that when compressive stresses are present, pre-existing Griffith cracks close before the tensile stress at the crack tip reaches the critical value for fracture initiation. To open these closed cracks, higher stresses are required in order to overcome the shear resistance resulting from the interlocking of irregular crack faces. The concept of crack closure was also able to explain the initial nonlinearity in the stress-strain curve of rocks.

McClintock and Walsh (61) were the first to modify the Griffith criterion with consideration given to the effects of crack closure. The fracture criterion in mathematical form given by McClintock and Walsh is as follows:

If

$$\sigma_n = \frac{1}{2}\ (\sigma_1+\sigma_3) + (\sigma_1-\sigma_3)\cos 2\psi_c < 0\ , \qquad (5.4a)$$

fracture initiation occurs when

$$\sigma_3 = \sigma_1\ \frac{\sqrt{1+\mu^2}+\mu}{\sqrt{1+\mu^2}-\mu}\ + \sigma_c \qquad (5.4b)$$

where

σ_n is the normal stress acting across the crack faces causing the cracks to close,

σ_c is the uniaxial compressive strength of the material,

μ is the internal coefficient of friction between the crack faces, and

σ_1, σ_3 are the major and minor principal stress components, as before.

For this condition of crack initiation, crack propagation direction is given by

$$\tan 2\psi_c = 1/\mu \qquad (5.5)$$

where ψ_c is measured from the minor principal stress axis.

Comparison of Equations 5.2 and 5.4 shows that the McClintock-Walsh criterion is based on the actual compressive strength of the material and also takes into account the effect of crack closure. Also, note that the original Griffith criterion given by Equations 5.1- 5.3 is valid whenever $\sigma_n > 0$, so that the normal stress acting across the crack does not cause crack closure.

It should be realized that both Griffith and McClintock-Walsh modified Griffith criteria refer to fracture initiation only, which is not the same as fracture (62). They do not consider factors such as the energy of plastic deformation; orientation, density, and interactions of existing microcracks, difference between the stress levels causing fracture initiation and those causing the ultimate strength failure; crack propagation velocity and other dynamic effects. Nevertheless, experimental results obtained by Hoek and Bieniawski (63) for a wide variety of rocks show a remarkable agreement with those predicted theoretically by the Griffith and McClintock-Walsh modified Griffith criteria. They, however, replaced the internal crack friction coefficient, μ, by fracture surface coefficient of friction, μ_f, which was obtained experimentally for each rock type tested. For igneous rocks, the value of μ_f has been found to lie between 1.0 and 1.5 (39, 59)

D. Properties Used in Analytical Studies

Even though field tests have been conducted on Missouri red granite, for the theoretical analysis, Dresser basalt was found to

be more suitable as it contains very little or no quartz. Also, the thermal and elastic properties for basalt as a function of temperature were readily available (14, 47, 58, 64).

1. Temperature Analysis

The available finite element temperature code is not capable of handling temperature dependent thermal properties. However, for Dresser basalt, the thermal conductivity and diffusivity show only small variations with temperature, as shown in Figures 14 and 15. The upper limit of 700°C for the temperature range was chosen in view of the fact that the modulus of elasticity for temperatures above 700°C becomes very small, as seen from Table II . The effect of this low value of Young's modulus is that, regardless of the steepness of temperature gradients, in the region where temperatures are higher than 700°C, the stresses will be very small. In other words, the upper limit, 700°C, of the temperature range for curves shown in Figures 14 and 15 is taken as the temperature at which the rock becomes plastic. Hence, the nonlinearities in the thermal properties will have a very small effect, if any, on the stresses which contribute to fracture.

In order to simplify the analysis, the assumption of temperature independent properties has been employed in most of the rock related investigations. Under this assumption, properties corresponding to the average temperature of the material are usually selected. This procedure has been shown to yield analytical results well within the range of experimental errors (45, 65-68).

For this analysis, average values of thermal conductivity and diffusivity were obtained from Figures 14 and 15. The input properties for the finite element code, however, are the conductivity, specific heat and specific gravity. Even though the specific heat values as a

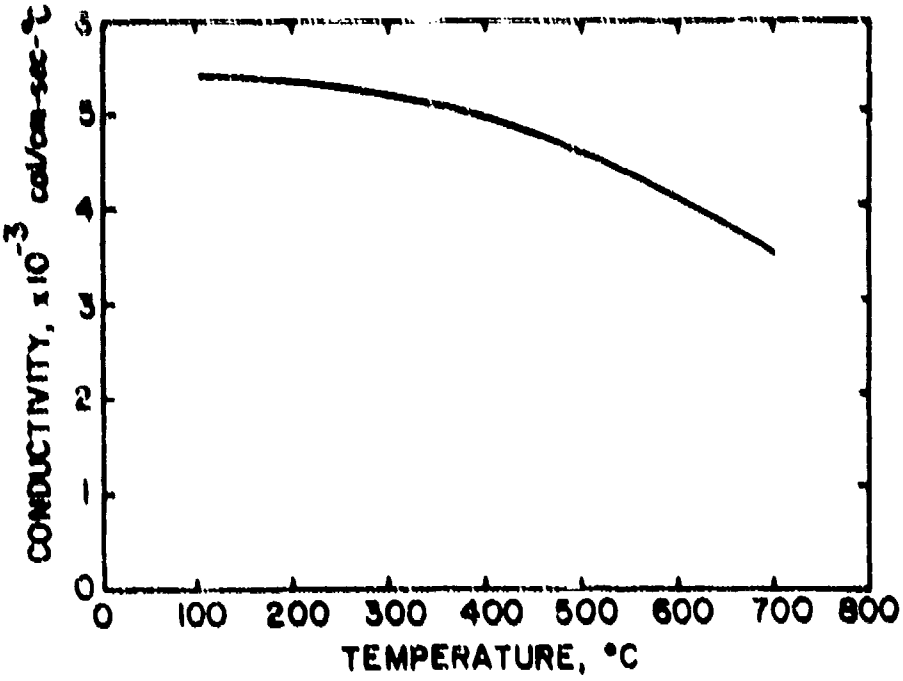

Figure 14. Variation of Conductivity of Dresser Basalt with Temperature (47)

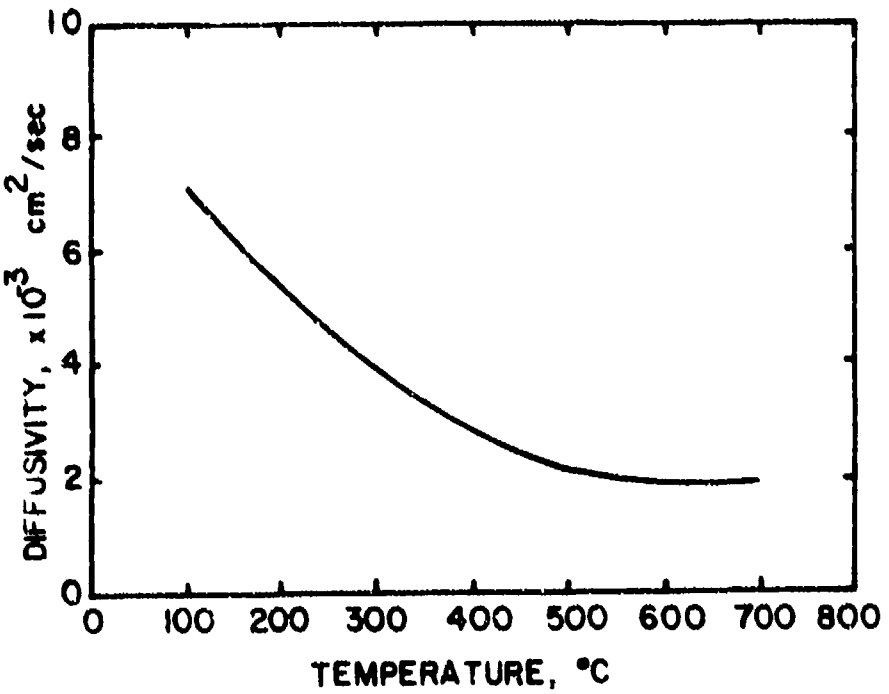

Figure 15. Variation of Diffusivity of Dresser Basalt with Temperature (47)

function of temperature were readily available for basalt (49), the following procedure was found to be more efficient. The specific gravity of the material was assumed to be constant, equal to that at room temperature. The average value of the specific heat was then obtained from the average values of the thermal conductivity and the diffusivity using the well-known relationship (69)

$$\kappa = \frac{k}{\rho c} \quad (5.6)$$

where

κ = average value of thermal diffusivity

k = average value of thermal conductivity

ρ = the specific gravity of material, and

c = the average value of the specific heat.

Values of the properties used for the temperature analysis are tabulated below.

TABLE 6

Property Data Used in Temperature Analysis of Dresser Basalt (47, 64, 70)

Thermal conductivity, k, cal/cm-sec - ^{o}C	0.0042
Specific heat, c, cal/gm - ^{o}C	0.293
Density, ρ, gm/cm^3	2.97
Melt Temperature, T_m	1250^{o}C
Surface convection coefficient, h, cal/cm^2 - sec - ^{o}C	0.00021

*For solids, no distinction is generally made between specific heat at constant pressure, c_p, and that at constant volume, c_v. Nevertheless, it shouldbe noted that in this equation c refers to c_p.

2. Stress Analysis

Unlike the temperature analysis, the stress analysis was performed using temperature dependent material properties. This was necessary due to the fact that the variations of the stress related properties with temperature greatly influence, as explained later on, the resulting stress field and consequently, the fracture predictions.

The stress related properties include the coefficient of thermal expansion, α, modulus of elasticity (Young's modulus), E, and the Poisson's ratio, ν. Table 7 gives the values of these properties used in the stress analysis.

TABLE 7

Property Data Used in Stress Analysis of

Dresser Basalt (4, 14, 52)

Temperature, T ^{o}C	Young's Modulus E, 10^6 psi	Poisson's Ratio ν	Coeff. of Thermal Expansion, α, $10^{-6}/^{o}C$
100	14.5	0.24	2.6
162	14.1	0.23	6.0
287	13.5	0.21	8.2
412	12.6	0.19	10.2
537	10.7	0.145	11.2
610	8.3	0.105	11.7
630	6.4	0.09	11.8
650	4.6	0.07	11.9
670	2.8	0.05	12.0
690	0.9	0.02	12.0

As was mentioned earlier, the rock is assumed to become plastic at 700°C as its elastic resistance for higher temperatures becomes very small.

In order to explain the strong influence of the stress related properties on the probability of fracture, the concept of fragmentation potential was introduced by Thirumalai (14). This concept is based on the observation that the thermal load vector is proportional to the factor

$$F = \frac{E \alpha T}{1 - \nu} \tag{5.7}$$

and thus, in the absence of mechanical loading, the resulting stress field depends directly on F (71).

In the nondimensional form, Thirumalai defines the fragmentation potential as

$$F^* = \frac{F}{F_{max}} \tag{5.8}$$

where F_{max} denotes the maximum value of F.

Figure 16 shows the variation of F^* with temperature for Dresser basalt. If the properties were assumed to be constant, the variation in F^* would have been linear as shown by the broken line. The difference between the ordinates for the solid and the broken line is an indication of the influence of the stress field of the nonlinear, temperature dependent properties as given in Table 7. Another method of predicting whether or not the temperature dependence of the thermoelastic properties will have a significant effect on the stress field is through the use of what will be referred to as the nonlinearity coefficient. This coefficient will be defined as

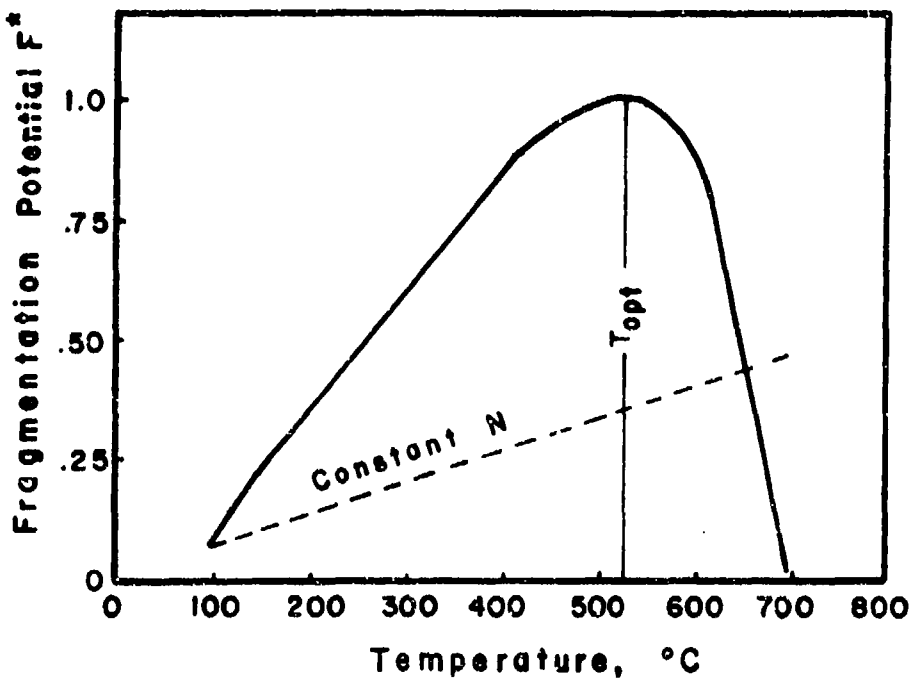

Figure 16. Fragmentation Potential of Dresser Basalt at Elevated Temperatures (14)

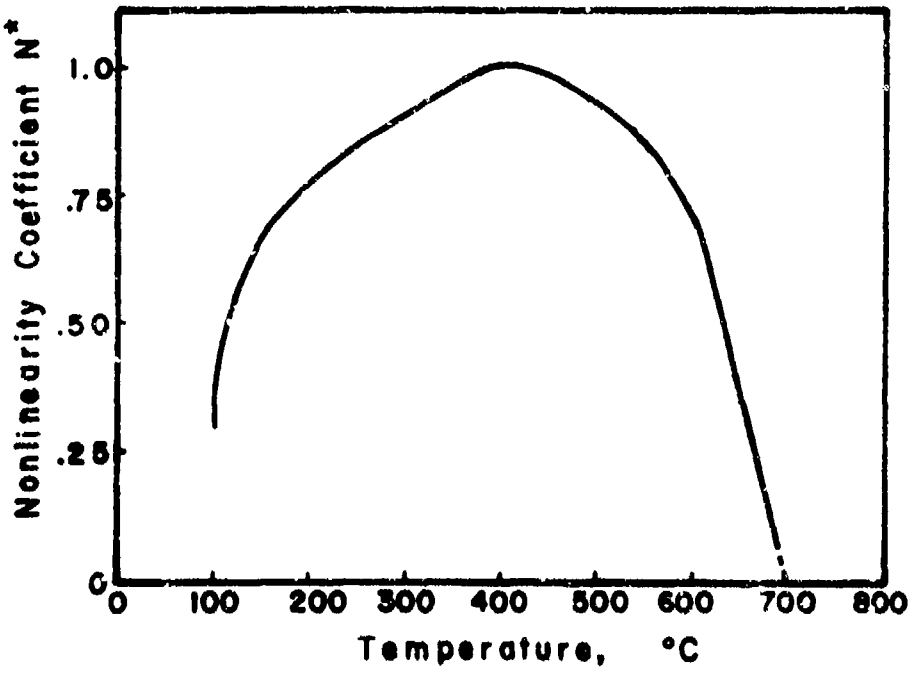

Figure 17. Nonlinearity Coefficient of Dresser Basalt at Elevated Temperatures

$$N^* = \frac{N}{N_{max}} \tag{5.9}$$

where

$$N = \frac{E\alpha}{1 - \nu} \quad , \tag{5.10}$$

and N_{max} denotes the maximum value of N.

The usefulness of this definition lies in the fact that, for a homogeneous solid under pure thermal loading it is the variation of N^* which influences the stress field rather than the individual variations of each of the thermoelastic properties. Thus, for materials exhibiting thermoelastic properties, it is possible to obtain quite accurate stress solutions provided the nonlinearity coefficient, N^*, remains fairly constant.

Variation of the nonlinearity coefficient for basalt is shown in Figure 17. The highly nonlinear nature of this curve indicates that for a reasonably accurate solution, the thermoelastic properties should be allowed to vary with temperature in the stress analysis.

3. Fracture Predictions

Fracture analysis is performed based on the Griffith and McClintock-Walsh modified Griffith criteria. Once the principal stresses have been obtained from the stress analysis, the following properties are required in order to predict the initiation of fracture: uniaxial tensile strength, σ_t, uniaxial compressive strength, σ_c, and the fracture surface coefficient of friction, μ_f, of the material.

Confining pressure is known to increase the strength of the rock. This effect, however, is neglected here since this investigation is concerned with rocks a few feet below the surface of the earth (41).

Temperature, on the other hand, has a weakening effect on the rock strength (41). This, too, is neglected in view of the localized nature of heating and the observation that the major portion of thermally fractured rock volume experiences only a small average increase in temperature.

Table 8 gives the properties used in the fracture analysis.

TABLE 8

Properties of Basalt used for Fracture Predictions (39, 59, 63, 72)

Uniaxial tensile strength, σ_t	2,195 psi
Uniaxial compressive strength, σ_c	42,399 psi
Fracture surface coefficient of friction, μ_f	0.9

Chapter VI

MATHEMATICAL FORMULATION AND METHOD OF ANALYSIS

The three-dimensional thermoelasticity problem and its reduction to three two-dimensional mathematical models were considered in Chapter VI. In Chapter V, hard rock characteristics were discussed and simplifying assumptions introduced for theoretical studies. In this chapter, analytical aspects such as mathematical formulation of equations and methods of their solution are considered.

The thermal fragmentation analysis considered here involves relatively low stress levels and very low strain rates as compared to conventional explosive and nuclear blasting techniques. Under these conditions, the effects of thermoelastic coupling are negligible. Thermal inertia effects are also neglected as the time rate of temperature change is very slow. Thus, the general problem can be formulated within the framework of the linear, uncoupled theory of thermoelasticity. For this formulation, the problem becomes explicit, that solutions can be obtained in two distinct steps; solution to a well-defined heat conduction problem, and solution of the stress problem with known temperature distribution.(68, 71).

A. Heat Conduction Problem

The geometries for the slot and the hole models considered in this investigation are shown in Figure 18a and b. Parameters used to describe these geometries are as follows:

c = center-to-center distance between the hole (or slot) axes,
d = hole diameter (or slot width),
A = total hole (or slot) depth,
a = melt depth,
L = fracture propagation length.

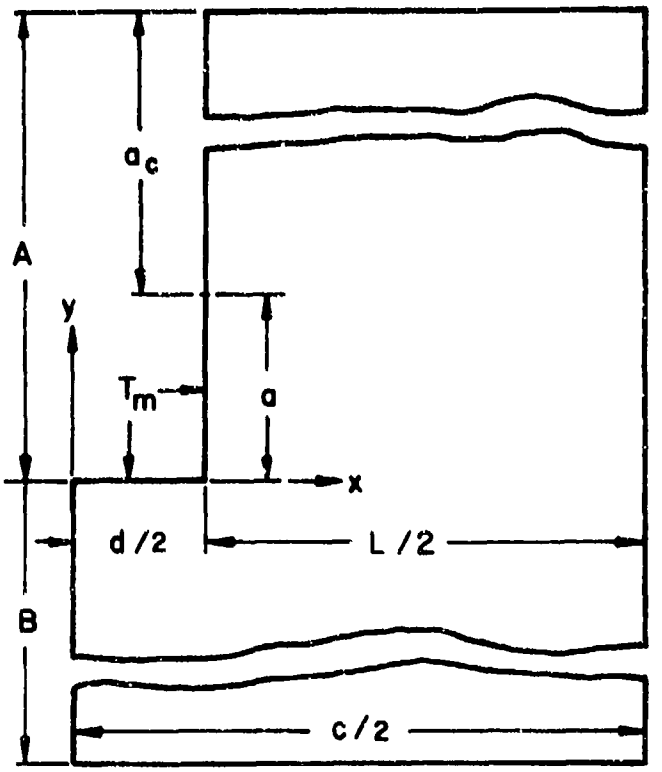

(a) SLOT MODEL

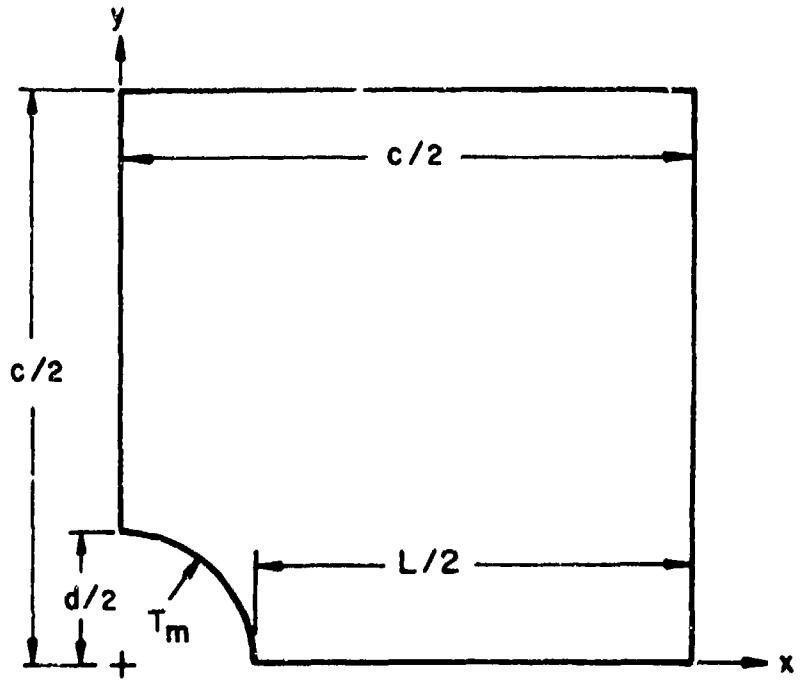

(b) HOLE MODEL

Figure 18. Nomenclature for Plane Models.

In the subsequent discussion, the remaining hole or slot depth, A-a, is referred to as convection depth, a_c. Parameter B is chosen arbitrarily but large enough so as to satisfy both the traction free and ambient temperature conditions on boundary y = -B of the slot model.

In the absence of internal heat generation, the governing equation of two-dimensional heat conduction for a homogeneous, isotropic solid with constant properties is given by

$$k\left(\frac{\partial^2 T}{\partial x^2}+\frac{\partial^2 T}{\partial y^2}\right)=\rho c\,\frac{\partial T}{\partial t} \tag{6.1}$$

where

k = thermal conductivity

ρ = density

c = specific heat, and

T = T(x,y,t) denotes the temperature at point (x,y) at time t

For notational convenience, the ambient temperature is assumed to be zero so that the initial condition becomes

$$T(x,y,0)=0 \tag{6.2}$$

The boundary conditions for the slot model are:

$$\frac{\partial T}{\partial x}=0\ , \qquad \begin{cases} x=0\ ,\ y<0 \\ x=c/2 \end{cases} \tag{6.3}$$

$$\frac{\partial T}{\partial x}+hT=0, \qquad x=d/2,\ y>a \tag{6.4}$$

$$\frac{\partial T}{\partial y}+hT=0, \qquad y=A \tag{6.5}$$

$$T=T_m, \qquad \begin{cases} 0\le x\le d/2,\ y=0 \\ x=d/2,\ 0\le y\le a \end{cases} \tag{6.6}$$

$$T=0, \qquad y=-B. \tag{6.7}$$

The boundary conditions for the hole model are:

$$\frac{\partial T}{\partial x} = 0, \qquad \begin{cases} x = 0, \; y < d/2 \\ x = c/2 \end{cases} \tag{6.8}$$

$$\frac{\partial T}{\partial y} = 0, \qquad \begin{cases} x > d/2, \; y = 0 \\ y = c/2 \end{cases} \tag{6.9}$$

$$T = T_m, \qquad x^2 + y^2 = d^2/4. \tag{6.10}$$

In the above equations, T_m denotes the melt temperature of the material and h is the coefficient of convection heat transfer.

Solution Techniques

A great deal of work has been done on solving problems of unsteady state or transient heat conduction (69, 73-76). Analytical tools include such classical techniques as separation of variables, integram transforms, Green's functions and those based on variational principles. The integral methods introduced by Goodman (77) and the Galerkin's variational method (78) are widely used to obtain approximate closed form solutions. Each method has some advantages over the others; however, each has its own limitations and the choice of the method to solve a particular problem depends largely on the nature of the problem itself.

With the advent of high-speed, large scale digital computers, the approximate numerical finite difference and finite element methods have become more popular due to their ease of application and capability of handling today's highly nonlinear, complex problems.

Even though the temperature problem considered in this investigation is linear in that constant average thermal properties are used,

the boundary conditions are quite complex. Also, for the stress analysis part, properties are allowed to vary with temperature which makes obtaining a closed form solution extremely difficult. Thus, closed form temperature solutions will be of little advantage and since a two-dimensional code was readily available, the numerical finite element solution was chosen.

Application of the finite element method for the solution of problems governed by a general quasi-harmonic differential equation is discussed by Zienkiewicz(79). The well-known Laplace and Poisson equations are particular cases of the general quasi-harmonic equation and govern such frequently encountered problems as those of heat conduction, seepage flow, distribution of electromagnetic potential, and torsion and bending of prismatic members. The finite element conduction code used in this analysis was developed based on the formulation given by Wilson and Nickell (80). Details of this code are proprietary in nature and hence are not given here.

B. Stress Problem

The problem of linear, uncoupled thermoelasticity involves fifteen equations with fifteen unknowns; six stress components, six strain components, and three displacement components. The field equations in index notation are as follows:

Equilibrium equations:

$$\sigma_{ij,j} + f_i = 0 \tag{6.11}$$

Stress-strain relations:

$$\sigma_{ij} = \delta_{ij}\lambda\varepsilon_{kk} + 2\mu\varepsilon_{ij} - \delta_{ij}(3\lambda+2\mu)\alpha T \tag{6.12}$$

Strain-displacement relations:

$$\varepsilon_{ij} = 1/2(u_{i,j}+u_{j,i}) \tag{6.13}$$

where

σ_{ij} = the stress tensor

ϵ_{ij} = the strain tensor

u_i = the displacement vector

f_i = the body force vector

δ_{ij} = the Kronecker delta

α = the coefficient of thermal expansion, and

λ, μ = Lame's constants.

It should be noted that the stress tensor, $\left.\begin{matrix}\sigma_{ij} = \sigma_{ji} \\ \epsilon_{ij} = \epsilon_{ji}\end{matrix}\right\}$ $i \neq j$.

Also, since six strain components are expressed in terms of only three displacement components, the following compatibility relations must be satisfied:

$$\gamma_{prm}\gamma_{qsn}\epsilon_{rs,\,mn} = 0 \tag{6.14}$$

where

γ_{ijk} is the alternating tensor.

Plane Theory of Thermoelasticity

For simply connected regions, in the absence of body forces, the general formulation given above simplifies for the plane theory of thermoelasticity to the solution of the biharmonic equation

$$\nabla^2\nabla^2 F + cE\nabla^2(\alpha T) = 0 \tag{6.15}$$

where

$\nabla^2 = \frac{\partial^2}{\partial x^2} + \frac{\partial^2}{\partial y^2}$, the Laplacian

$c = \begin{cases} 1, & \text{plane stress} \\ \frac{1}{1-\nu}, & \text{plane strain} \end{cases}$

ν = Poisson's ratio

E = Young's modulus, and

α = coefficient of thermal expansion

Once the Airy stress function F is determined, the stresses can be obtained from the following relations:

$$\sigma_x = \frac{\partial^2 F}{\partial y^2} \tag{6.16}$$

$$\sigma_y = \frac{\partial^2 F}{\partial x^2} \tag{6.17}$$

$$\tau_{xy} = -\frac{\partial^2 F}{\partial x \partial y} \tag{6.18}$$

It is important to note that the solution to the biharmonic equation is to be obtained subject to the boundary conditions. Since both the slot and the hole models considered in this investigation involve mixed boundary conditions, that is, specified tractions as well as specified displacements, solution of the biharmonic equation in itself becomes quite complicated. Further complications are introduced due to the temperature variations of the thermoelastic properties, E, ν, and α. No attempt was therefore made to obtain closed form solutions. Rather, approximate numerical solutions were sought using the finite element method which due to its generality of application provides a powerful tool for the solution of complex structural problems with arbitrary geometries and nonlinear material properties.

Numerous finite element codes have been developed in recent years for the solution of elasto-plastic and thermal stress problems. However, no suitable code was available for the transient thermoelastic stress analysis. The available codes for thermoelastic analysis are quasi-static in nature and can handle stationary temperature distributions only. This means that for a given problem geometry, the temperature distribution at each time step must be run separately through the stress program to determine the stress distribution as a function of

time. This procedure becomes highly inefficient as the program recomputes the entire stiffness matrix and load vector for each of the sets of temperature data.

A new finite element code was, therefore, developed for the transient thermal stress analysis. This code is identified by the acronym "TRATSA" (TRAnsient Thermal Stress Analysis) and can be used for plane or axisymmetric bodies with temperature-dependent material properties. The code is based on theoretical formulations given by Zienkiewicz (79) and Jones and Crose (81). These formulations assume linear displacement between nodes, resulting in constant stress elements. Both triangular and quadrilateral elements can be used. The input instructions and the program listing are given in Reference 82.

C. Fracture Analysis

The fracture predictions made in this investigation are exploratory in nature and are based on the stress field which is obtained by assuming the material to remain a continuum. In practice, however, initiation of a crack will change the temperature field which, in turn, effects the stresses. Cracks also tend to relieve the stresses, but at the same time, they also act as stress raisers. A rigorous treatment of the problem would require progressive introduction of additional convection and traction free boundary conditions with the creation of new fracture surfaces.

If the propagation of a crack is to be followed, the numerical treatment of the thermoelasticity problem becomes coupled in the sense that once the crack initiation is predicted from the known stress field, one must go back and recompute the temperature distribution for the next time step allowing for the newly developed fracture surfaces.

For an extensive investigation such an approach becomes impracticable due to the amount of work involved in the reformulation of the problem at each time step and the resulting prohibitively large amount of machine time. Apart from this, for problems not involving dynamic fracture, there is little justification in using a progressive fracture approach as the crack propagation of nondynamic nature, in actual practice, is largely governed by the orientation of the pre-existing microcracks and the interactions between them; factors of which no theoretical knowledge is available.

The fracture predictions in this analysis are based on the Griffith and the McClintock-Walsh modified Griffith criteria. These fracture theories are themselves approximate as they are derived from an energy formulation and neglect the effects of stress concentrations and the interactions between the cracks. These theories, therefore, can at best be considered statistical in nature. This is evidenced by the results of Lauriello (68) and Bieniawski (60) who obtained "statistically" good correlations between the experimentally observed fracture fields and those predicted theoretically using the Griffith and the modified Griffith fracture criteria.

Fracture Propagation Studies

During the preliminary analysis, it was found that, predicting the initiation of a crack and following its propagation even under the assumption that the presence of a crack does not effect the temperature and stress fields, requires a rather large number of stress runs with very small time steps. Stress runs with large time steps, on the other hand, result in large fracture zones giving no indication whatsoever of the actual crack propagation path. This observation

necessitated some sort of approximate procedure that could serve as a compromise between the two extremes and would yield practically comprehensible propagation data.

A procedure was devised based on a concept referred to hereafter as the concept of fracture intensity level. With this concept, the crack can be predicted to lie within a small narrow band rather than a whole large fractured zone as obtained from the stresses using large time steps. The fracture intensity level is defined in terms of the stress magnitude in excess of that necessary for fracture. Thus, a fractured element, A, having a higher excess stress than some other fractured element, B, will be identified by a fracture intensity level higher than that of element B.

This procedure, of course, does not eliminate the trial and error method necessary in finding the solution associated with the complete fracture of the solid; that is, solution when fracture reaches a free surface. Once this solution is obtained, excess stresses associated with fractured elements are computed. The total range from minimum to maximum excess stress magnitude is divided into a number of intervals and labeled in terms of the fracture intensity levels. The computer code is written to plot the fractured elements together with their respective stress intensity levels. From the plotted output, it is possible to trace the approximate crack propagation path; with the crack initiating at the point of the highest stress intensity level and progressing in the direction of decreasing fracture levels.

D. Summary

The thermal fragmentation analysis is performed in three steps. The first step involves the temperature solutions obtained by using a finite element conduction code. Average thermal properties are used in this part of the analysis. The temperature results are then used as input into the finite element stress code TRATSA. Thermoelastic properties are allowed to vary with temperature for the stress analysis. Principal stresses are computed and read through the fracture code. Fracture predictions are based on the Griffith and the McClintock-Walsh modified Griffith criteria. The solid is assumed to remain a continuum and the effects of crack initiation on temperature and stress fields are neglected. The concept of fracture intensity level, based on the stress magnitude in excess of that required for fracture was introduced to obtain an approximation to the fracture propagation path.

Chapter VII

SLOT MODEL ANALYSES

As mentioned in Chapter IV, the slot model is obtained by passing a cutting plane along a series of holes and observing the geometry that is projected on the cutting plane. This model was designed for the parametric study of the fracture which occurs on a plane perpendicular to the hole axes passing approximately through the thermal inclusions. This fracture is parallel to the working face and makes possible the removal of a layer equal to the depth of the thermal inclusions. In the subsequent discussion this subsurface fracture, due to its orientation with respect to the working face, is referred to as the parallel fracture. The significance of the process parameters which are the hole diameter, hole depth, hole spacing and the depth of heating on the actual removal of the layer can be approximated by studying their influence on the parallel fracture. The slot model studies, therefore, are of primary importance.

In order to study the significant process parameters, twenty different slot models were analyzed. Effects of hole diameter and hole spacing were studied by using three different values of each; the combinations giving nine different fracture lengths. Effects of convection depth and melt depth were investigated using various combinations of these values for a given hole diameter and hole spacing. Parametric description of these models is given in Table 9 .

A. Grid Size Effects

Accuracy of the finite element solution depends largely on the size of the elements; the smaller the element size, the more accurate the solution. However, computer time increases with an increase in the number of elements. Hence, it is necessary to adjust the finite

TABLE 9

Parametric Description of Slot Models

Model	Hole Diam d,in.	Spacing c,in.	Fracture Length L = c-d	Melt Depth a,in.	Conv. Depth a_c = A-a
1A	1.0	4.0	3.0	0.5	1.5
1A-1				2.0	0.0
1A-2				2.0	2.0
1A-3				4.0	0.0
1B	1.0	8.0	7.0	0.5	3.0
1C	1.0	12.0	11.0	0.5	5.0
2A	2.0	4.0	2.0	0.5	1.0
2A-1				1.2	0.8
2A-2				0.5	0.1
2B	2.0	8.0	6.0	0.5	3.0
2B-1					0.1
2C	2.0	12.0	10.0	0.5	5.0
2C-1					3.0
2C-2					0.1
3A	1.5	4.0	2.5	0.5	1.5
3B		8.0	6.5		3.0
3C		12.0	10.5		5.0
11A	2.0	5.0	3.0	0.5	1.5
13B		8.5	6.5		3.0
13C		12.5	10.5		5.0

element grid so that acceptable solutions can be obtained economically. Fairly large elements can be used in the areas where low stresses are expected, whereas regions of high stress concentrations should be divided into very fine grids. Thus, the problem geometry and the boundary conditions should be given primary consideration in drawing the finite element grid. For thermal stress problems, the magnitude of the temperature gradient must also be taken into consideration as it greatly influences the stress field.

For the slot model analysis, effects of element size and time increment were investigated. A value of 0.2 seconds for the time increment for a typical grid shown in Figure 19 was found to yield quite accurate results. Size of the smallest elements used in this grid is 0.025 in. square.

B. Melt Depth Studies

The stress State in the elastic rock surrounding the heater and molten rock inclusion depends on the temperature field and mechanical constraints in the form of specified displacement boundary conditions. Due to the poor thermal conductivity of rocks, the resulting thermal gradients are very steep. This requires very small sized elements for a reasonably accurate analysis. It is necessary, therefore, to reduce the semi-infinite problem geometry to a finite region for numerical treatment.

The experimentally observed fractures occur in the vicinity of the slot base. This location for the secondary fractures is highly desirable from an economical viewpoint. Hole depths used in the field tests varied from 12.0 in. to about 30.0 in. and the thermal inclusions were observed to be in the range from 4.0 in. to 12.0 in. in length.

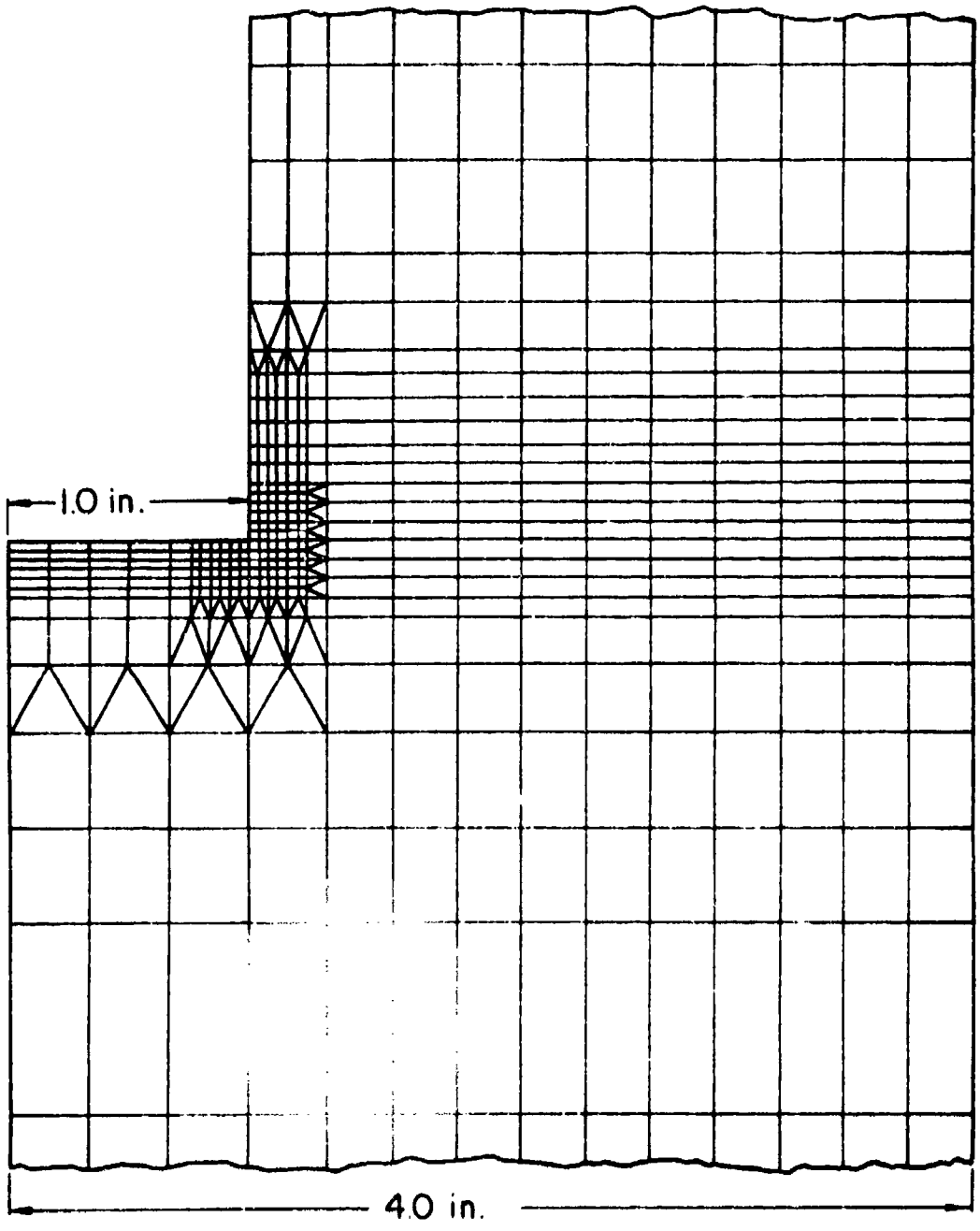

Figure 19. Typical Finite Element Grid for the Slot Model Analysis

These values were much too high to be used for the numerical finite element analysis. However, for a given geometry under identical mechanical constraints, the stress field in an area depends only on the temperature field in that area. Thus, it is possible to obtain a reasonably accurate stress field in the vicinity of the slot base by using small melt depths provided the temperature field in this area remains fairly constant for different melt depths.

Effects of different melt depths and convection depths on the temperature field in the vicinity of the slot base were investigated using models 1A-1, 1A-2, and 1A-3. Parametric description of these models is given in Table 9.

Results of these studies are plotted in Figures 20-25 which show the temperature plots for two different time values. Temperature contours are plotted in increments of 100°C except for the 50°C contour. The melt temperature used in the analysis was 1250°C. Comparison of these results show that the temperature field in the vicinity of the slot base does remain fairly constant for different combinations of melt depth and convection depth values. However, it should be realized that for the above statement to be true, there exists a lower limit on the value of the melt depth, a. A value of 0.5 in. was found to be sufficiently high in order to obtain an invariant temperature field in the immediate surrounding of the slot base. The subsequent analysis was, therefore, completed using a melt depth value of 0.5 in.

C. Convection Depth Studies

As seen from the results shown in Figures 20-25, the temperature distribution in the vicinity of the slot base is independent of the convection depth. However, for small melt depths, the stress field

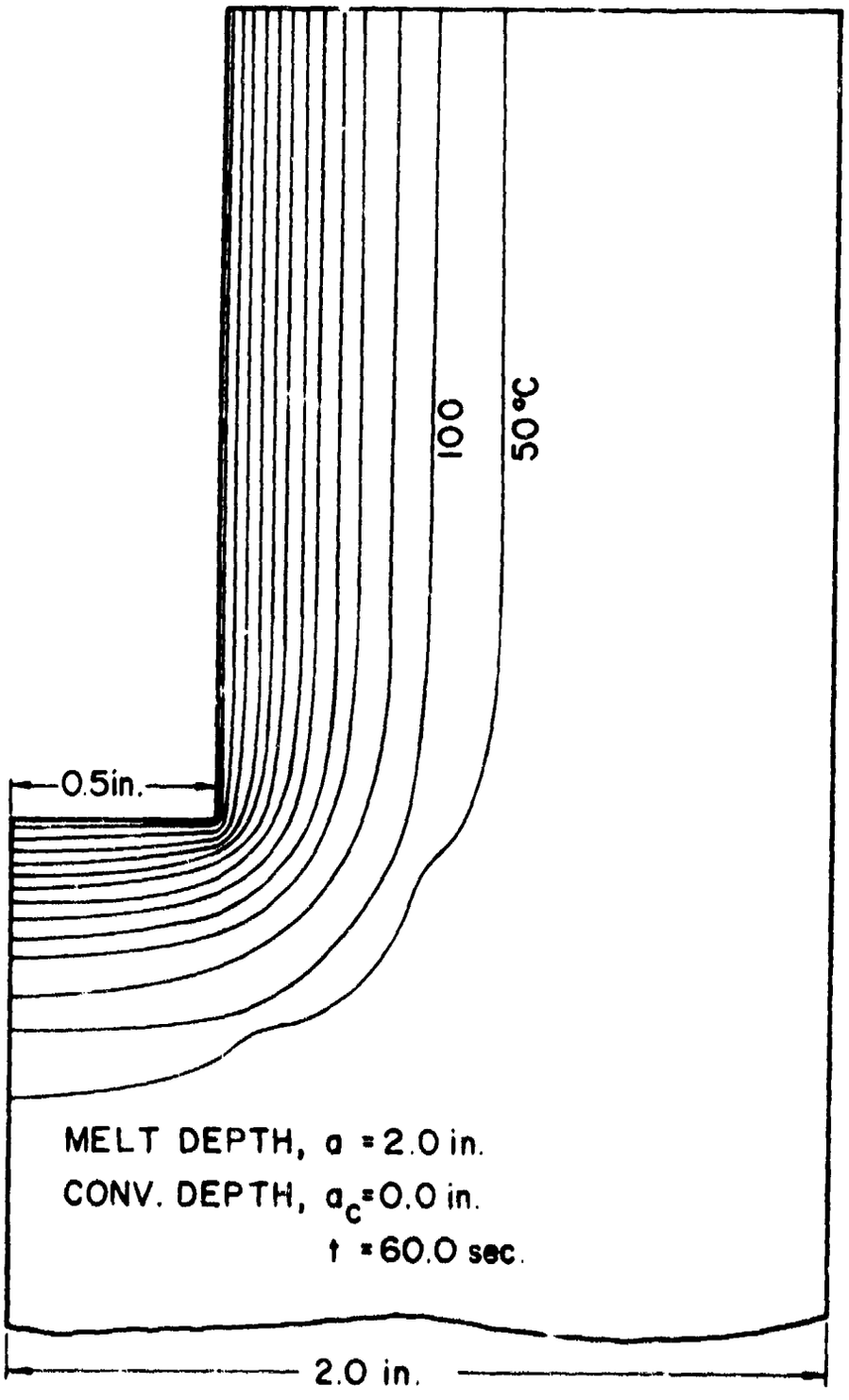

Figure 20. Temperature Distribution, Model A-1, t = 60 sec.

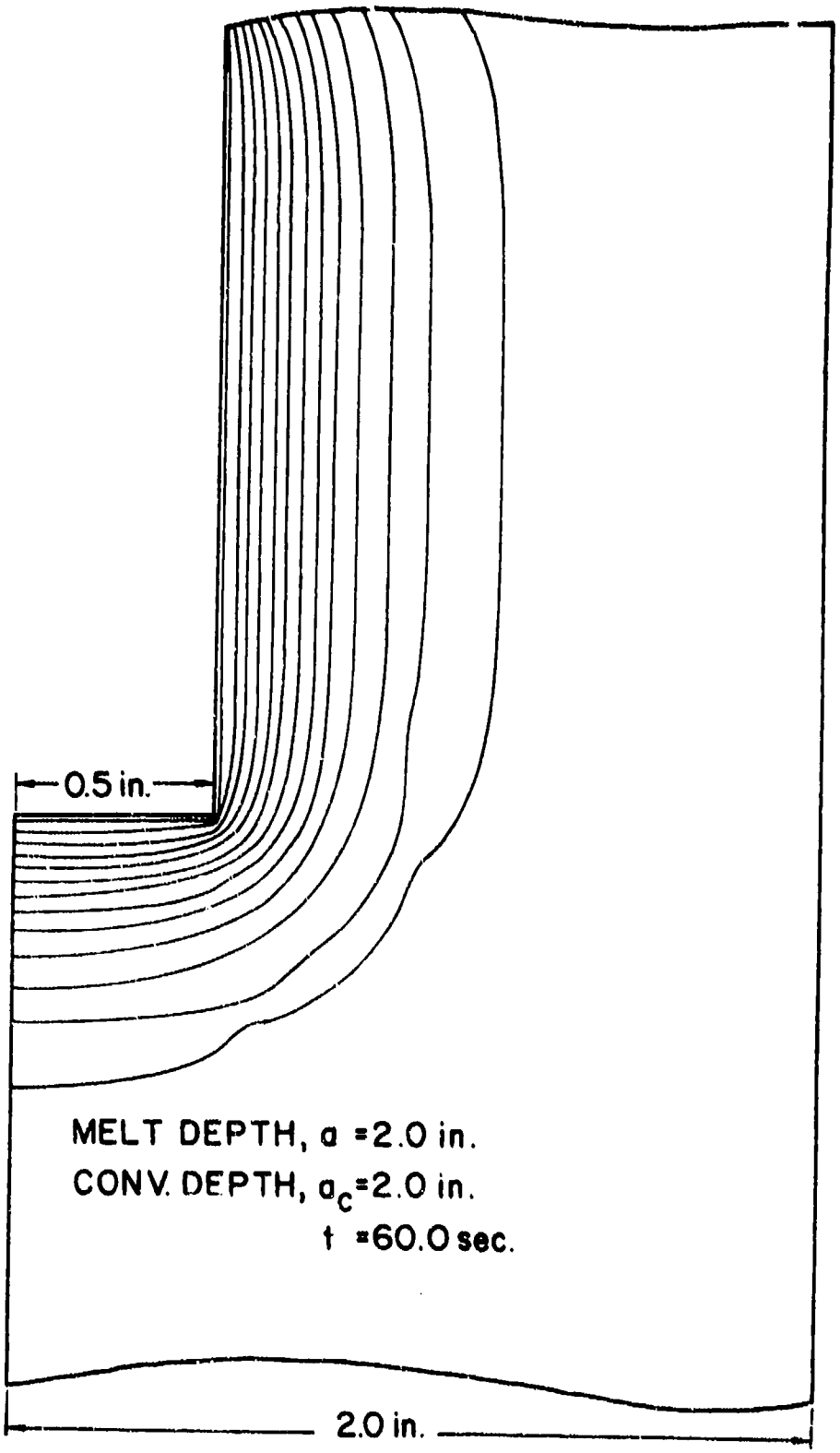

Figure 21. Temperature Distribution, Model 1A-2, t = 60 sec.

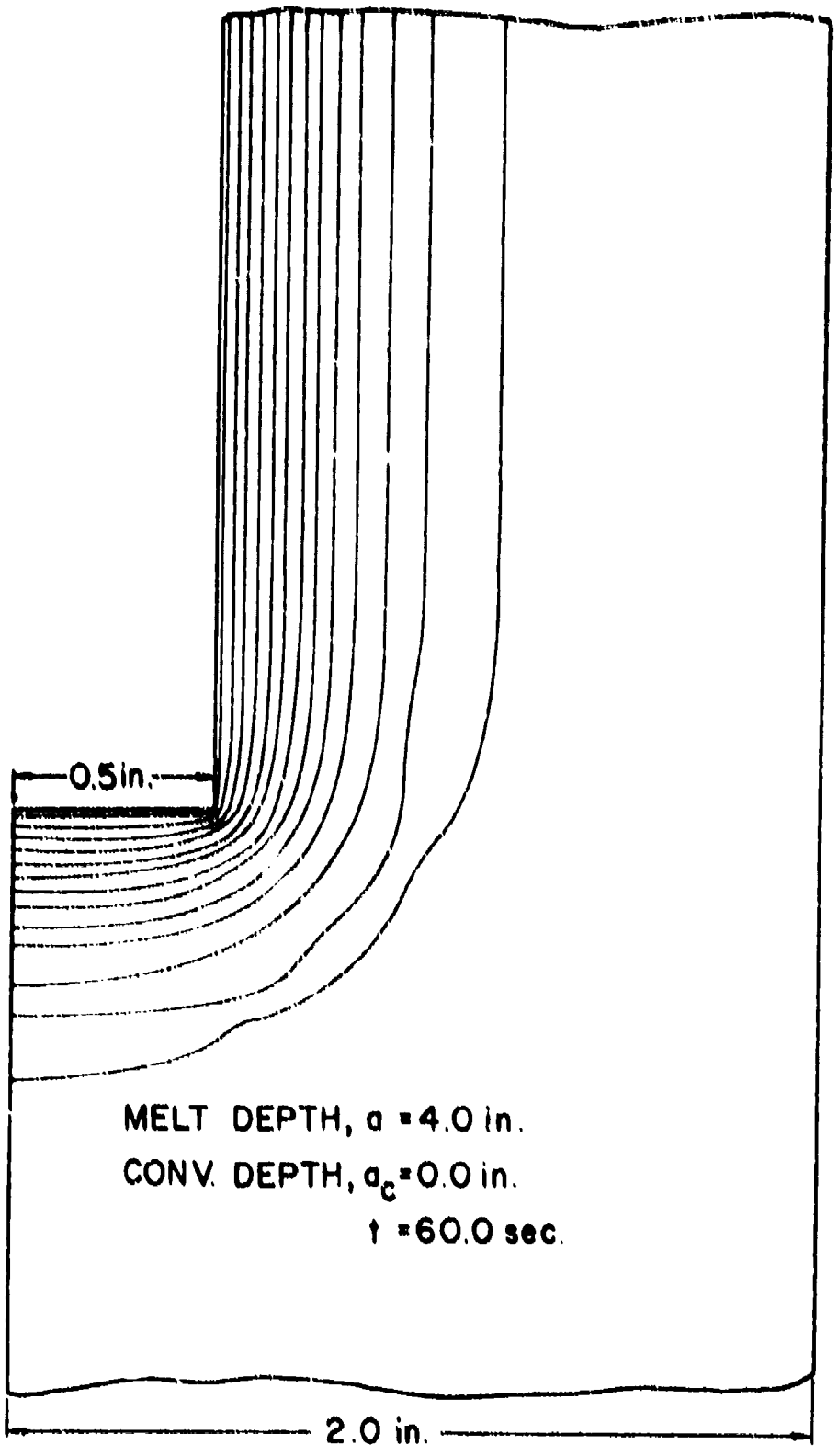

Figure 22. Temperature Distribution, Model 1A-3, t = 60 sec.

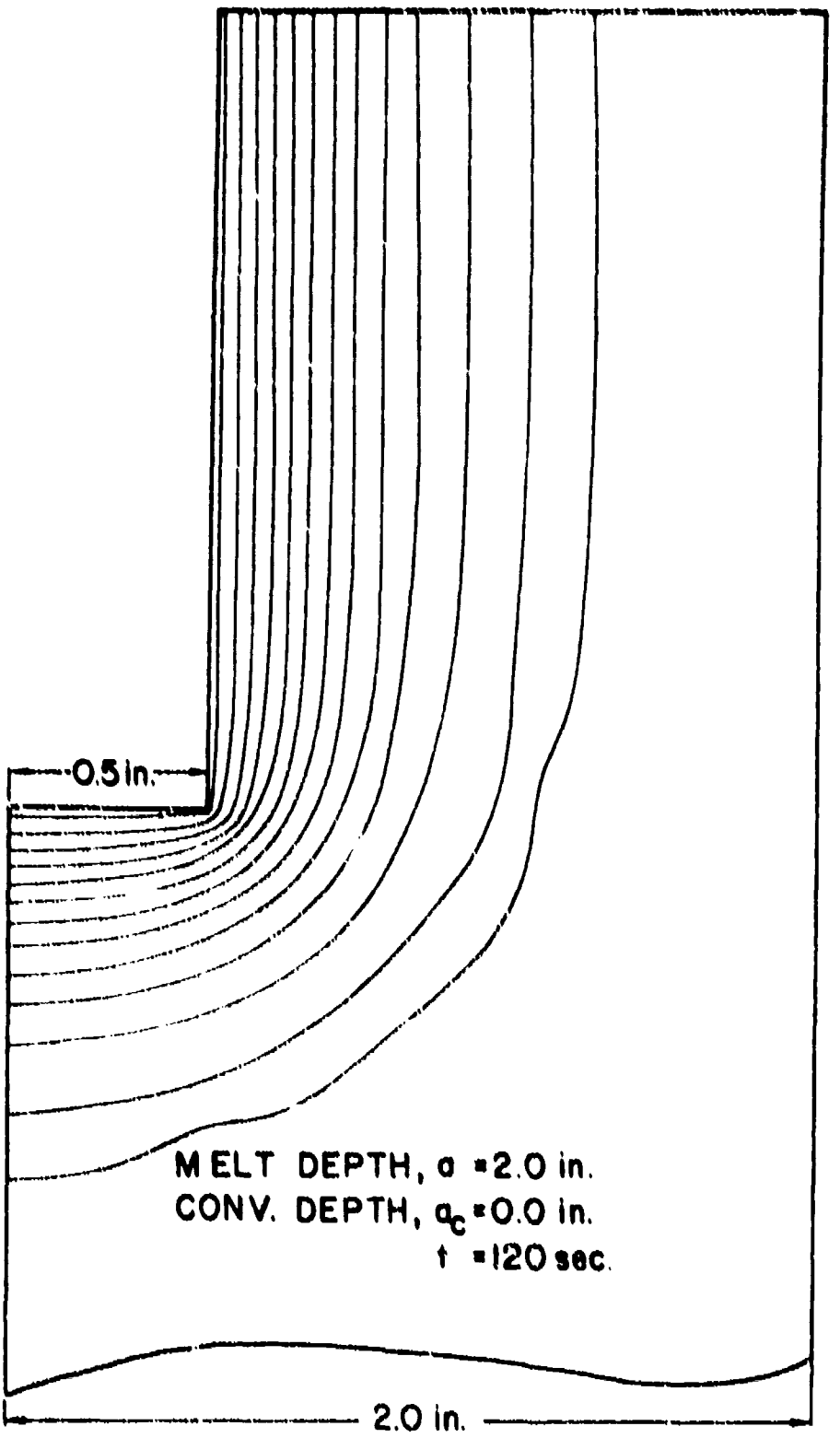

Figure 23. Temperature Distribution, Model 1A-1, t = 120 sec.

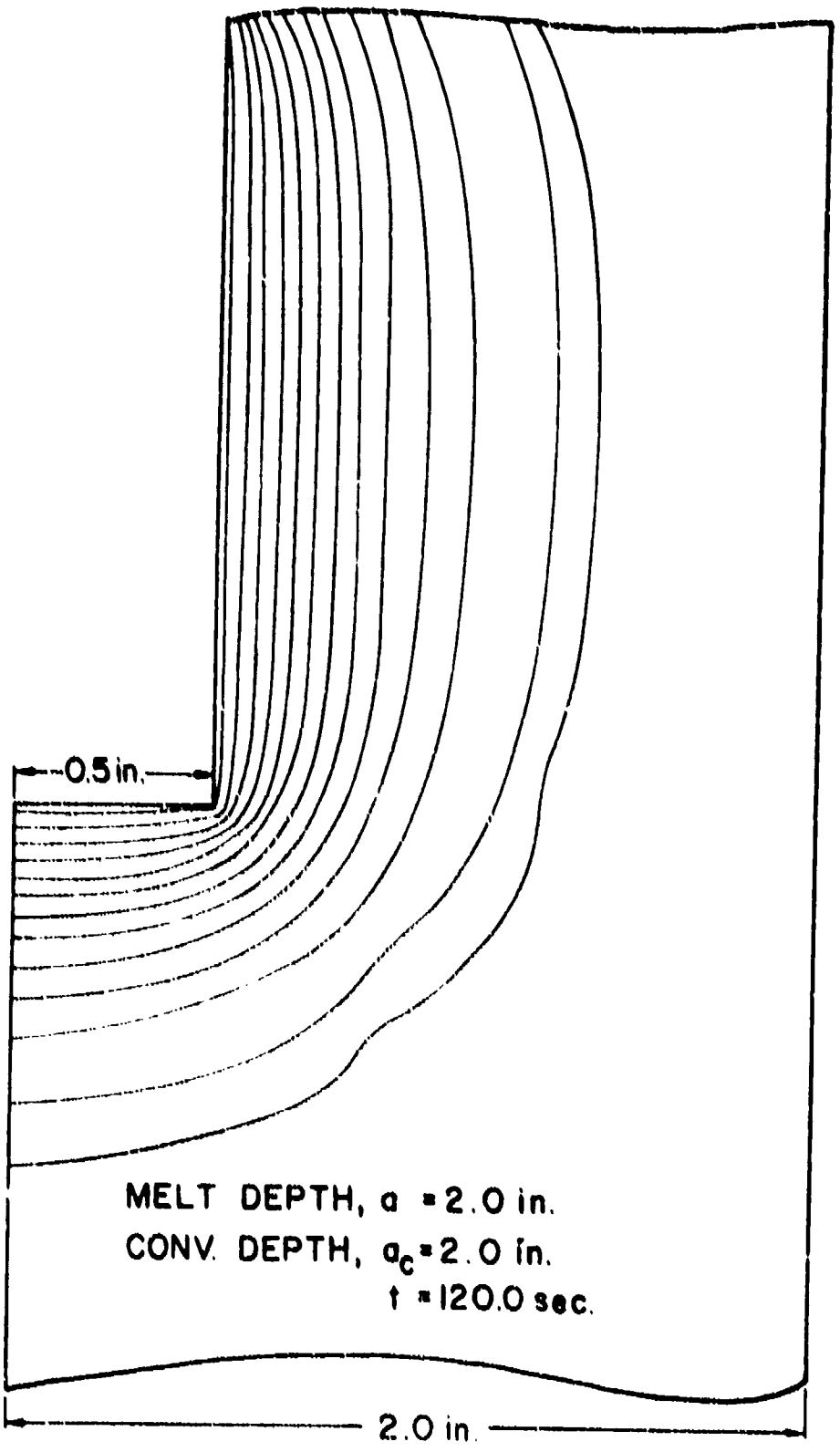

Figure 24. Temperature Distribution, Model 1A-2, t = 120 sec.

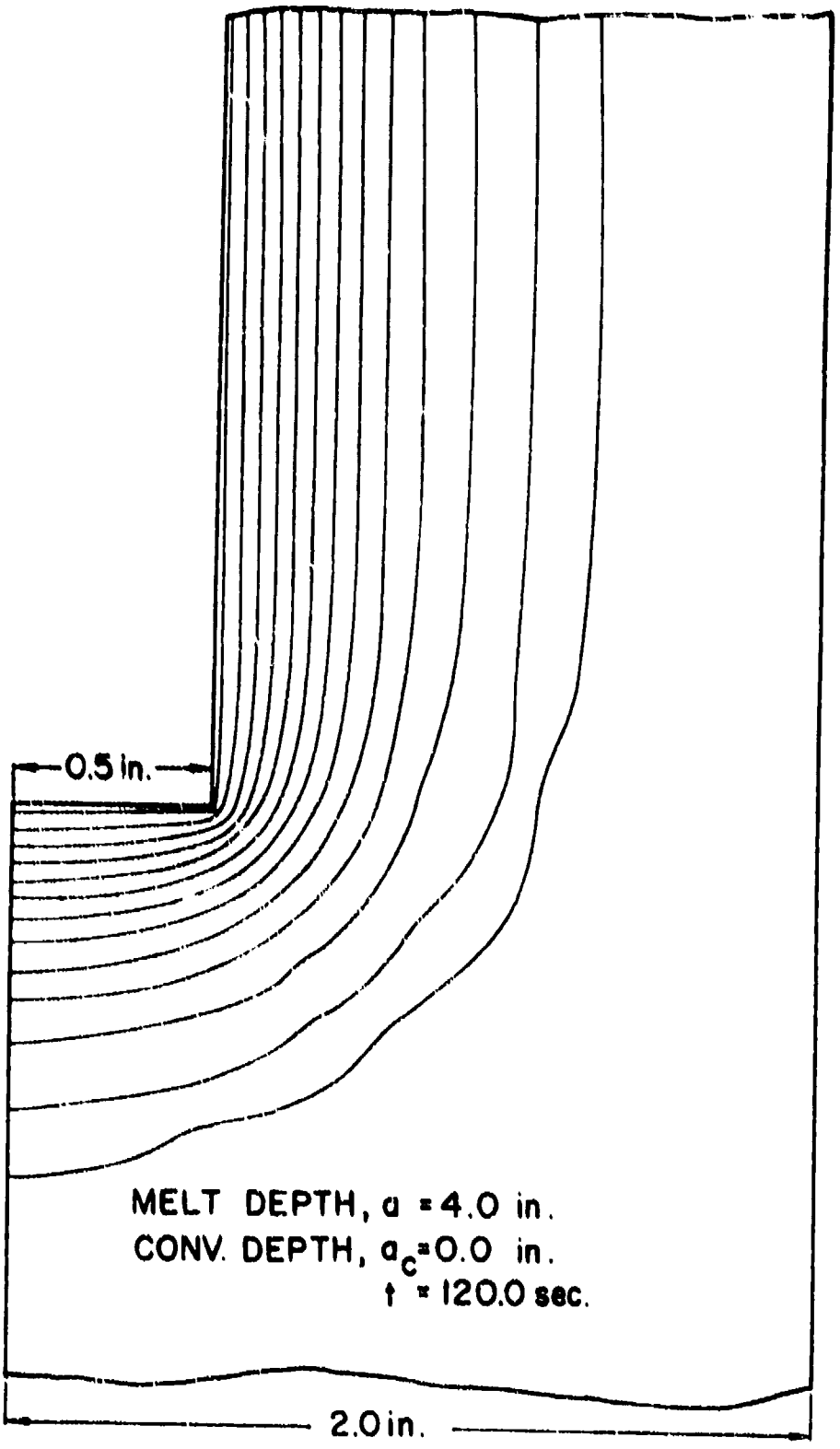

Figure 25. Temperature Distribution, Model 1A-3, t = 120 sec.

in this region is highly dependent on the convection depth. This effect results from two factors. Although the temperature distribution as seen from Figures 20-25 is approximately one-dimensional in the melt-depth section, thermal gradients near the point of transition from melt condition to convection condition are highly localized. These highly localized gradients give rise to very high stress concentrations. Also, due to the localized heating, the thermal expansion of this area is restrained by the relatively large cold zone. This thermally induced constraint induces very high compressive stresses in the heated zone and tensile stresses in the cold zone. For a given temperature distribution, the severeness of the thermal constraint increases with increase in the volume of the cold zone, up to a certain critical value. Once the cold zone volume reaches this critical value, any further increase has no effect on the stress field. For the slot models, since the volume of the cold zone depends directly on the convection depth, there exists a critical value of the convection depth beyond which any increase in the convection depth has no significant effect on the fracture inducing stresses.

The convection depth studies were conducted using models 2A, 2A-1, 2A-2; 2B, 2B-1; and 2C, 2C-1, 2C-2. The hole diameter for these models was kept constant. Three values of hole spacing were considered, giving three different fracture lengths. For models of equal fracture length, convection depths were varied, the highest value being approximately equal to half the fracture length. Parametric description of these models is given in Table 9.

The results of these studies are shown in Figures 26-33. In view of the assumption that the material above 700°C has no elastic resistance, the problem geometry is modified using the 700°C isotherm.

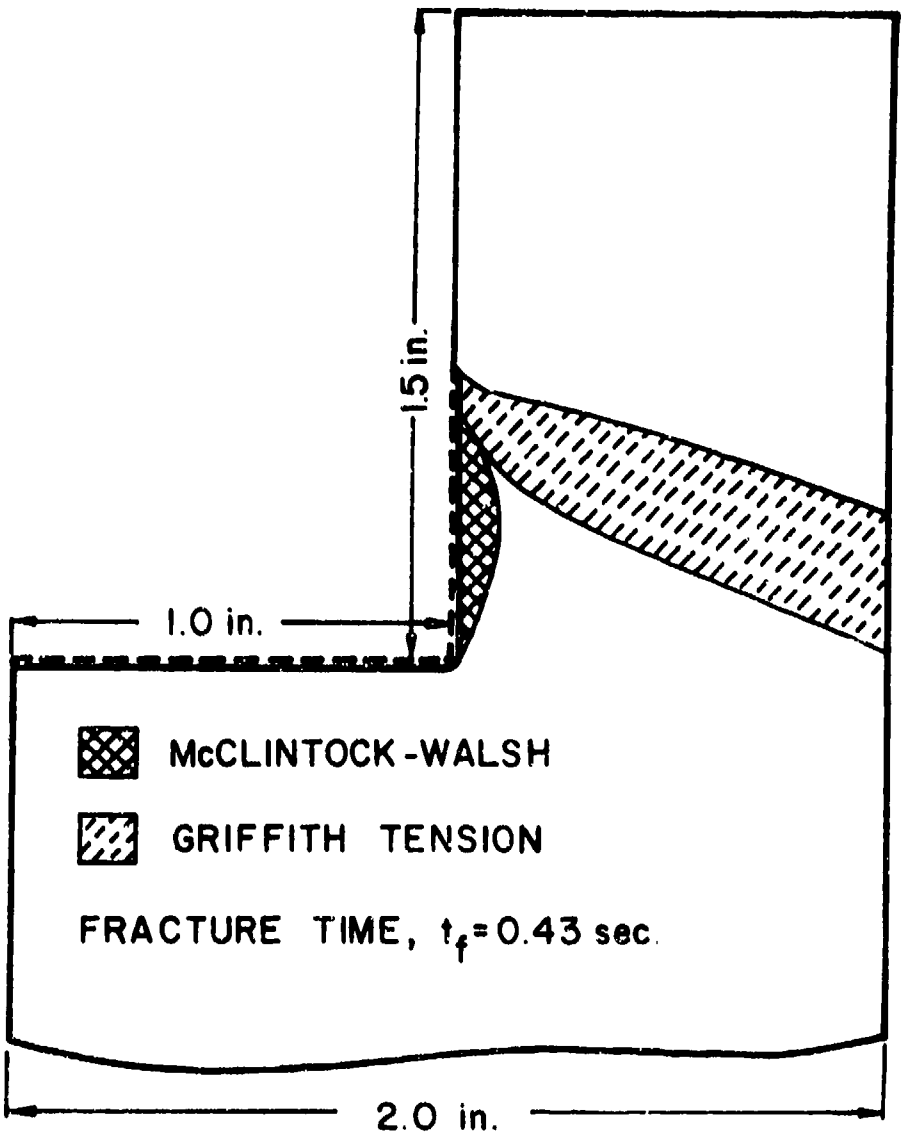

Figure 26. Fracture Zones, Model 2A

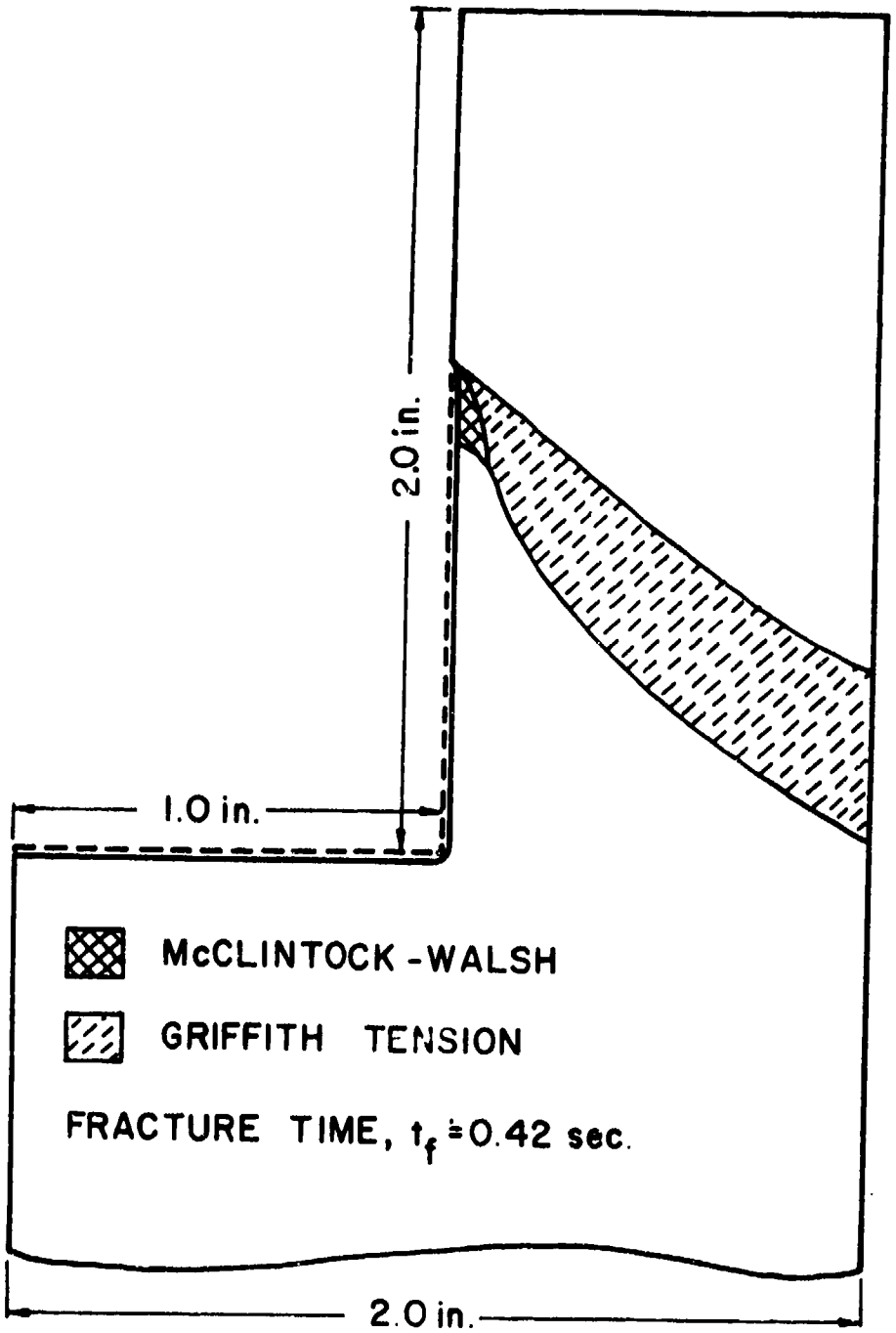

Figure 27. Fracture Zone, Model 2A-1

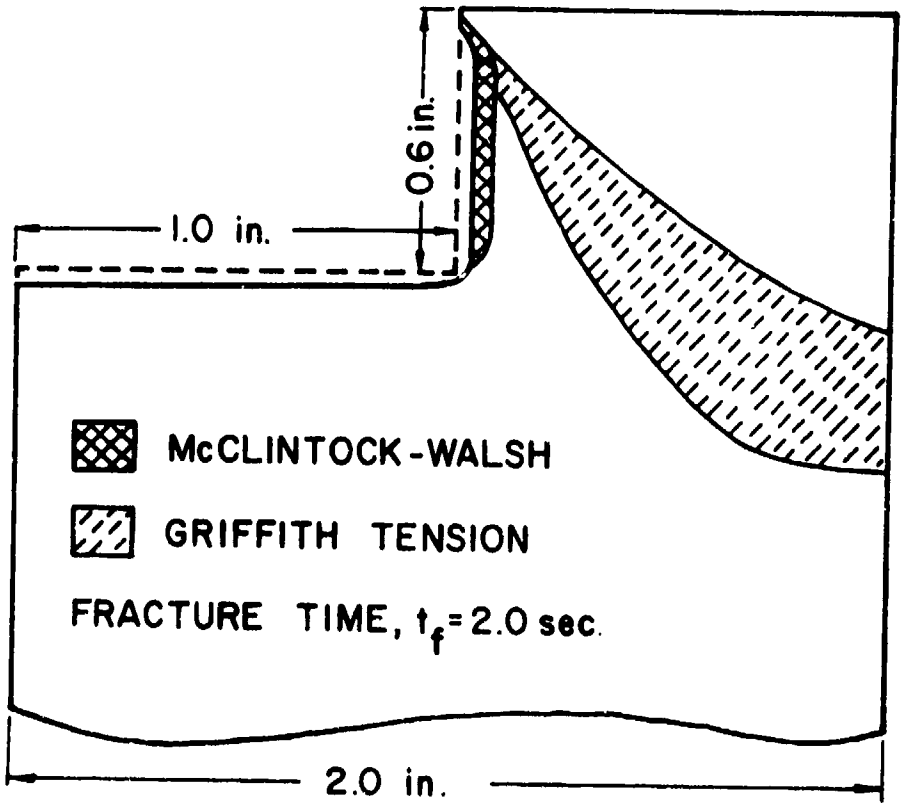

Figure 28. Fracture Zones, Model 2A-2

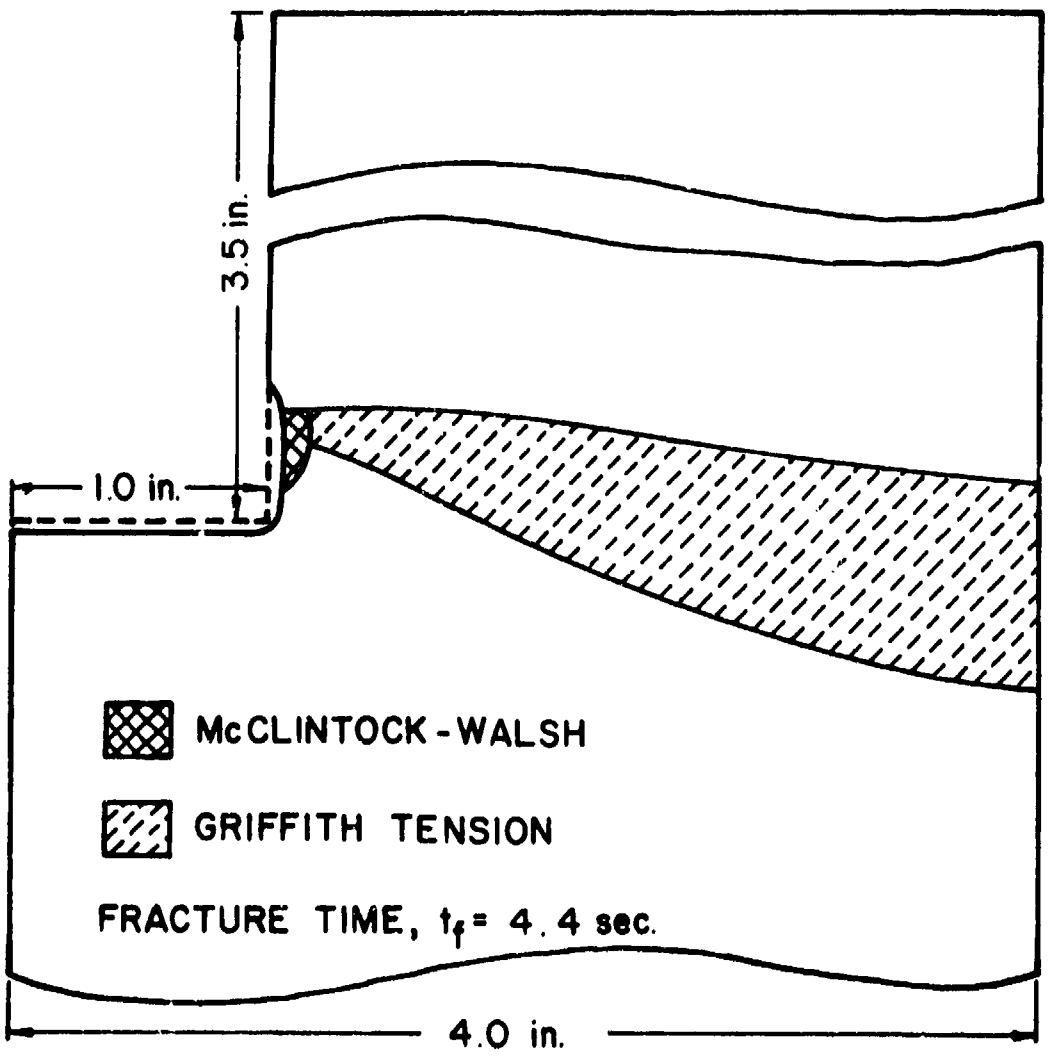

Figure 29. Fracture Zones, Model 2B

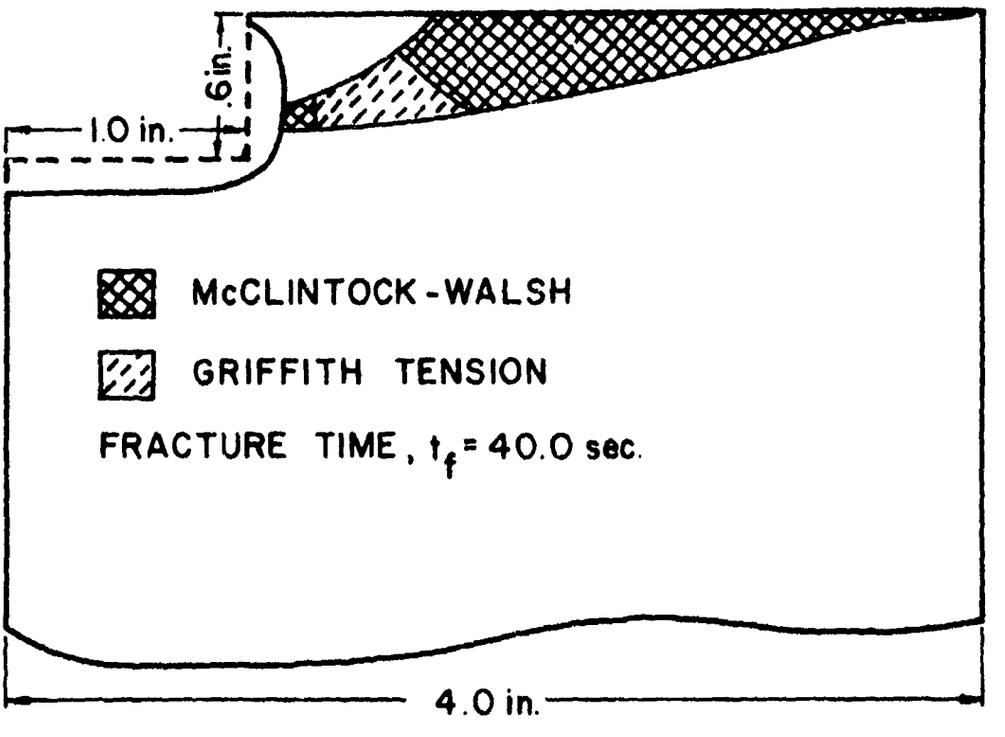

Figure 30. Fracture Zones, Model 2B-1

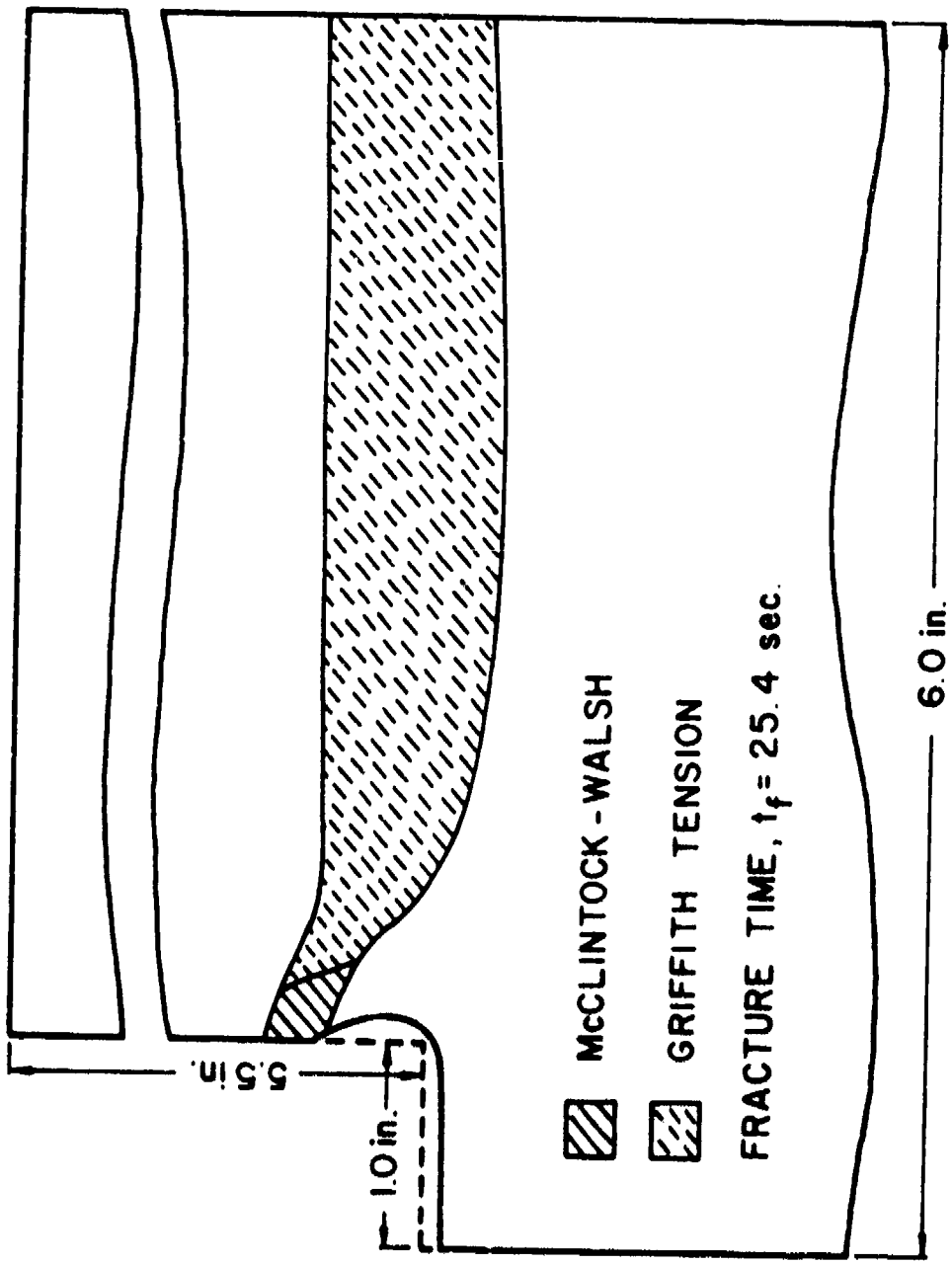

Figure 31. Fracture Zones, Model 2C

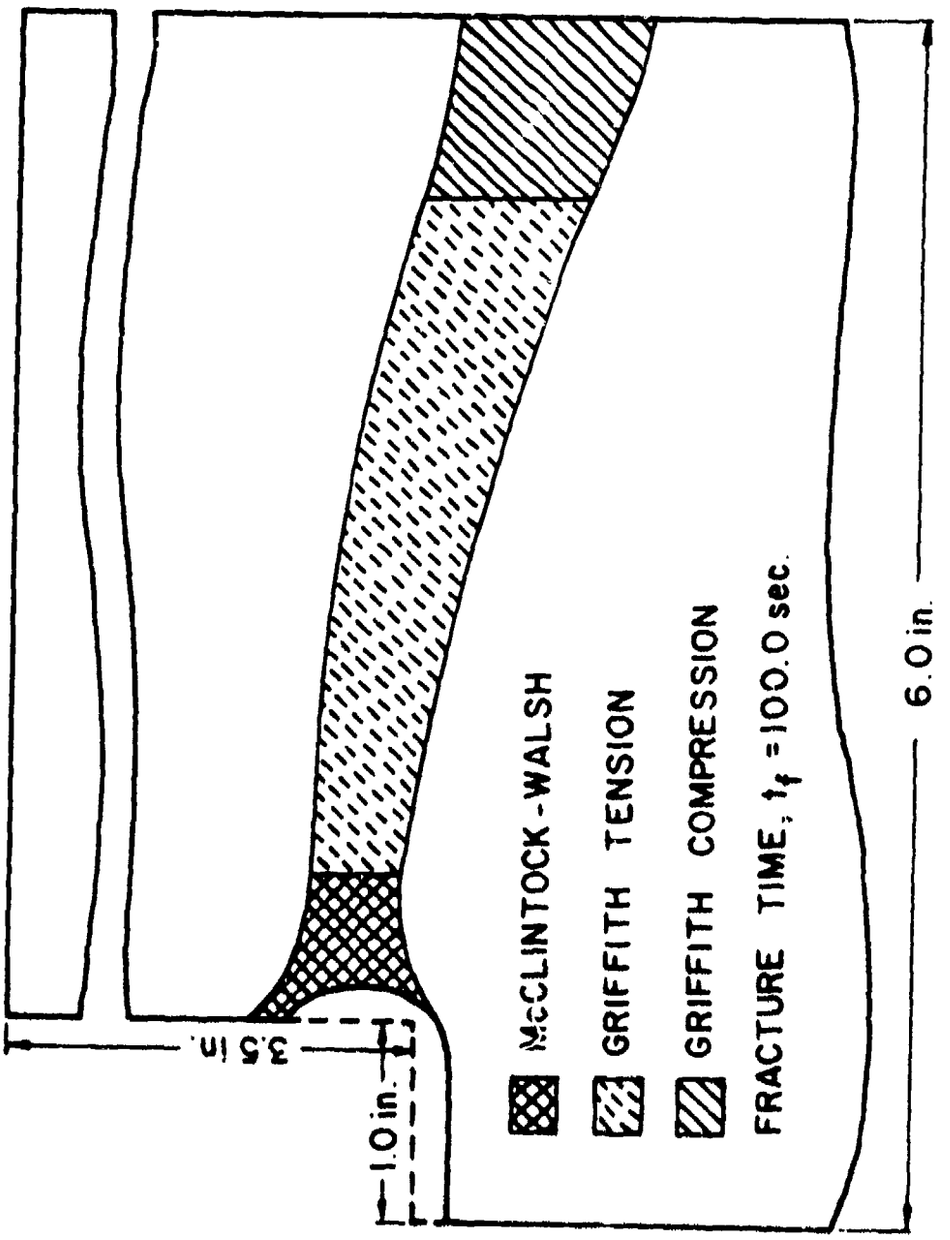

Figure 32. Fracture Zones, Model 2C-1

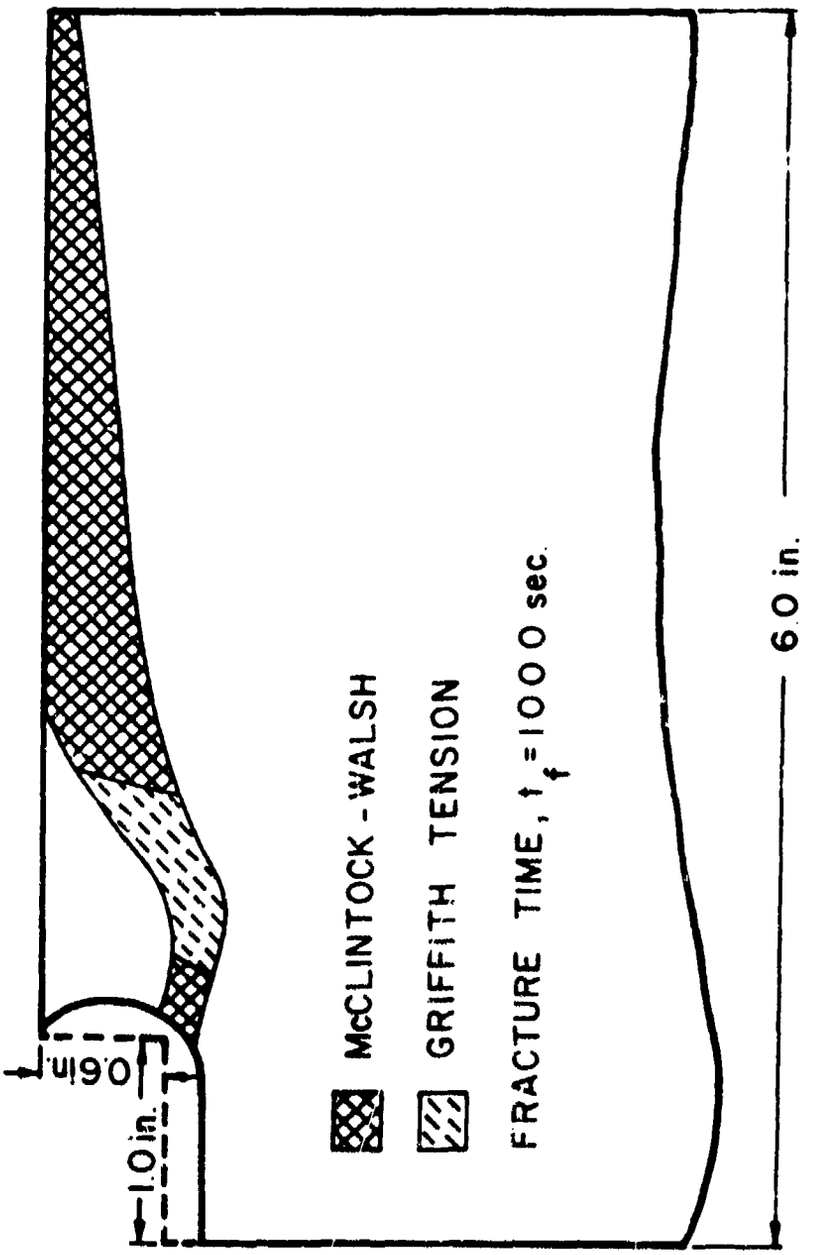

Figure 33. Fracture Zones, Model 2C-2

The fracture completion time is denoted by t_f, and the probable fracture zones at this time are shown by the cross-hatched area. The doubly cross-hatched area shows the fracture zone governed by the McClintock-Walsh modified Griffith criterion, Equation 2.4. The remainder of the fracture zone is governed by the original Griffith criterion, Equations 2.1 and 2.2. In the subsequent discussion, the two types of fracture zones are referred to as the McClintock-Walsh zone and the Griffith zone, respectively.

The McClintock-Walsh zone is associated with very high compressive stress components. For very small or no convection depths, the fracture is characterized by a McClintock-Walsh zone in the high temperature region followed by a small Griffith tension zone in the low temperature area and a large secondary McClintock-Walsh zone extending to the line of symmetry. The increase in the cold zone volume and the consequent thermal constraint as a result of the increase in the convection depth has relatively little influence on the McClintock-Walsh zone in the high temperature area and the small Griffith zone immediately following it. This is due to the fact that the stress state in these zones result primarily from the temperature gradients and that changes in the convection depth have very little effect on the temperature field in this region.

The McClintock-Walsh zone in the cold region is, however, greatly influenced by convection depth changes. As the convection depth is increased, the thermal constraint becomes more severe. As a result, the high compressive stress components in the cold region start to decrease in magnitude and the tensile stress components increase sharply. The net effect of these changes in the stress components is that the

secondary McClintock-Walsh zone begins to shrink. If the convection depth is continuously increased, a stage is reached when the secondary McClintock-Walsh zone completely disappears and transforms into the Griffith tension zone which now extends to the line of symmetry. In this discussion, the convection depth associated with the completion of the above transformation is referred to as the critical convection depth.

The critical convection depth was found to be approximately equal to half the fracture length. From the results for convection depths approximately equal to the critical value, it is seen that the total fracture zone consists of a small McClintock-Walsh zone in the high temperature region followed by a Griffith tension zone in the low temperature region and extending all the way to the line of symmetry.

For convection depths smaller than the critical value, the fracture time shows only small variations with changes in convection depth. However, as the convection depth approaches the critical value, the McClintock-Walsh zone rapidly transforms into the Griffith tension zone, and because of the tensile strength of the rock being much lower than its compressive strength, the fracture time is drastically reduced. Once the fracture mode transformation is completed, the fracture time shows a negligibly small decrease with any further increase in the convection depth.

The fracture zones in Figures 26-33 show another very important effect of the convection depth changes. This effect involves the location of the parallel fracture. The optimum location of the parallel fracture requires the crack initiation to occur very close to the hole base and the crack propagation in a plane approximately parallel

to the hole base. The fracture zones in Figures 26-33 indicate that, in order to obtain the optimum location, the thermal inclusion should be concentrated at the very base of the hole while the convection depth should, at least, be equal to half the fracture length, and that any further increase in the convection depth has only a trivial influence on the location of the parallel cracks and the fracture time.

D. Hole Diameter and Spacing Studies

Hole diameter and the hole spacing are, perhaps, the two most significant parameters in the study of rock fragmentation using subsurface thermal inclusions. The hole diameter affects the fracture length as well as the size of the thermal inclusion. The hole spacing, however, is the more important factor as it directly controls the volume of the rock removed.

In order to investigate the effects of the hole diameter and the hole spacing, nine fracture lengths were considered. Hole spacings of 4.0 in., 8.0 in., and 12.0 in. were used and for each hole spacing, hole diameter values of 1.0 in., 1.5 in., and 2.0 in. were considered.

In Table 9, the models used for the hole diameter and the hole spacing studies are identified as 1A, 1B, 1C; 2A, 2B, 2C; and 3A, 3B, 3C. The melt depth and the convection depth values were selected based on the results of the melt depth and the convection depth studies as described in the beginning of this chapter. The melt depth value was kept constant at 0.5 in. for all models. For a given model, the total hole depth considered was such that the convection depth was approximately equal to the critical value, that is, approximately half the fracture length.

1. Temperature Field Characteristics

The temperature distribution at the time of fracture completion was found to be far from stationary and highly localized in the vicinity of the slot base. Plots of the typical temperature fields at the time of fracture completion are shown in Figures 34-36. As seen from these plots, the major portion of the fractured volume does not experience any temperature change. Thus, the stresses in this region occur entirely due to the load vector resulting from the thermal constraint. The natural thermal expansion of the high temperature region is resisted by the cold volume. As a consequence of this constraint, the hot region undergoes a compressive loading while the cold zone is under a tensile load condition. In view of the equilibrium of forces, the compressive load vector integrated over the entire high temperature region must equal the tensile load vector integrated over the cold zone volume. Since the rock fracture is attributed to the tensile failure because of the tensile strength of rock being much lower than its compressive strength, only a small hot region is required to induce fracture causing stresses in a comparatively large cold zone.

As the hole spacing is increased, the cold zone volume also increases. A higher tensile load vector is therefore necessary in order to cause the fracture inducing stresses in the cold zone. This, in turn, requires a larger natural expansion of the hot region and, therefore, a larger volume of the hot zone and a longer time for fracture completion.

Thus, as the hole spacing is increased, the fracture completion time also increases. However, as seen from Figures 34-36, the increase in the fracture completion time is much higher than the corresponding

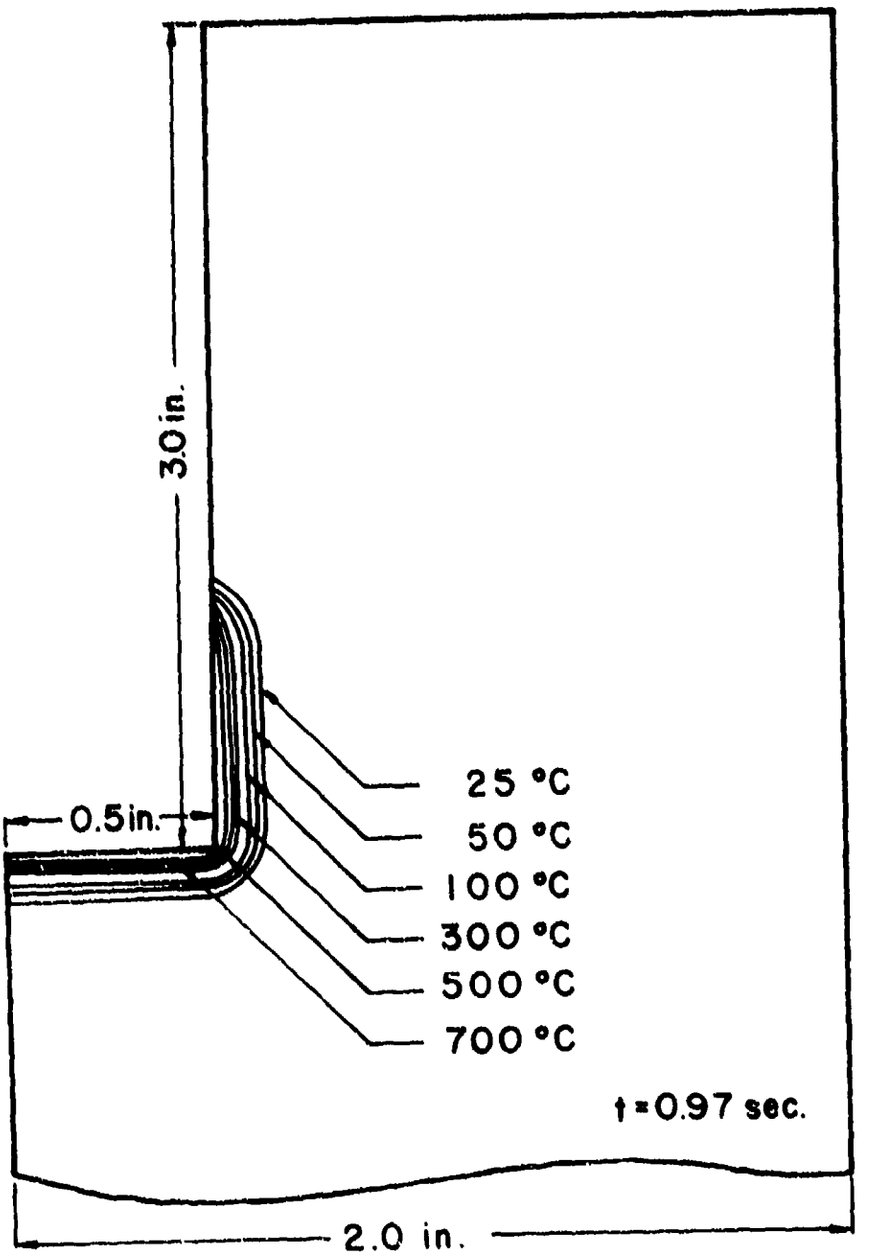

Figure 34. Temperature Distribution, Model 1A

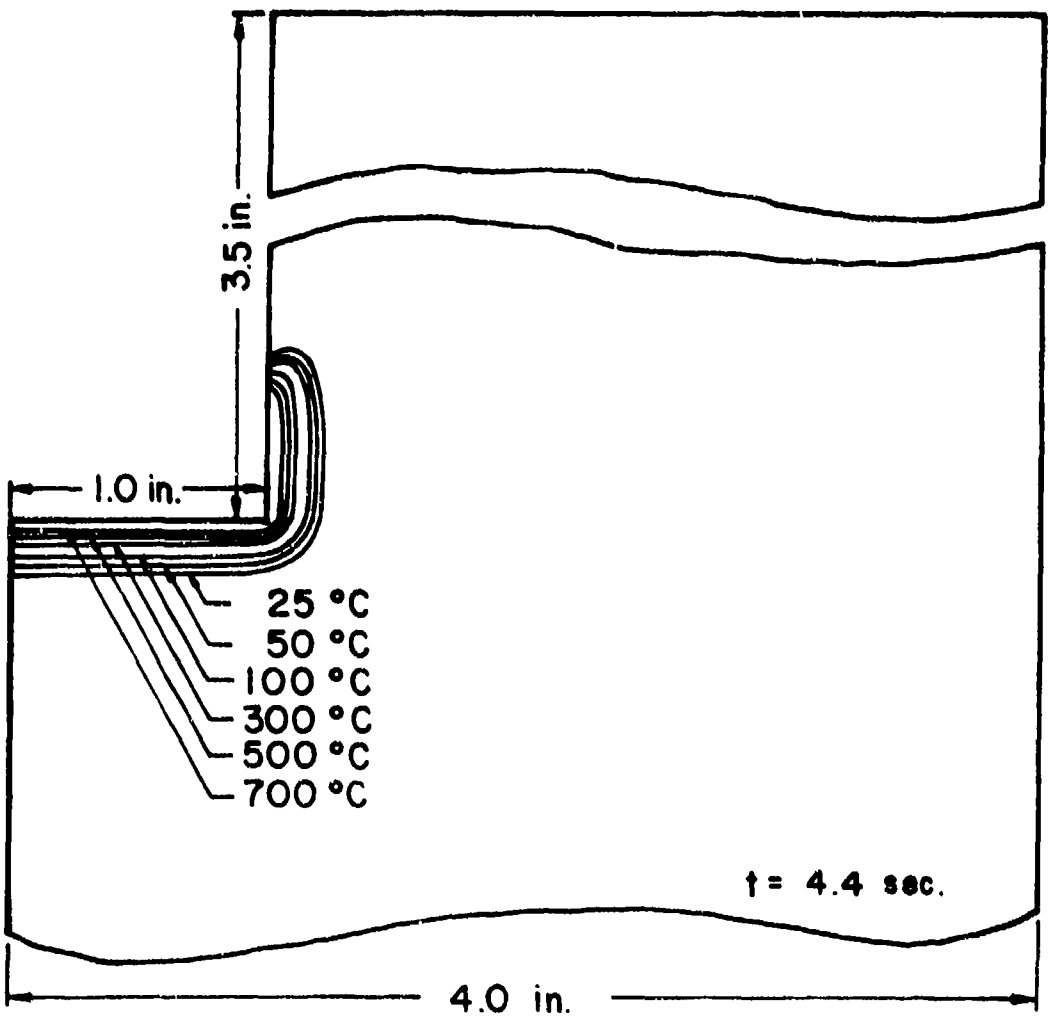

Figure 35. Temperature Distribution, Model 2B

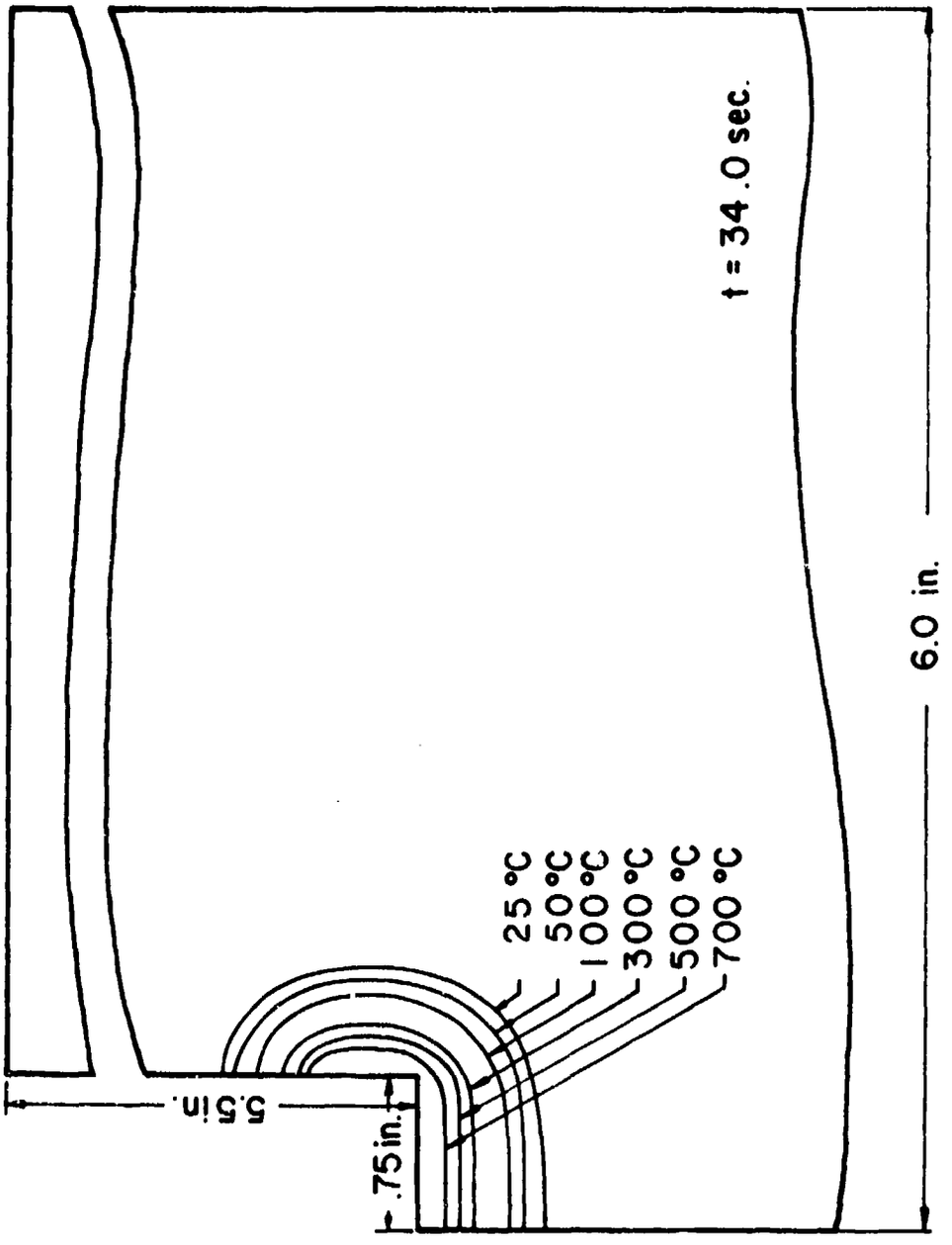

Figure 36. Temperature Distribution, Model 3C

increase in the hot zone volume. This is explained by the fact that while the thermal expansion and the resulting force vector are directly dependent on the volume of the hot zone, the volume of the hot zone itself is a complex function of the thermal conductivity and the thermal diffusivity, and for rocks the values of both these properties are extremely low.

2. Fracture Length Effects

From the above discussion, it is clear that while for a given hole diameter, increasing the hole spaci ıcreases the fracture completion time, it must also be true that for a given hole spacing, the fracture completion time will decrease if the hole diameter is increased. In other words, it is the change in the fracture length that affects the fracture completion time. This is demonstrated by the fracture zone plots shown in Figures 26, 29, 31, 37 - 39, and the fracture completion time versus the hole spacing plots shown in Figure 40.

It is possible, therefore, to study the effect of the change in hole diameter on the fracture time by keeping the hole diameter unchanged and changing the hole spacing such that the fracture length will remain the same. Models 11A, 13B, and 13C as described in Table 9 were designed in support of this hypothesis. These models were obtained by increasing the diameters of models 1A, 3B, and 3C to 2.0 in. and increasing the hole spacing correspondingly so as to keep the fracture lengths unchanged.

Plots of the fracture zones for models 11A, 13B, and 13C are shown in Figures 41-43. Comparison of fracture times and the fracture plots of these models with those of models 1A, 3B, and 3C shown in Figures 44, 38, and 39 confirms the above mentioned hypothesis.

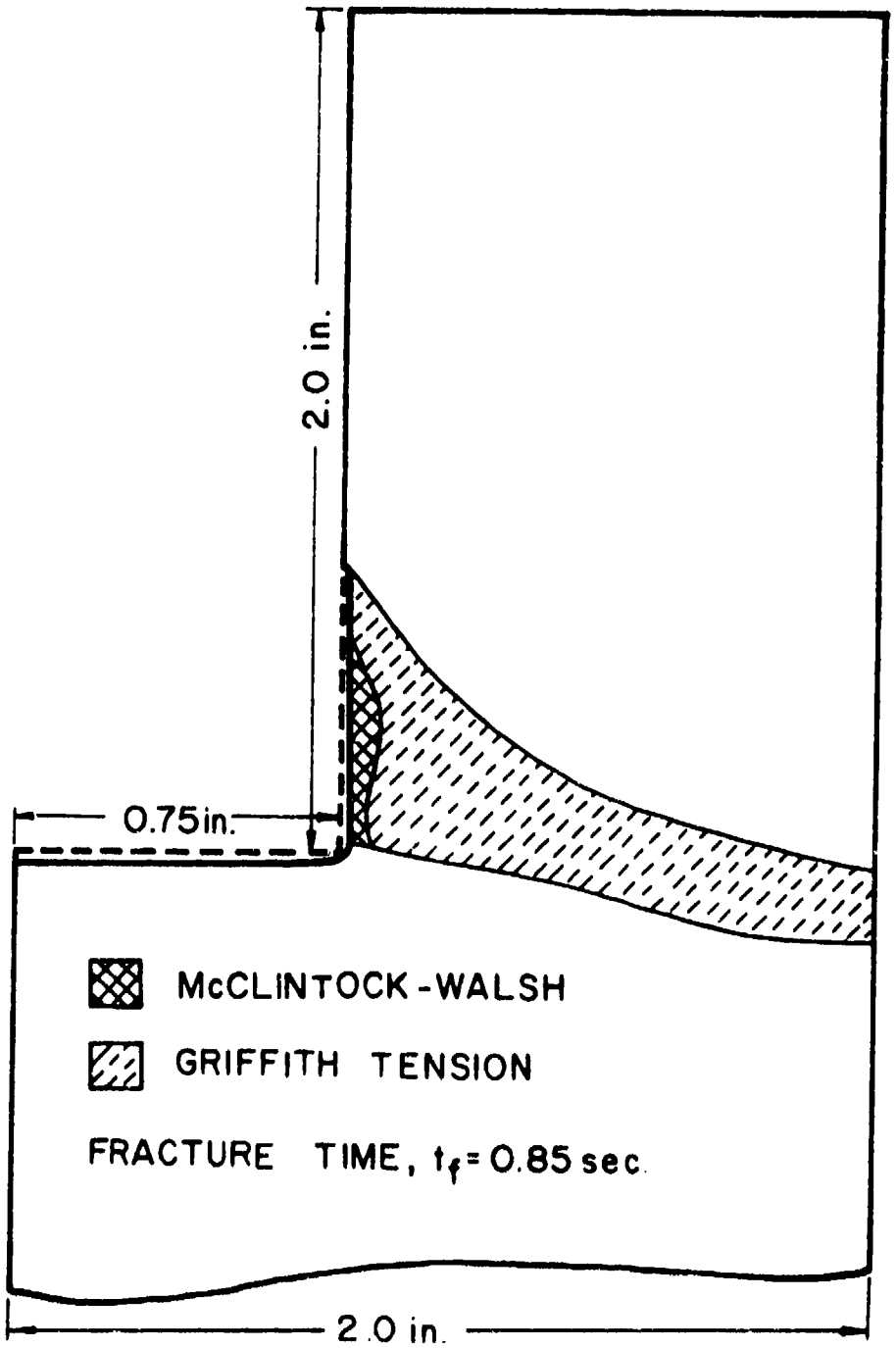

Figure 37. Fracture Zones, Model 3A

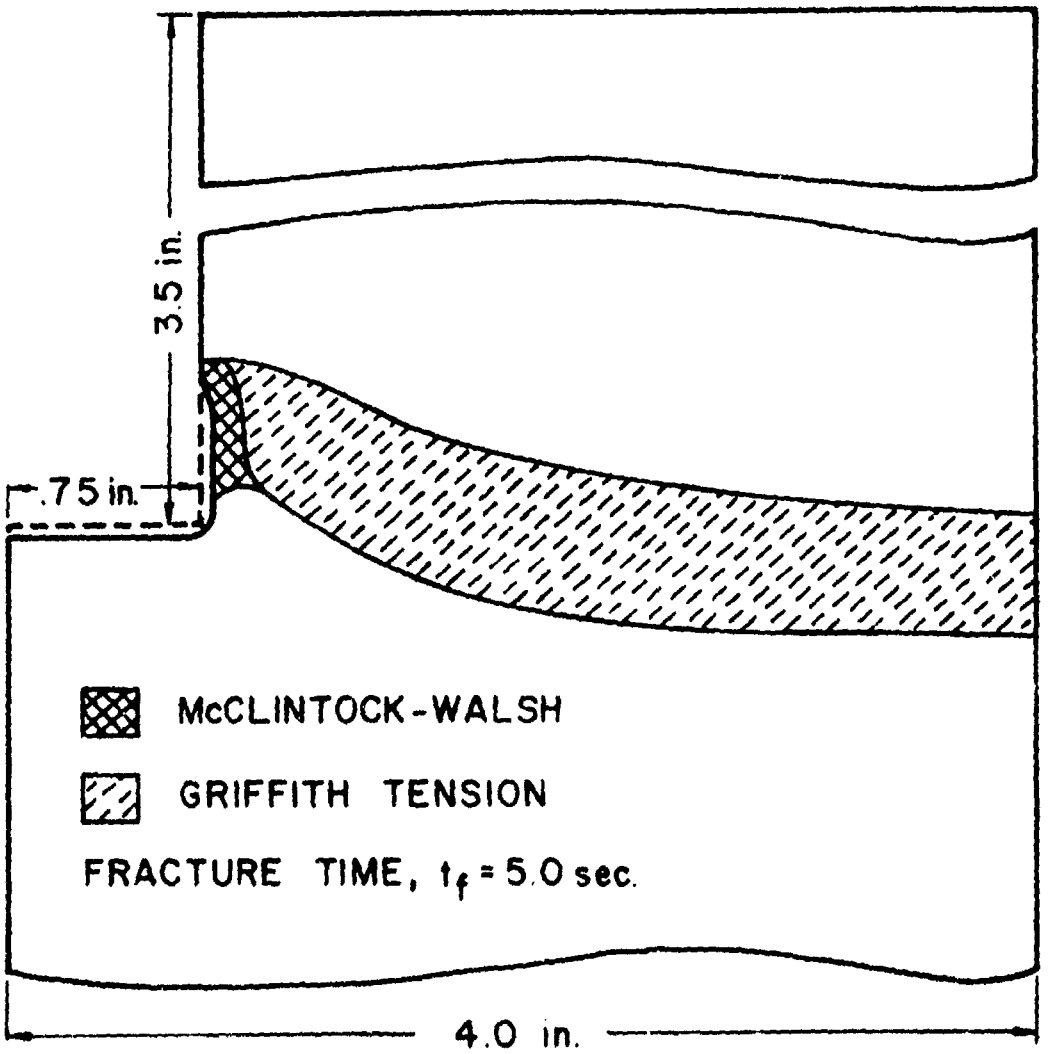

Figure 38. Fracture Zones, Model 3B

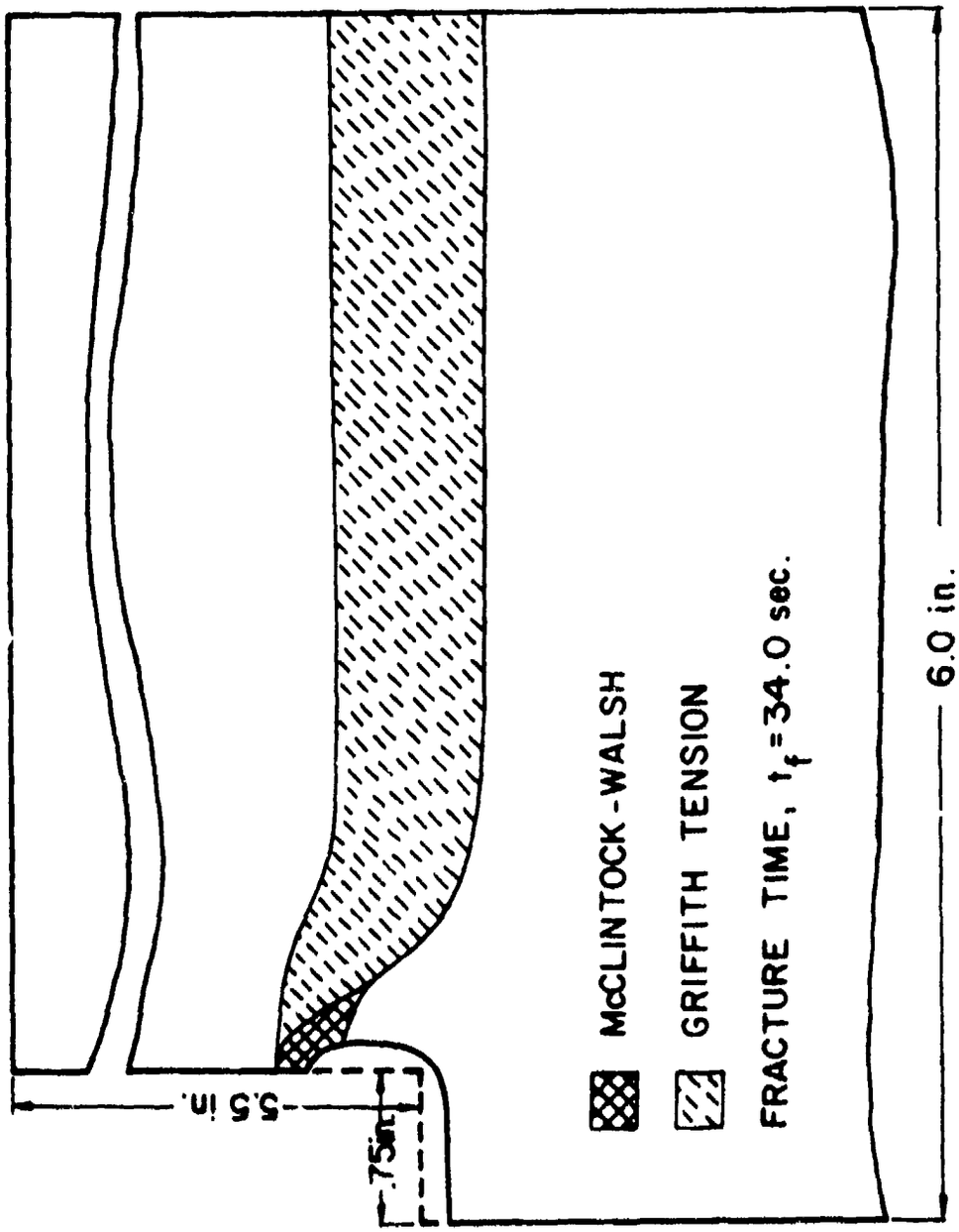

Figure 39. Fracture Zones, Model 3C

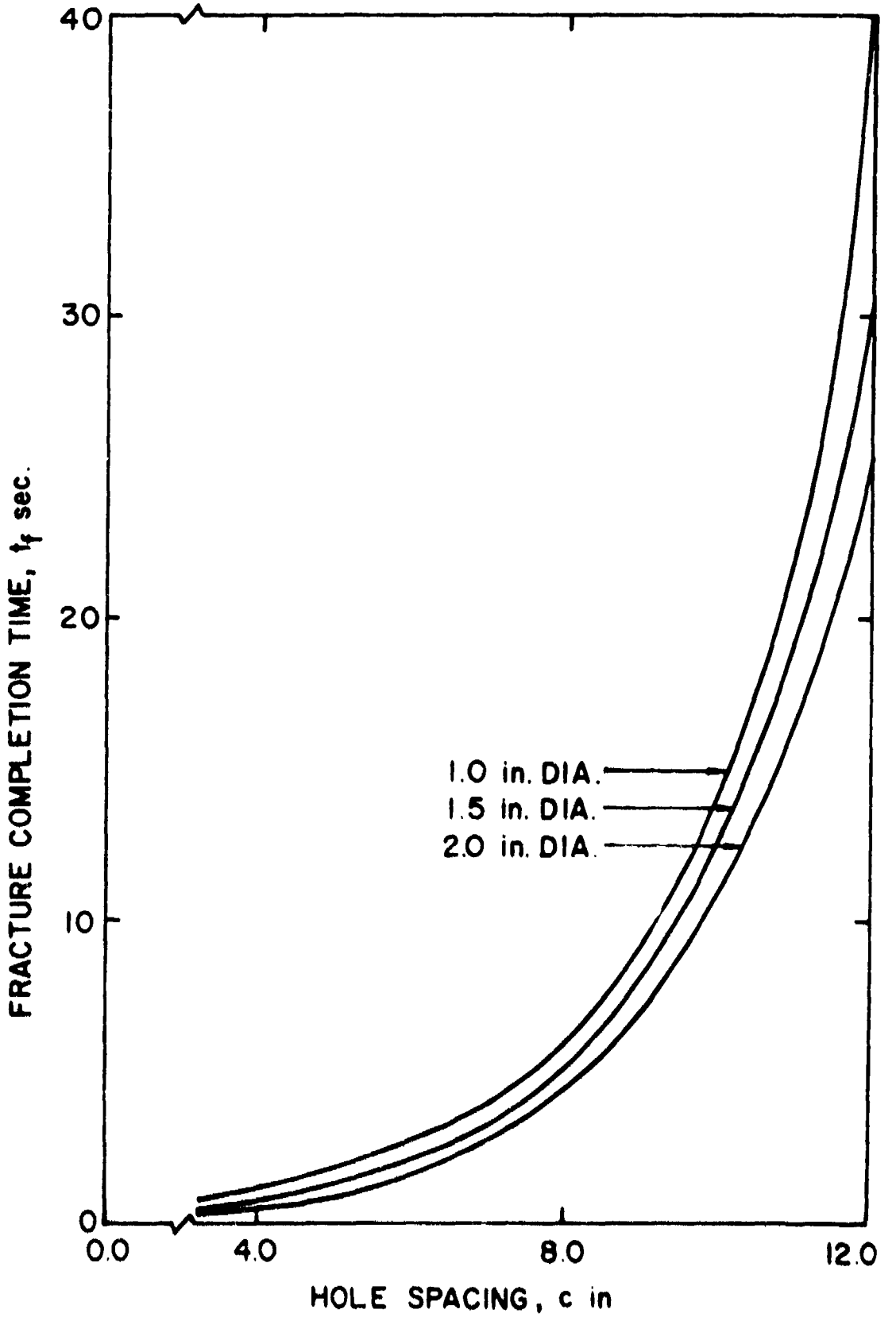

Figure 40. Fracture Time-Spacing Curves for Slot Models

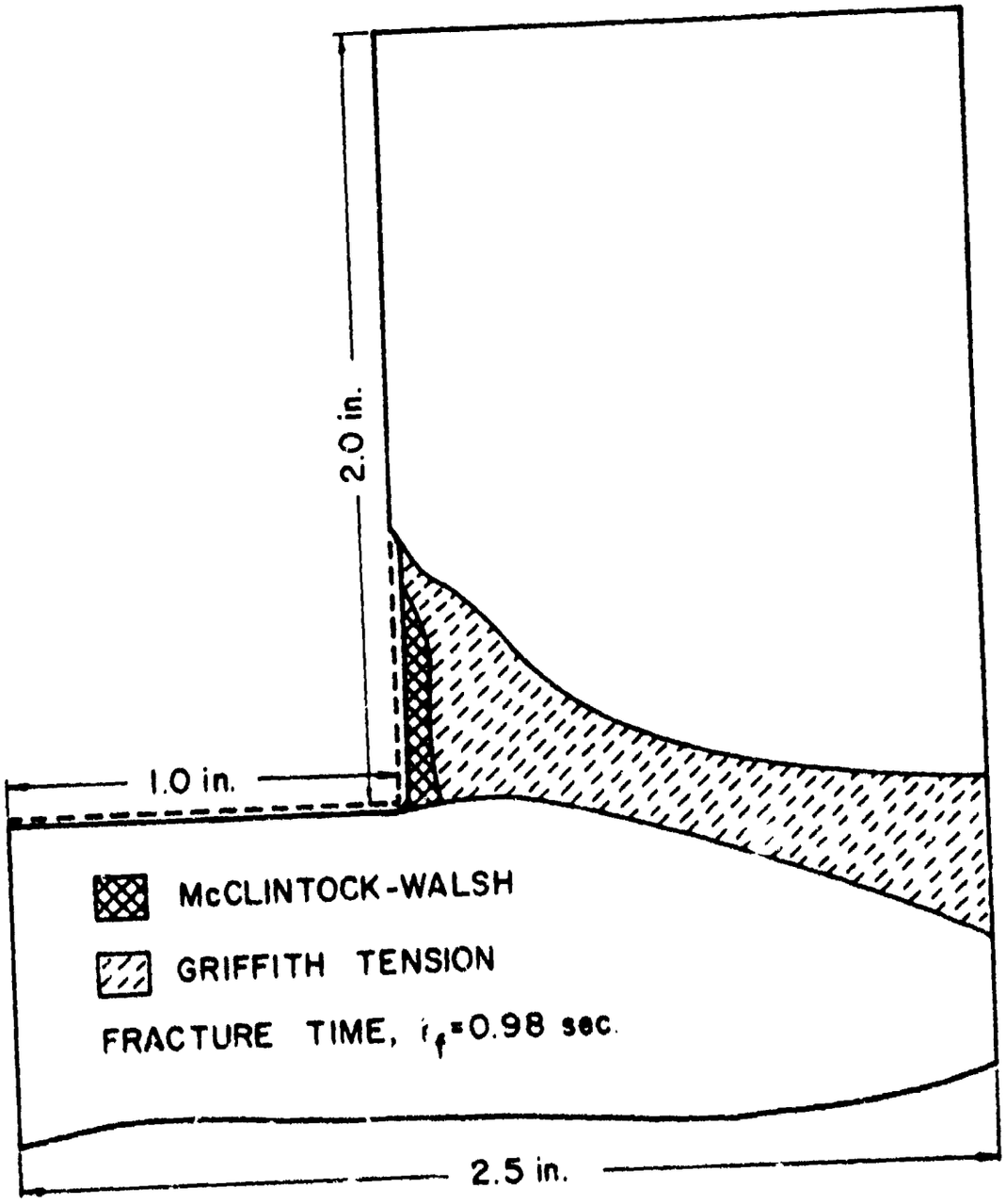

Figure 41. Fracture Zones, Model 13A

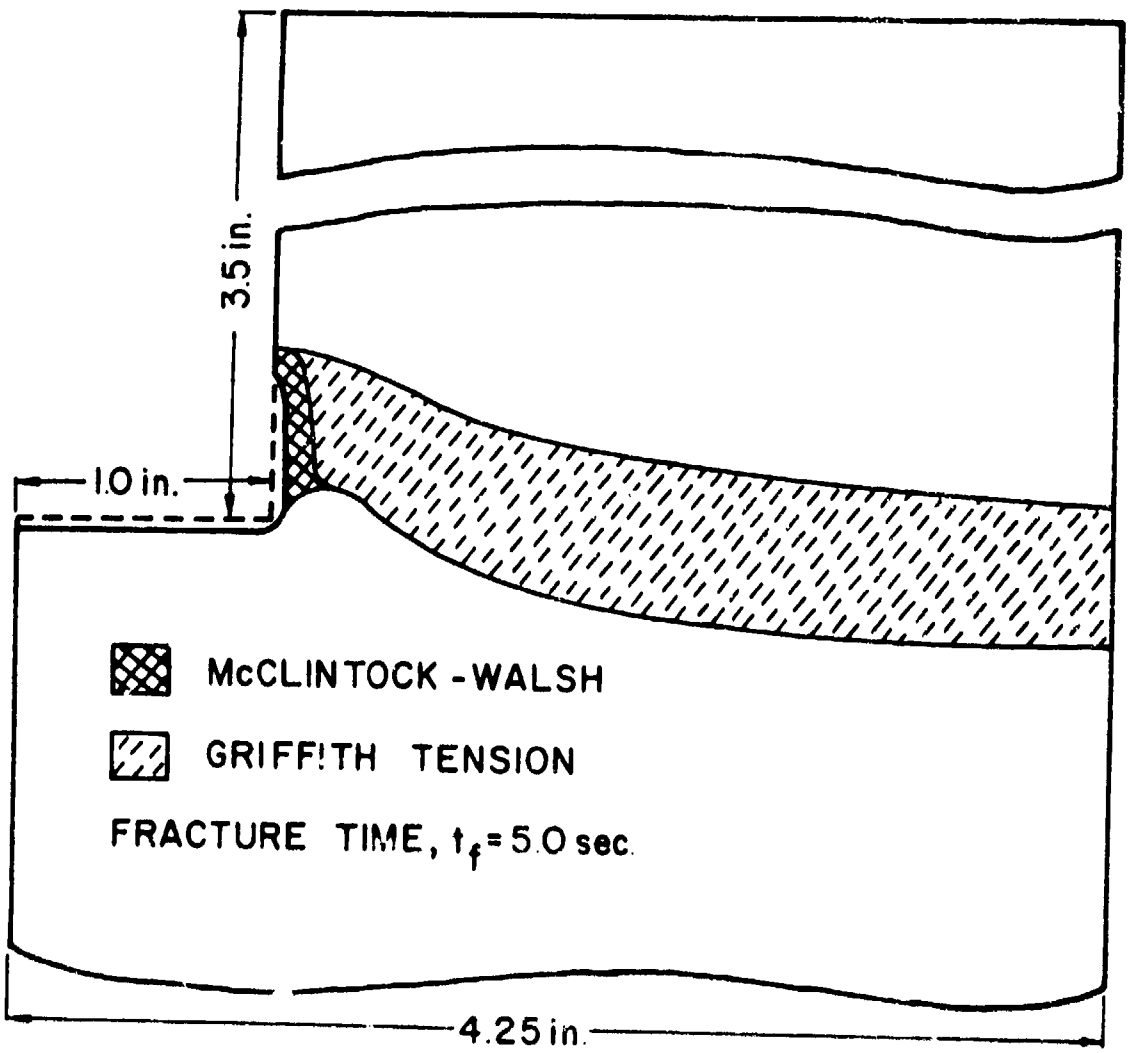

Figure 42. Fracture Zones, Model 13B

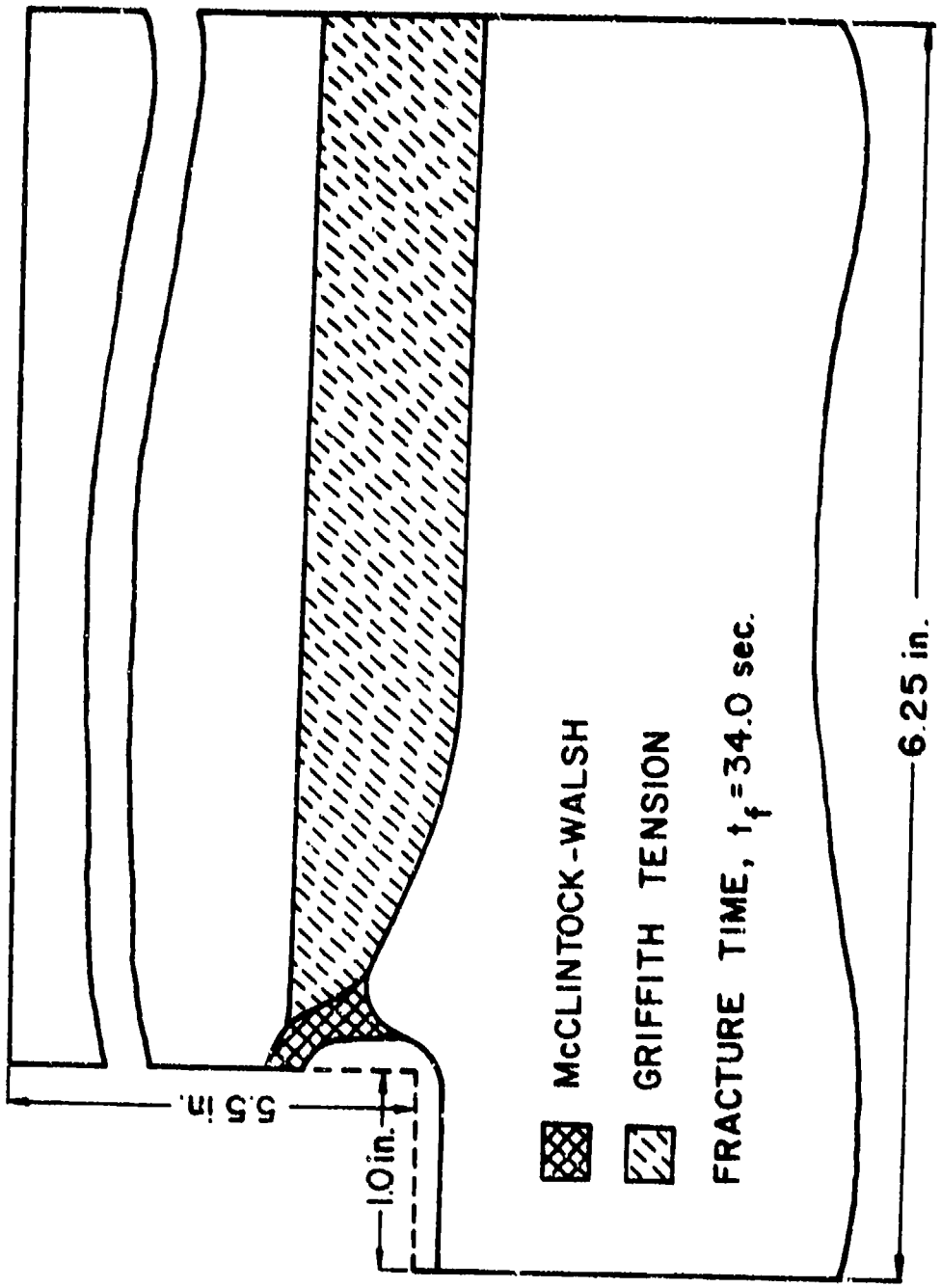

Figure 43. Fracture Zones, Model 13C

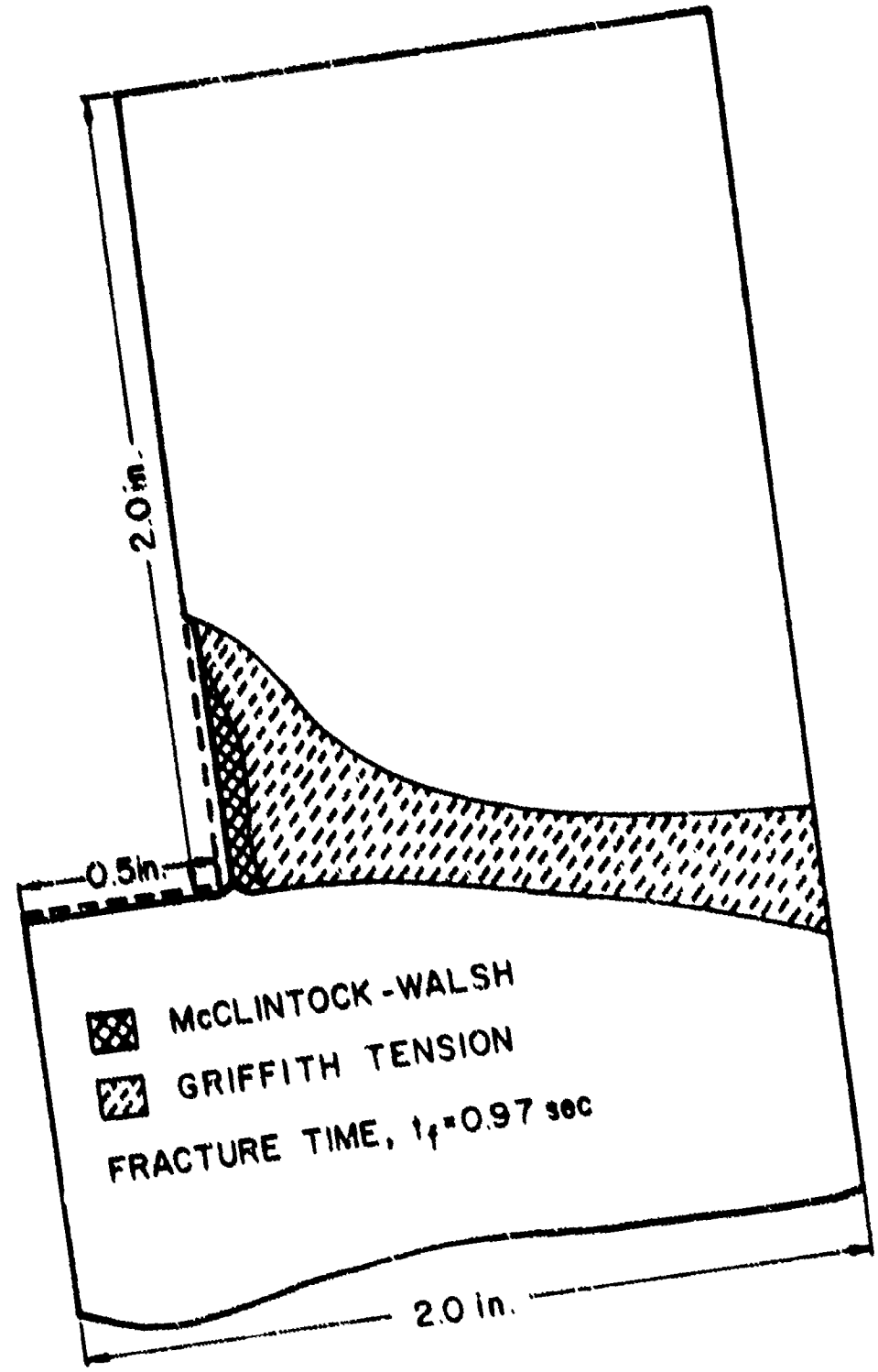

Figure 44. Fracture Zones, Model 1A

F. Fracture Length - Fracture Time Relation

Results presented for different models indicate that the fracture completion time can be expressed as a function of the single variable, the fracture length. Fracture completion times for models with convection depths approximately equal to the critical convection depth are listed in Table 10. Values from this table were used to compute the fracture length ratios and the corresponding fracture completion time ratios as given in Table 11. These values were plotted on a logarithmic scale as shown in Figure 45 from which the following relation was obtained:

$$t_f^* = L^{*2.7} \tag{7.1}$$

where t_f^* is the fracture completion time ratio, and L^* is the fracture length ratio.

The usefulness of Equation (7.1) lies in the fact that the fracture completion time for any given fracture length can be predicted from the data for a single test.

TABLE 10

Fracture Times for Slot Models with $a_c \sim L/2$

Model	Hole Diam d, in.	Spacing c, in.	Fracture Length $L = c-d$	Conv. Depth a_c, in.	Fracture Time t_f, sec.
1A	1.0	4.0	3.0	1.5	0.97
1B		8.0	7.0	3.0	5.82
1C		12.0	11.0	5.0	40.6
2A	2.0	4.0	2.0	1.0	0.43
2B		8.0	6.0	3.0	4.4
2C		12.0	10.0	5.0	25.4
3A	1.5	4.0	2.5	1.5	0.85
3B		8.0	6.5	3.0	5.0
3C		12.0	10.5	5.0	34.0
11A	2.0	5.0	3.0	1.5	0.98
13B		8.5	6.5	3.0	5.0
13C		12.5	10.5	5.0	34.0

TABLE 11

Fracture Length and Fracture Time Ratios for Slot Models with Convection Depths Approximately Equal to Half the Fracture Length

Length L_1	Length Ratio $L^* = \frac{L_2}{L_1}$	Time Ratio $t_f^* = \frac{t_2}{t_1}$	Length L_1	Length Ratio $L^* = \frac{L_2}{L_1}$	Time Ratio $t_f^* = \frac{t_2}{t_1}$
2.0	5.5	96.0	6.0	1.83	9.23
	5.25	80.2		1.75	7.23
	5.0	60.0		1.67	5.78
	3.5	13.73		1.16	1.322
	3.25	11.8		1.08	1.136
	3.0	10.38			
	1.5	2.28	6.5	1.69	8.12
	1.25	2.02		1.61	6.8
				1.53	5.09
2.5	4.4	47.4		1.07	1.165
	4.2	39.7			
	4.0	29.7	7.0	1.57	6.97
	2.8	6.78		1.5	5.84
	2.6	5.84		1.42	4.38
	2.4	5.14			
	1.2	1.13	10.0	1.1	1.59
				1.05	1.34
3.0	3.67	42.0			
	3.5	35.2	10.5	1.04	1.19
	3.33	26.3			
	2.33	6.02			
	2.17	5.17			
	2.0	4.55			

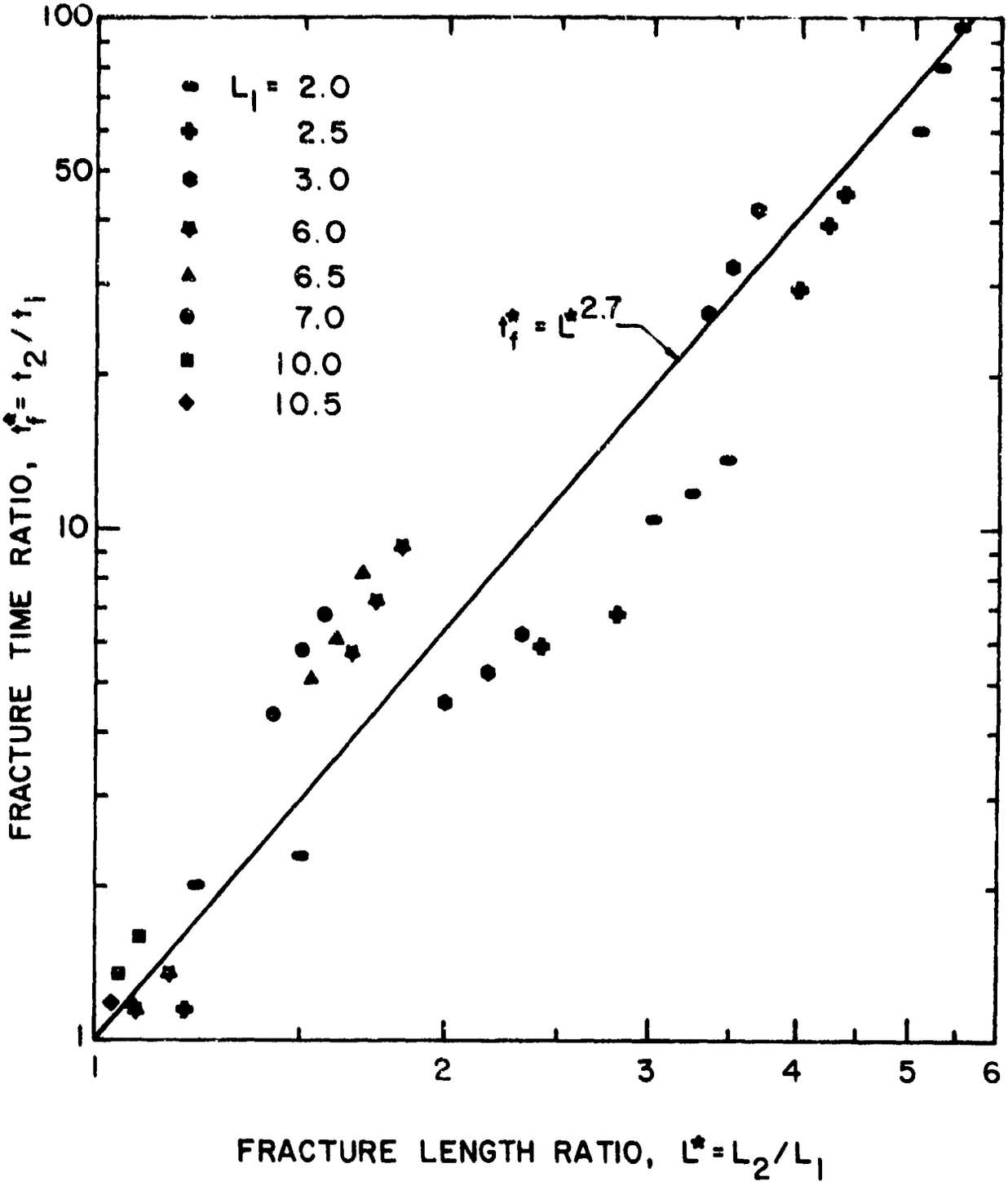

Figure 45. Dimensionless Fracture Time-Length Relationships

Chapter VIII
HOLE MODEL ANALYSIS

The hole model was designed to study the influence of the hole diameter and the hole spacing parameters on the fracture which occurs along the line of a series of holes. Because of its orientation with respect to the working face, this fracture in the subsequent discussion is referred to as the perpendicular fracture.

The model is obtained by passing a cutting plane, parallel to the working face, through the center of the thermal inclusions. The geometry of this model is therefore that of a thin uniform plate with a series of holes. For the plane, two-dimensional thermal stress analysis, the variations in the temperature and the stresses across the thickness are neglected. For the actual problem however, this is only true for the melt depth section as the hole is only partially heated, and as shown in the previous chapter, the fracture initiates in the vicinity of the point of transition from the melt condition to the convection condition and propagates to the surface. It was also shown that the fracture times for the parallel fractures using small or zero convection depths were much higher than those obtained by using convection depths approximately equal to or greater than half the fracture lengths. Thus, the results of the hole model analysis given in this chapter are representative of the upper bound solution of the three-dimensional problem with small hole depths heated along their entire length.

The hole model studies were conducted using three values each of the hole diameter and the hole spacing; the combinations giving nine

different fracture lengths as described in Table 12. The hole diameter and the hole spacing values for these models are the same as those for the parallel fracture studies using the slot models. A typical finite element grid used for the hole model analysis is shown in Figure 46.

TABLE 12

Parametric Description of Hole Models

Model	Hole Dia. d, in.	Hole Spacing c, in.	Fracture Length L = c - d
21A	1.0	4.0	3.0
21B		8.0	7.0
21C		12.0	11.0
22A	2.0	4.0	2.0
22B		8.0	6.0
22C		12.0	10.0
23A	1.5	4.0	2.5
23B		8.0	6.5
23C		12.0	10.5

A. Temperature Analysis:

As in the case of the slot model studies, the fracture time values for the hole models were observed to be small compared to those associated with the steady-state temperature distribution. As a result, the temperature field at the time of the fracture is highly localized in teh vicinity of the melt condition and is independent of the changes in the boundary conditions at the far end. Thus, the hole models are characterized by almost radial, one-dimensional temperature fields as typically illustrated in Figures 47-49.

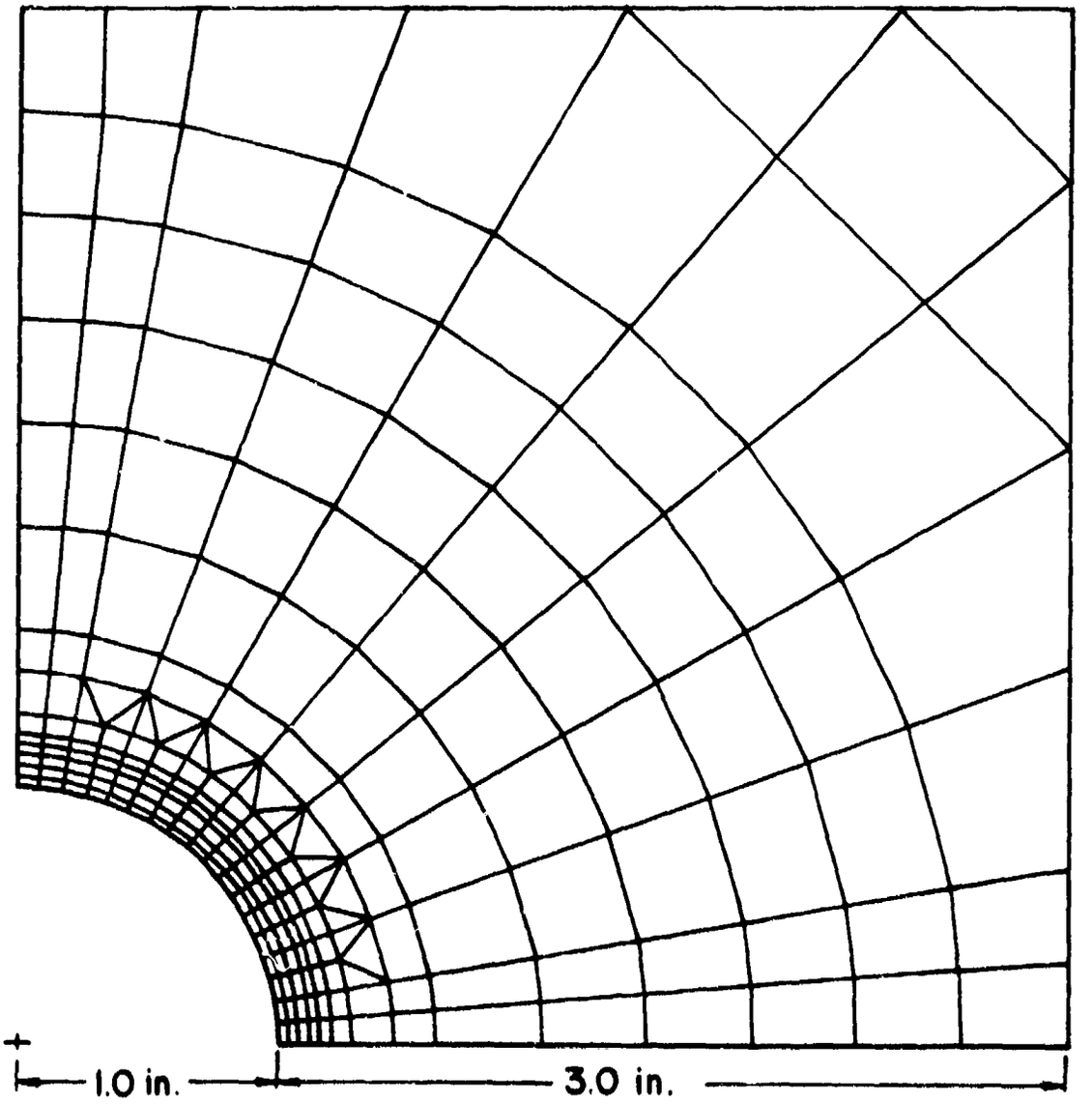

Figure 46. Typical Finite Element Grid for Hole Model Analysis

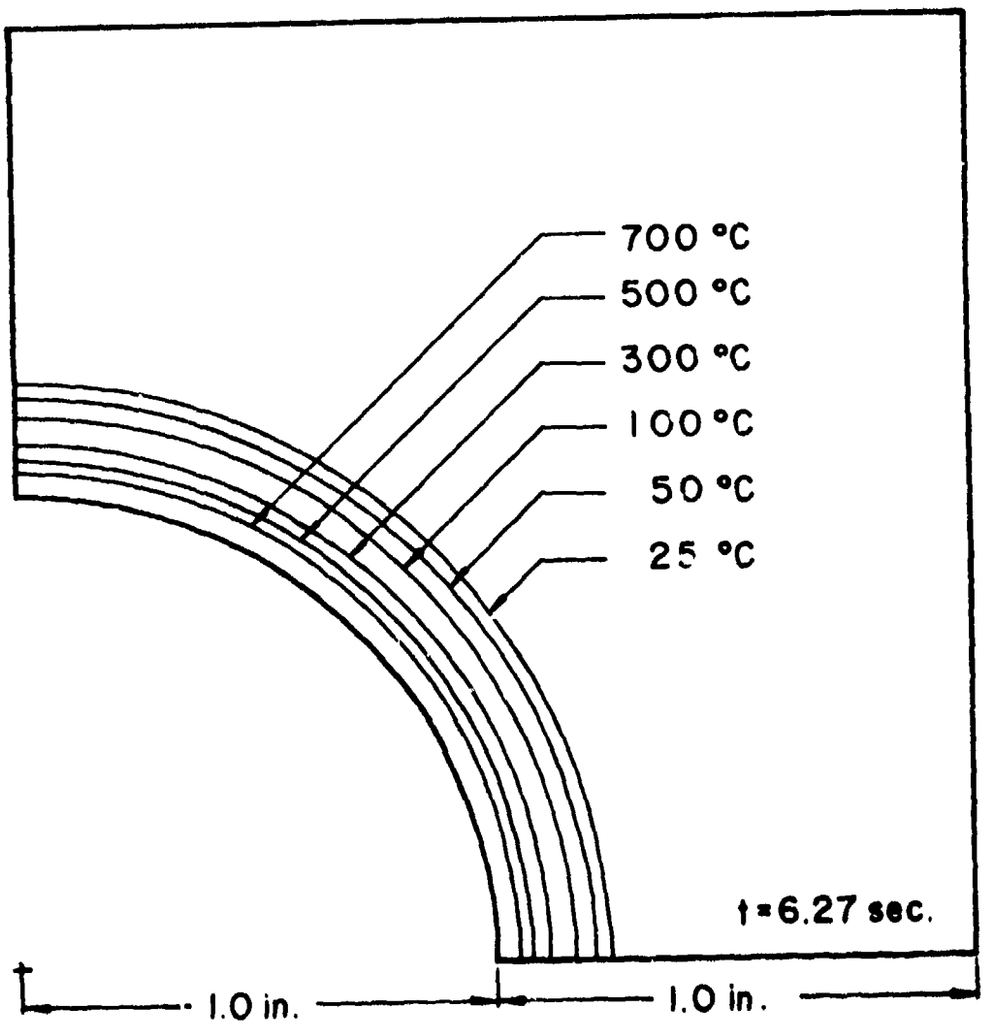

Figure 47. Temperature Distribution, Model 22A

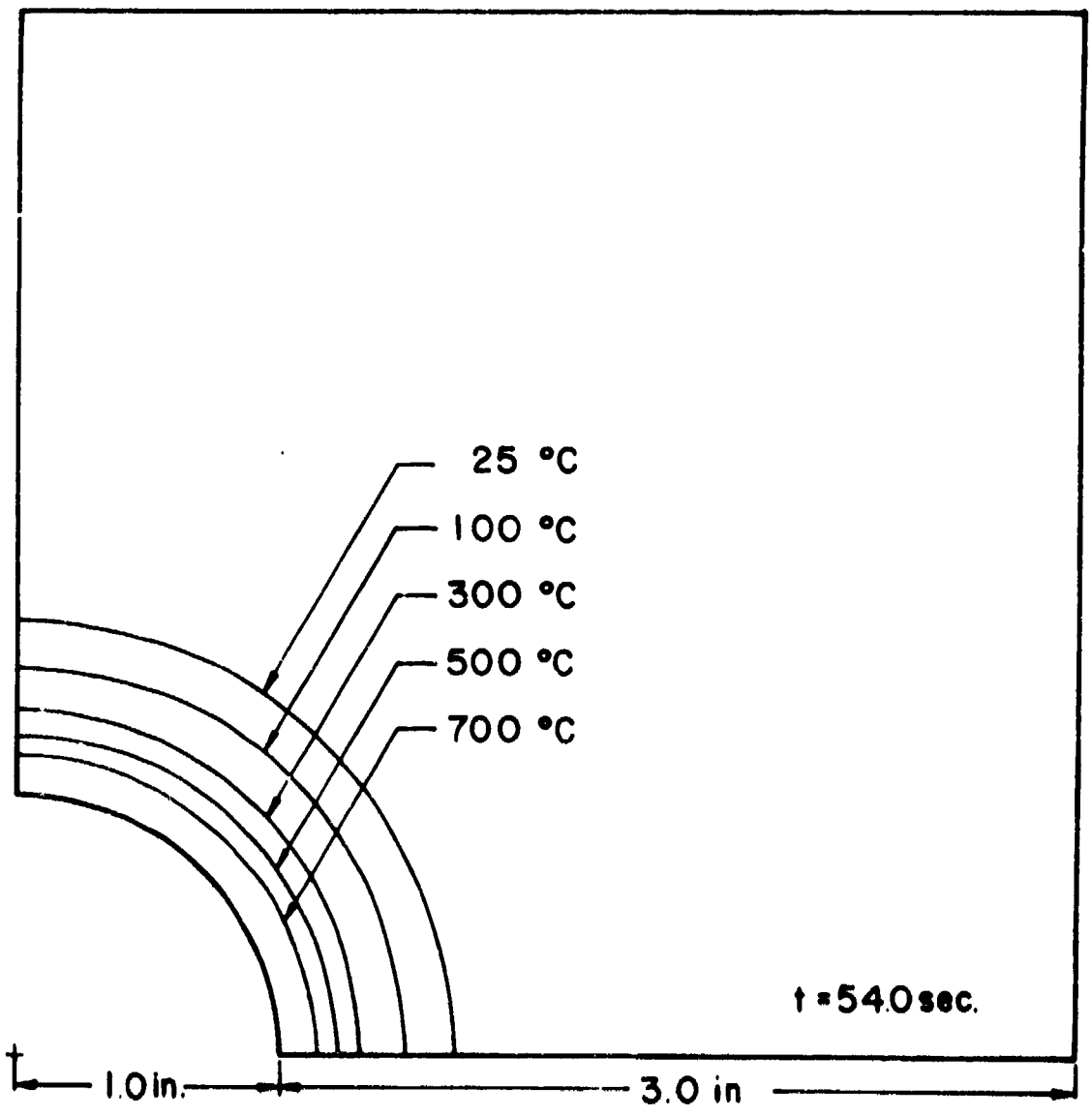

Figure 48. Temperature Distribution, Model 22B

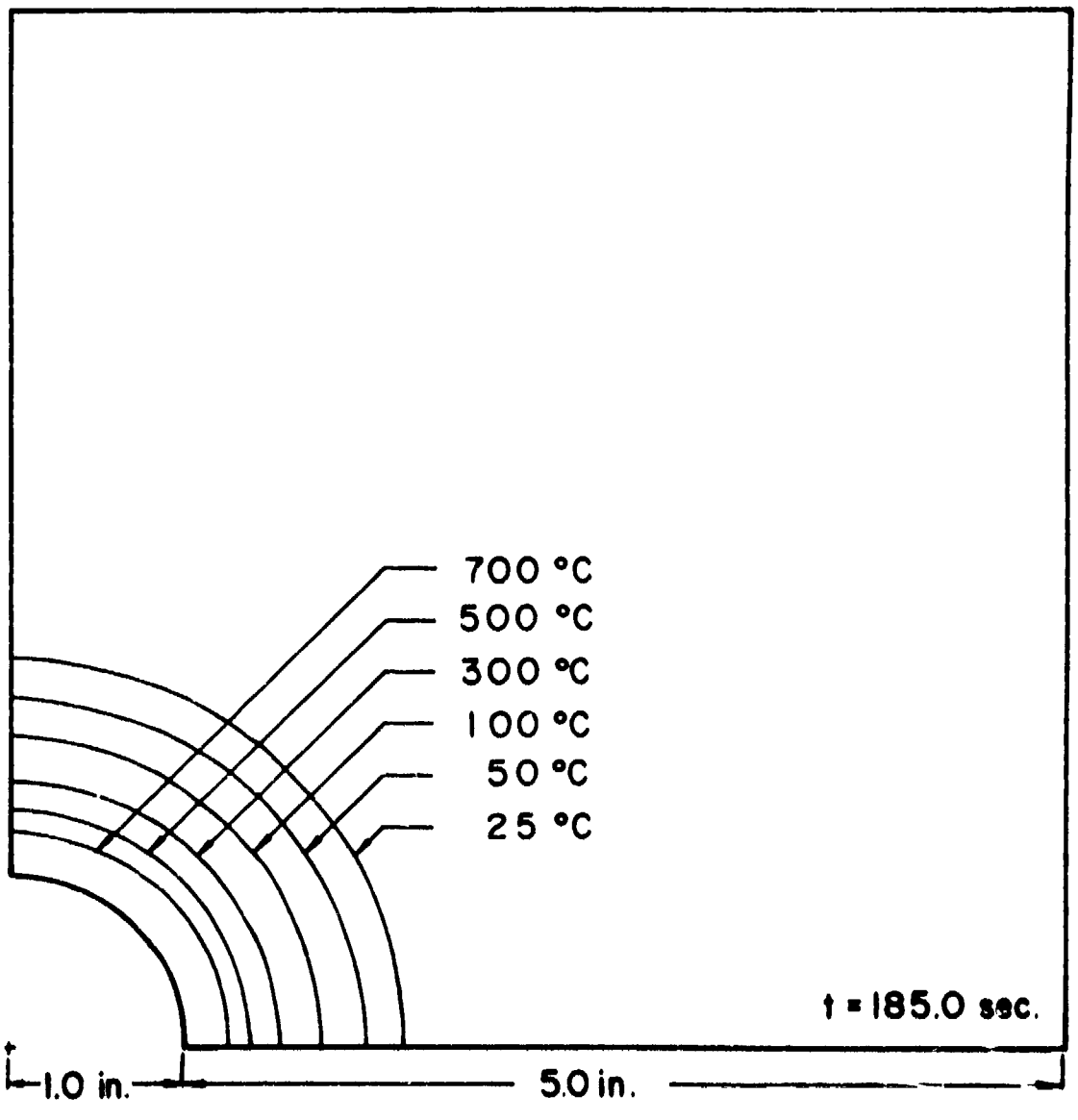

Figure 49. Temperature Distribution, Model 22C

B. Stress and Fracture Analysis:

Unlike the slot models, where the ratio of the cold zone volume to the hot zone volume varies with the convection depth, the volume ratio for a given hole model is constant. Thus, the fracture plots for the hole models are characteristic of those for the slot models with deep holes heated along their entire depth. For slot models with very small convection depths, it was shown in Chapter VII that the fracture zone consists of a McClintock-Walsh zone in the high temperature region, followed by a small Griffith tension zone and a large secondary McClintock-Walsh zone. Also, the fracture completion times for small convection depth models were found to be much higher than those given in Table 10 where convection depths used are approximately equal to the critical values. These two observations are also reflected through the hole model analysis as seen from the typical fracture plots shown in Figures 50-52.

From these results, it can be inferred that the fractures originate in the melt depth section across the holes and propagate to the surface. It can also be observed that, like the slot models, the fracture completion time in the case of the hole models is dependent only on the fracture length, and that the individual variations in the hole diameter and the hole spacing parameters will have no influence on the fracture time provided the fracture length is kept constant. This is obvious from the approximately parallel curves in Figure 53 which show the fracture time versus the hole spacing plots for the hole models with different diameters.

As seen from the temperature plots for the hole models shown in Figures 47-49 , a major portion of the fractured volume does not

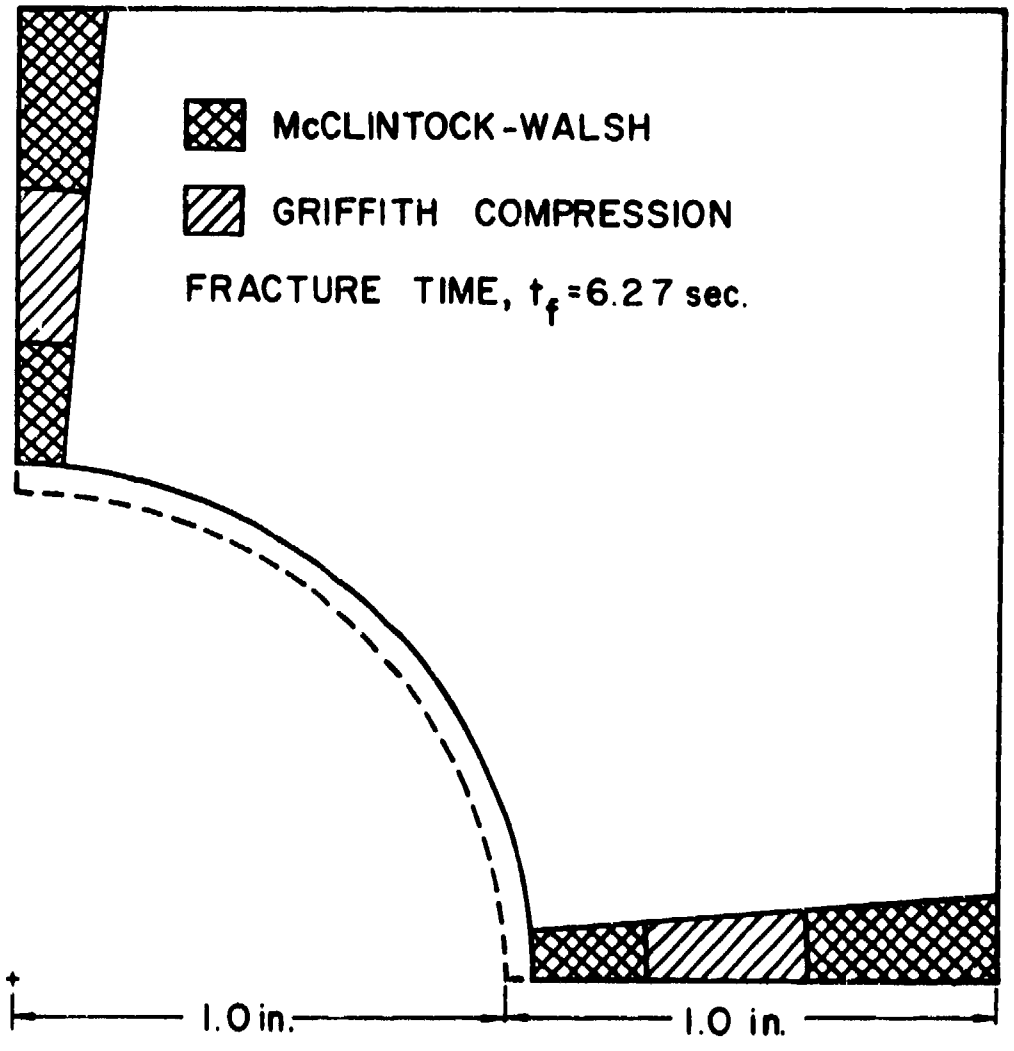

Figure 50. Fracture Zones, Model 22A

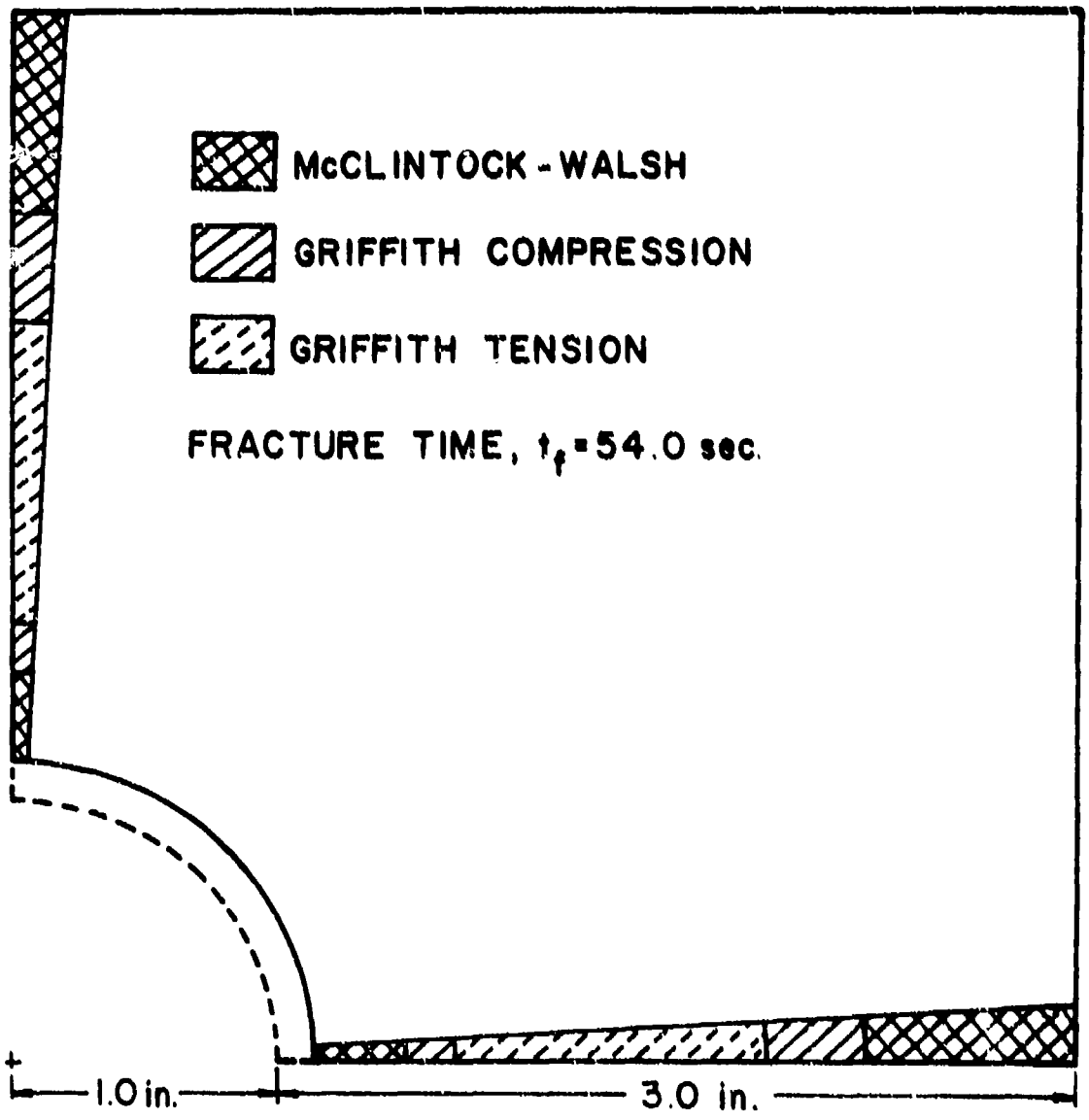

Figure 51. Fracture Zones, Model 22B

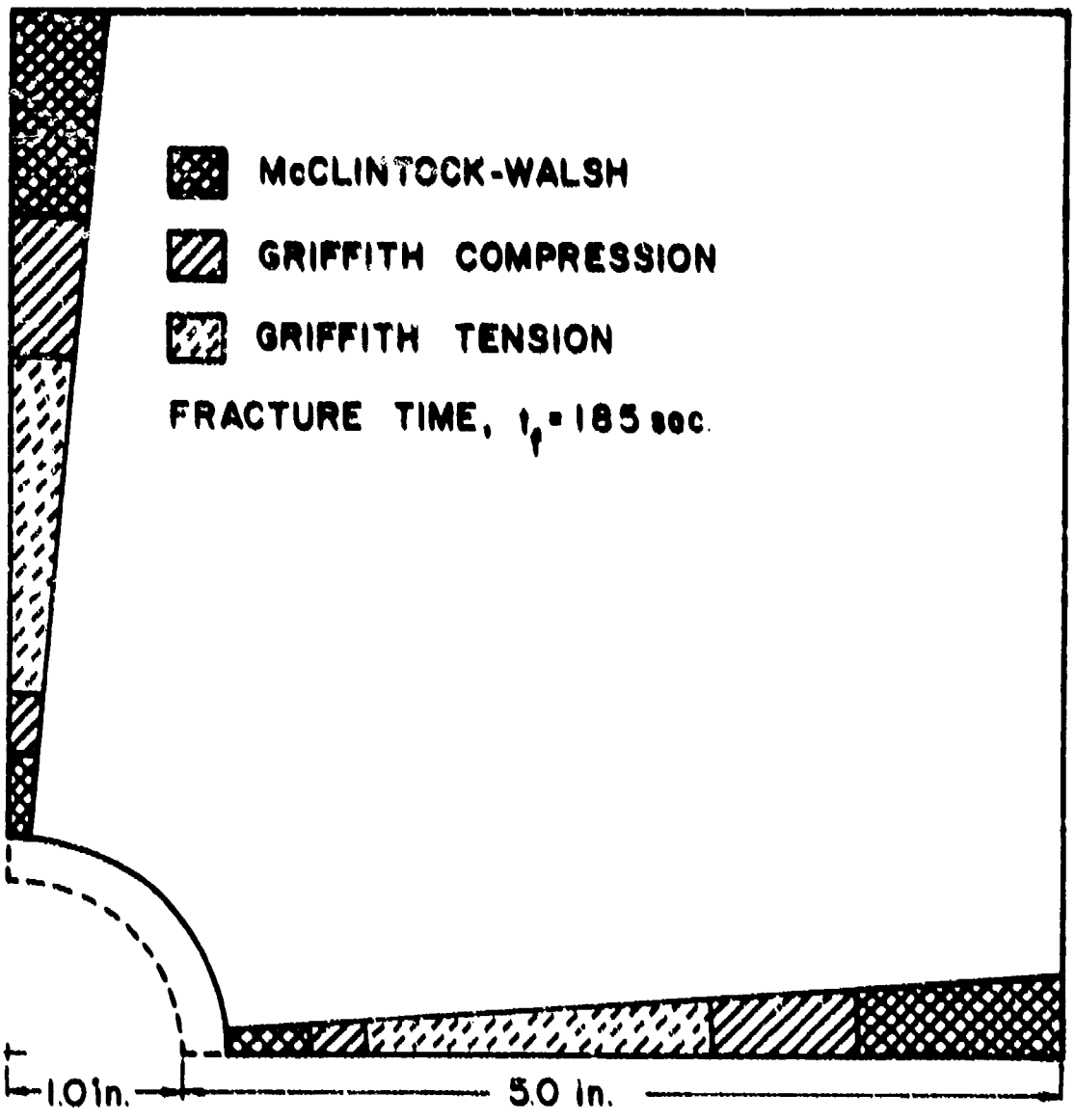

Figure 52. Fracture Zones, Model 22C

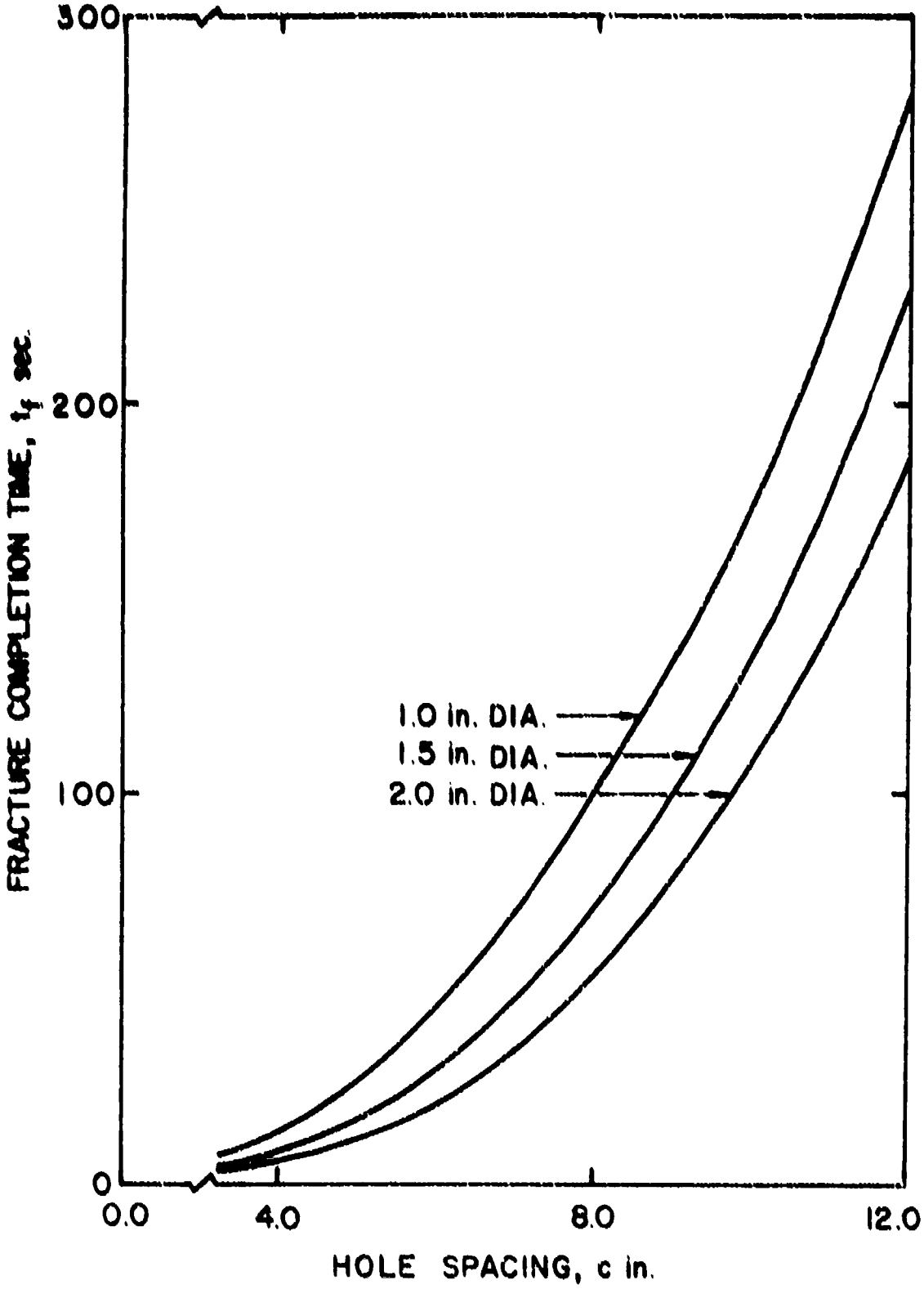

Figure 53. Fracture Time-Spacing Curves for Hole Models

experience any temperature change, and hence, the stresses in this region are due entirely to the load vector resulting from the thermally induced constraint. Thus, the explanation for the sharp increase in fracture completion time with increased hole spacing in the case of the slot models also applies to the hole models.

Comparison of Figures 40 and 53 shows a remarkable similarity between the parallel and the perpendicular fracture characteristics, although for a given problem geometry, the perpendicular fracture time using the hole model approximation is much higher than the parallel fracture time. However, as mentioned earlier, the hole model analysis involves small hole depths without any convection depths and thus, assumes a plane stress condition. In practice, however, the holes are rather deep and the problem appraoches a plane strain condition. Thus, the actual perpendicular fracture times as compared to the actual parallel fracture times will not be as high as theoretically predicted. It should also be realized that while the convection depth will greatly reduce the perpendicular fracture time as in the case of the parallel fracture, any increase in the convection depth will mean the heat source will have a greater burden against which to open cracks between the holes.

Chapter IX

HEAT TRANSFER IN ROCK MATERIALS OF SIMPLE GEOMETRIC SHAPE

The objective of this part of the research was to determine the temperature distribution within a rock material resulting from an internal cylindrical heater. The information obtained should provide a means of evaluating heater performance as well as insight into the appropriate boundary conditions at the internal rock surface due to primarily radiant heat sources. The heaters were constructed from Kanthal wire coils wound on alumina cylinders.

Discussion of Analytical Problem

For thermal rock fracturing processes there is a need for a method for solving transient heat transfer problems with variable thermal properties and/or radiation boundary conditions. The development and operation of a three-dimensional code would be expensive for complete nonlinear conditions. The equations of heat transfer for this type of problem are:

$$\nabla(k\nabla T) = \rho c \frac{\partial T}{\partial t} \tag{9.1}$$

$$h(T-T_\infty) = k \frac{\partial T}{\partial n_1} \tag{9.2}$$

$$\epsilon\sigma(T^4-T_0^4) = k \frac{\partial T}{\partial n_2} \tag{9.3}$$

The partial differential equation is nonlinear due to the temperature-dependence of the material properties. The radiation boundary condition is also nonlinear.

There are two-dimensionless codes available which will solve the linear transient heat transfer problem. A nonlinear, two-dimensional steady state code is also available. The available two-dimensional,

transient code is being modified to solve problems with temperature-dependent material properties.

Heat Transfer Study

The method of heat transfer from the Kanthal heaters to the rock surfaces is a complicated combination of convection, radiation and conduction. An exact analysis or even an experimental measurement of the temperature distribution inside a large rock mass would be difficult. However, the most important function which a boundary condition performs is to determine how much heat actually enters the rock body. The mode of heat transfer which is employed at the boundary is of secondary importance.

Discussion of Experimental Problem

An ideal experiment gives direct readings of physical events without analytical or experimental manipulation. Since it is not possible to measure the temperature directly inside a rock specimen, the experiment should be designed as close to the ideal experiment as possible. To minimize the analytical manipulation, a one-dimensional model was chosen.

A basic heat transfer study was devised to determine the heat flux entering the rock as a function of time. This study consisted of designing an experimental test which would have essentially one-dimensional heat flow and then measuring the temperature as a function of time. The temperature history will be used in future work to estimate the surface temperature as a function of time. Thus, a time-dependent temperature boundary condition will be available for further analytical studies.

The shape of the Kanthal heaters is cylindrical and the natural shape for the rock specimen would also be cylindrical. Figure 54 shows the heater, rock specimen, four thermocouples and two end plugs. The end plugs are used to prevent excessive convective currents.

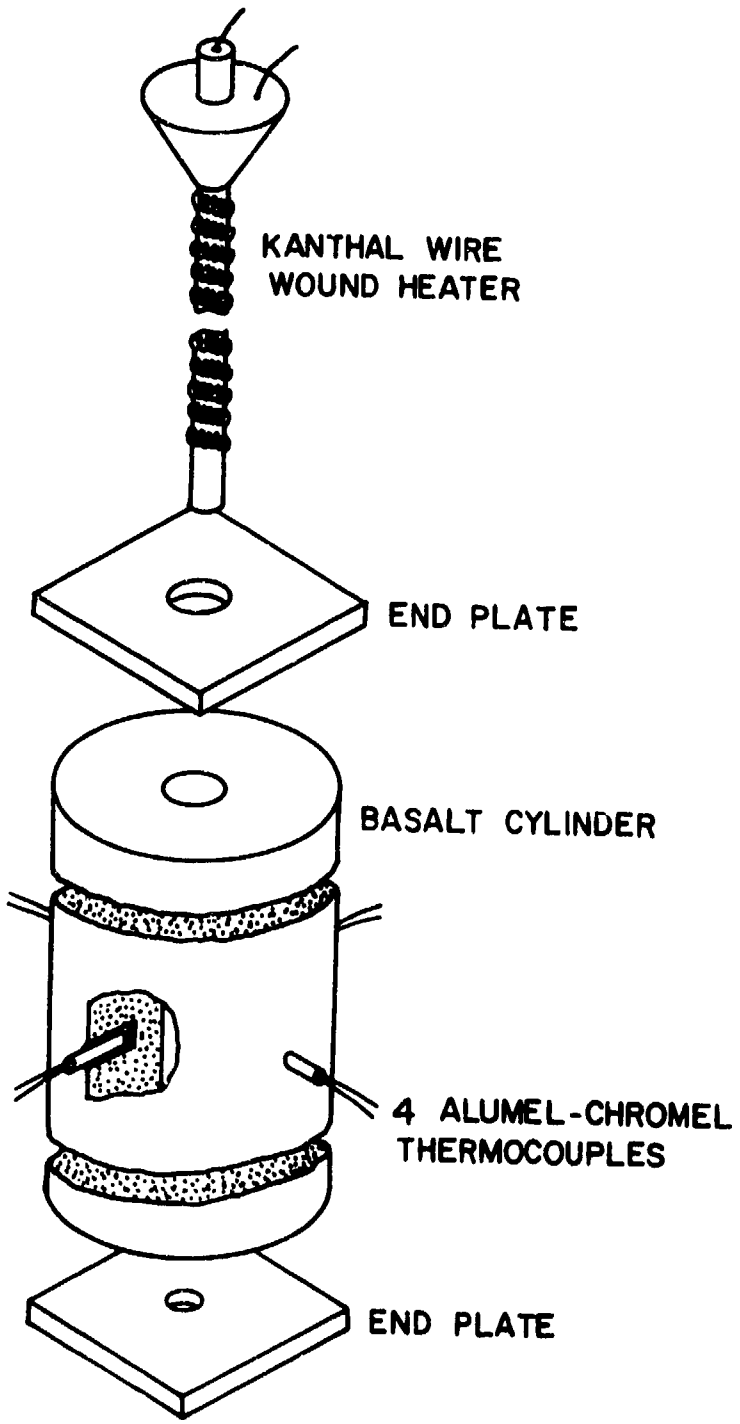

Figure 54. Experimental Configuration for Cylinder Tests

Since the basic shape was determined, the actual dimensions had to be determined. A special heater was built whose outside diameter was somewhat less than one inch. Also, the largest core drill presently available at the RMERC has a four-inch inside diameter. The outside diameter of the rock specimen then was, from logistical considerations, four inches and the inside hole diameter was one inch. The length of the rock specimen had to be determined so that nearly one-dimensional heat flow is experienced at the mid-plane of the cylinder. This length was to be determined by considering two important factors:

a) A steady state analysis will show the two-dimensional effects more strongly than a transient analysis, and

b) Through numerous tests with Kanthal wire heaters, the rock surface has never been melted.

Thus, if a two-dimensional model was designed based on a steady state analysis and an absolute maximum temperature condition, (i.e., the surface at the material melt temperature), then the design should be valid for transient conditions. The method of study was to select grids representing one-eighth (from symmetry and thermocouple placement) of the rock cylinder with boundary conditions of a melting inner surface and convection on the outer surface and find the steady state temperature distribution. A typical grid shown in Figure 55 was drawn for five length-to-depth ratios (L/D= 2-10) and the temperatures were calculated with constant conductivity and then temperature-dependent conductivity. Dresser basalt was chosen as the rock material for two reasons:

a) Material properties are given in Reference 64.

b) Basalt is easier to machine than most other hard rocks.

The value of h was given in Reference 68 as h = 1.57 Btu/hr-ft^2-°F. For the constant conductivity case the conductivity corresponding to zero degrees was used as a starting point of iteration.

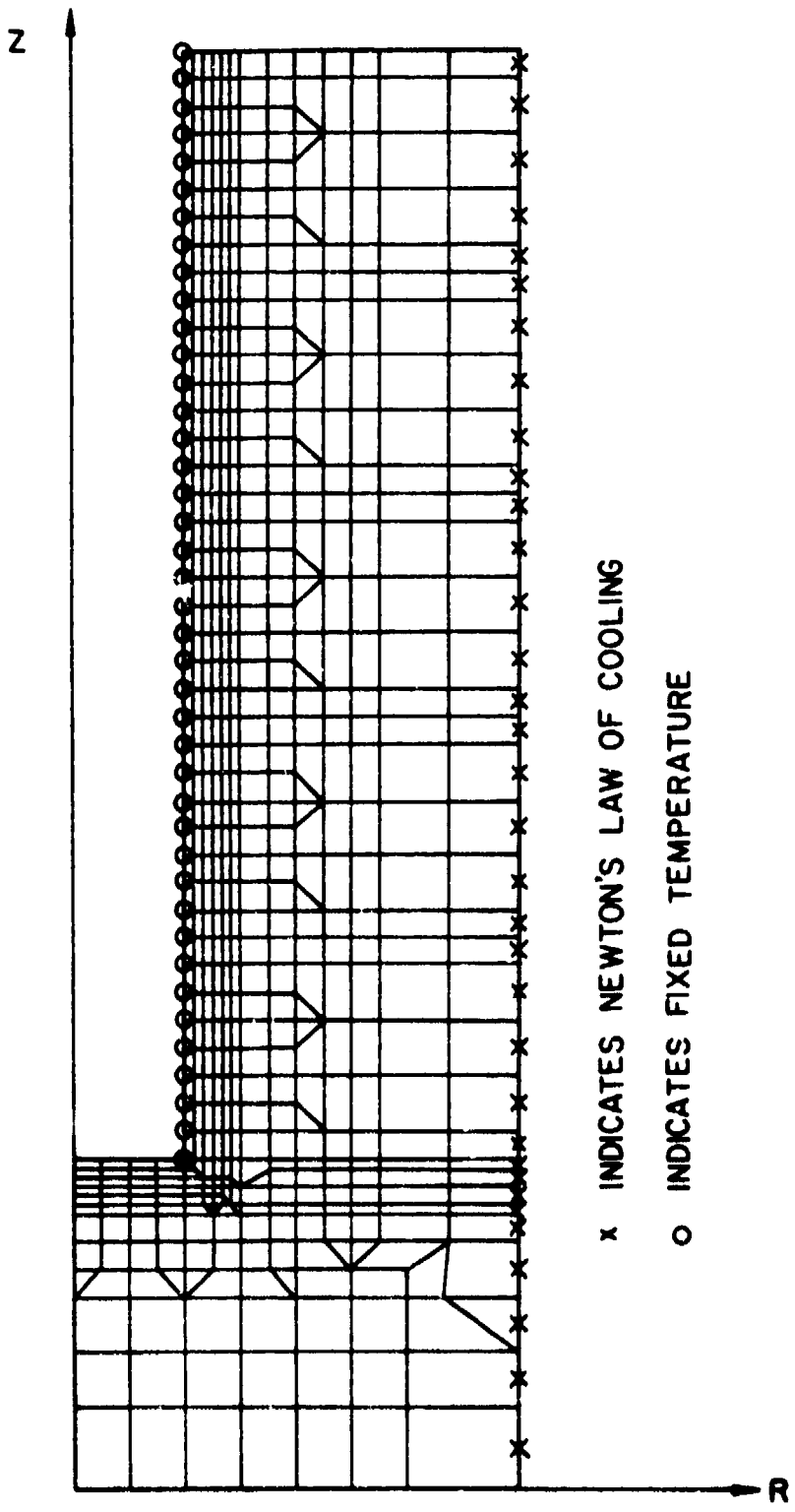

Figure 55. Typical Finite Element Grid for Cylinder Model (L/D=10)

The isotherm produced by the zero degree value of conductivity and the final value of conductivity are typically shown in Figures 56 and 57. The radius of the center hole is 1/2 in. and the data indicates that within 4 mm of the surface, the heat flow is essentially one-dimensional for all of the ratios of L/D.

A bound on the error due to placing a thermocouple in the rock cylinder was needed. A new grid (Fig. 58) was made which would represent 1/8 of the circular section of the cylinder. Then the material was designated as solid basalt and as basalt with a thermocouple, insulator and a small air space. The tip of the thermocouple was allowed to be at 1 mm, 2 mm, 3 mm, and finally at 4 mm. Boundary conditions were Newton's law of cooling on the outer surface and the basalt melting temperature (1250°C) on the inner surface. The values of conductivity for air, chromel-alumel and omegatite were assumed constant and are given in Table 13.

TABLE 13

Material	Conductivity Btu/hr ft °F
Air	.0303
Chromel-Alumel	24.08
Omegatite	14.5

Figures 59 - 62 show typical isotherms for the constant conductivity case and for the temperature-dependent case.

Table 14 gives values of the error produced by the thermocouple in the rock specimen by depth. The maximum value of 6.12 percent error is an acceptable amount considering that a steady state analysis was used and as an assumption in solving the grid of Figure 58, all

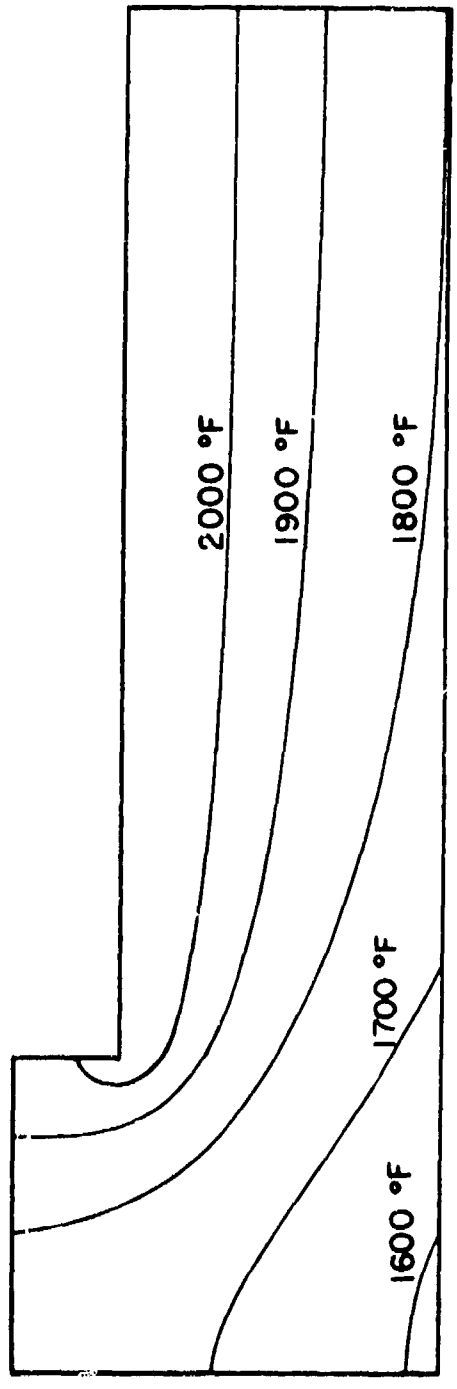

Figure 56. Steady State Temperature Distribution for Constant Thermal Conductivity (L/D=10)

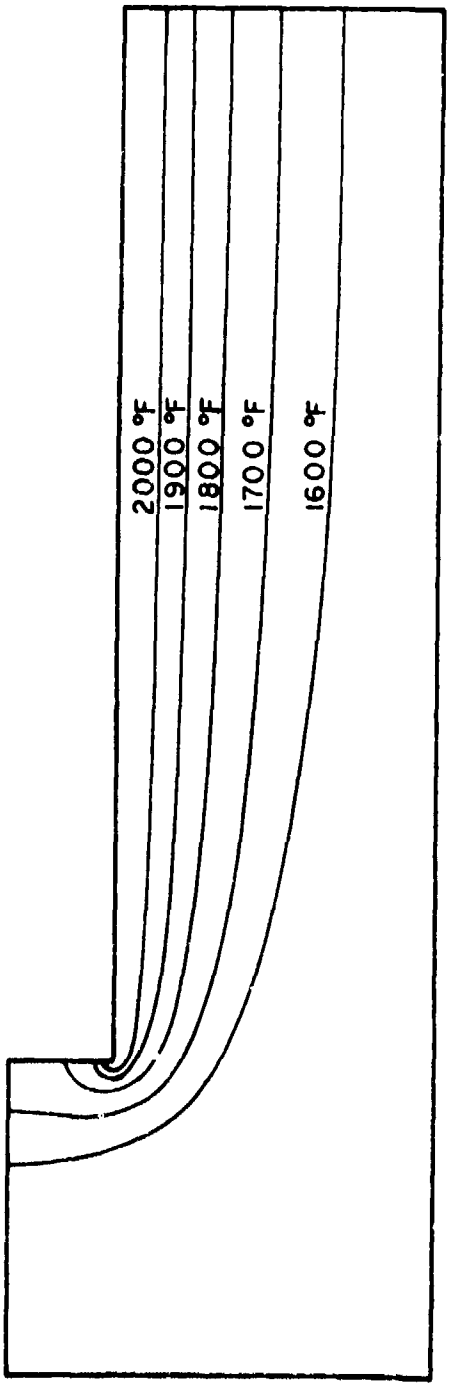

Figure 57. Steady State Temperature Distribution for Variable Thermal Conductivity (L/D=10)

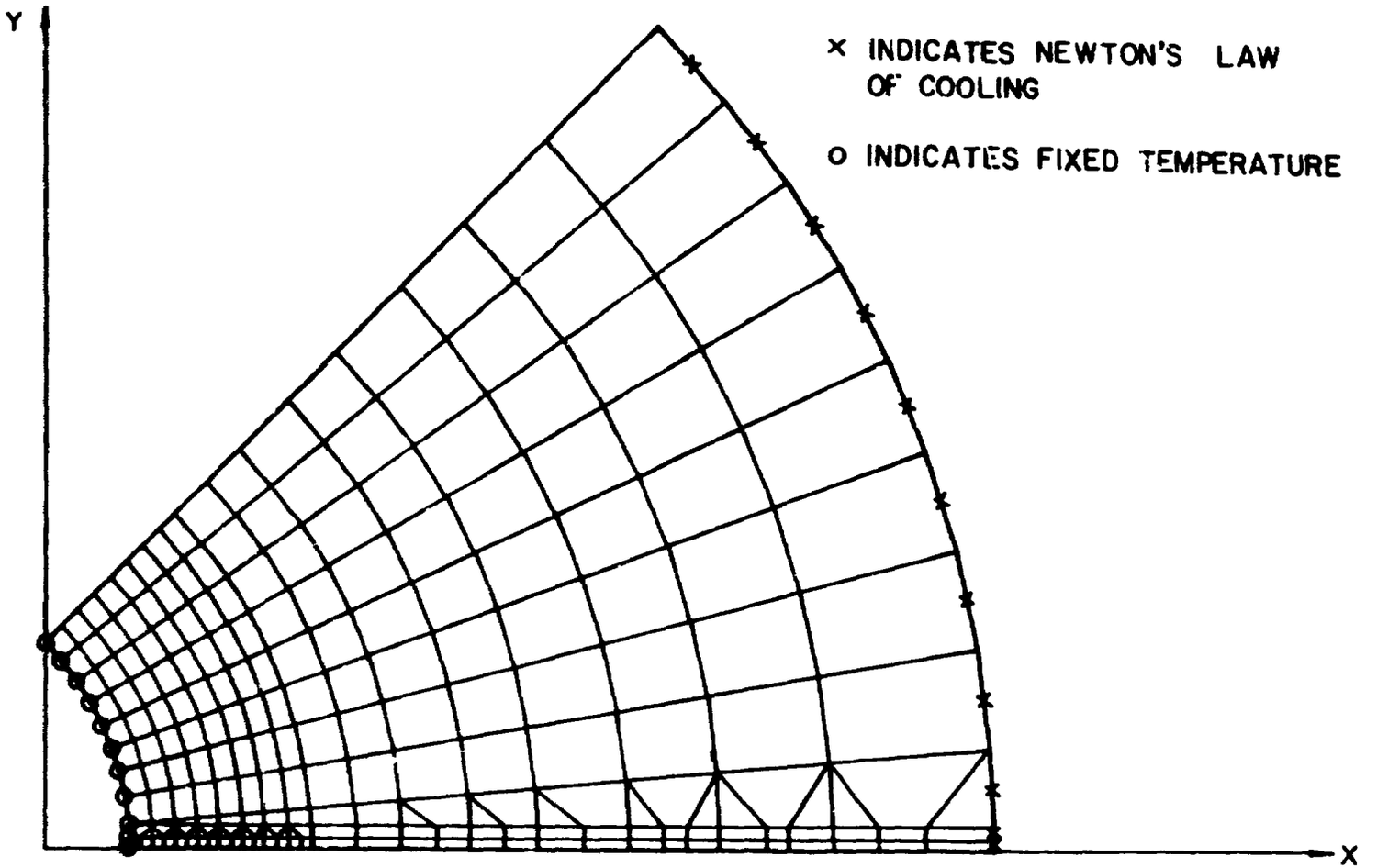

Figure 58. Typical Finite Element Grid for Cylinder Model with Thermocouple

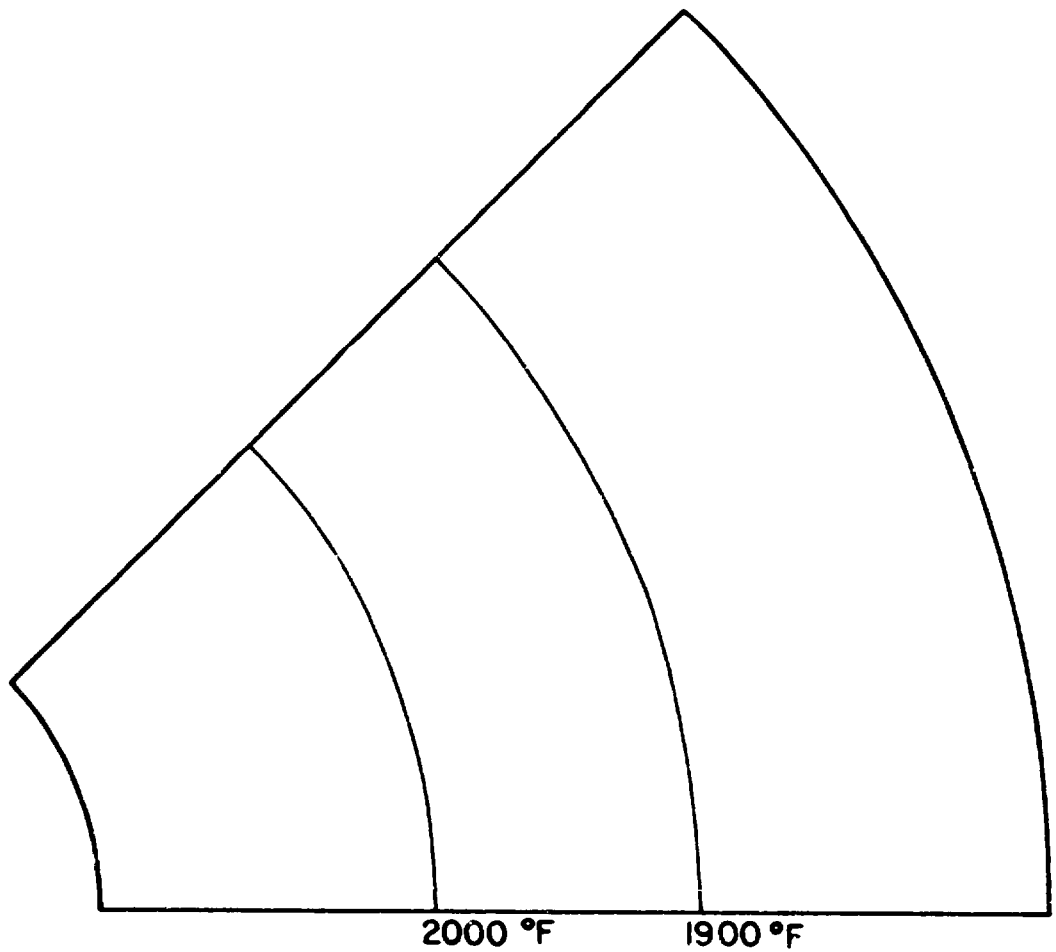

Figure 59. Steady State Temperature Distribution for Constant Thermal Conductivity without Thermocouples

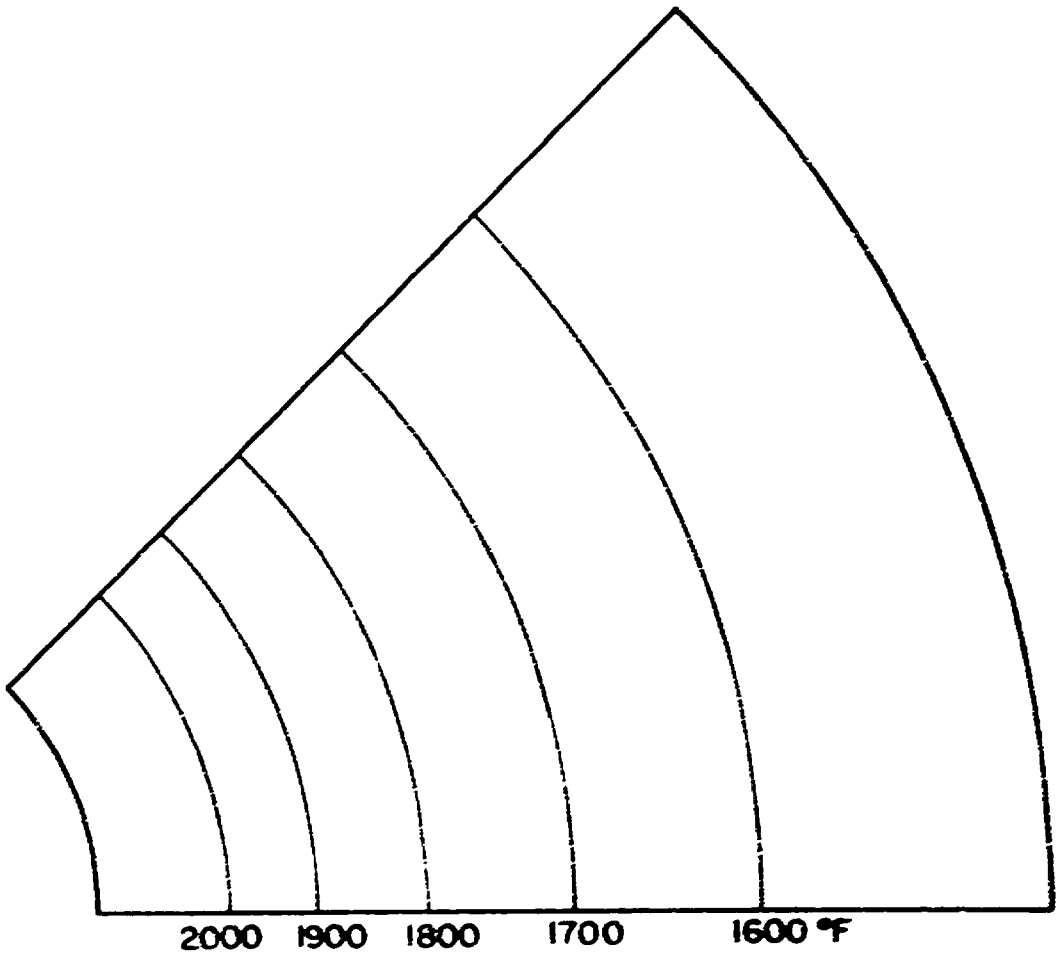

Figure 60. Steady State Temperature Distribution for Variable Thermal Conductivity without Thermocouples

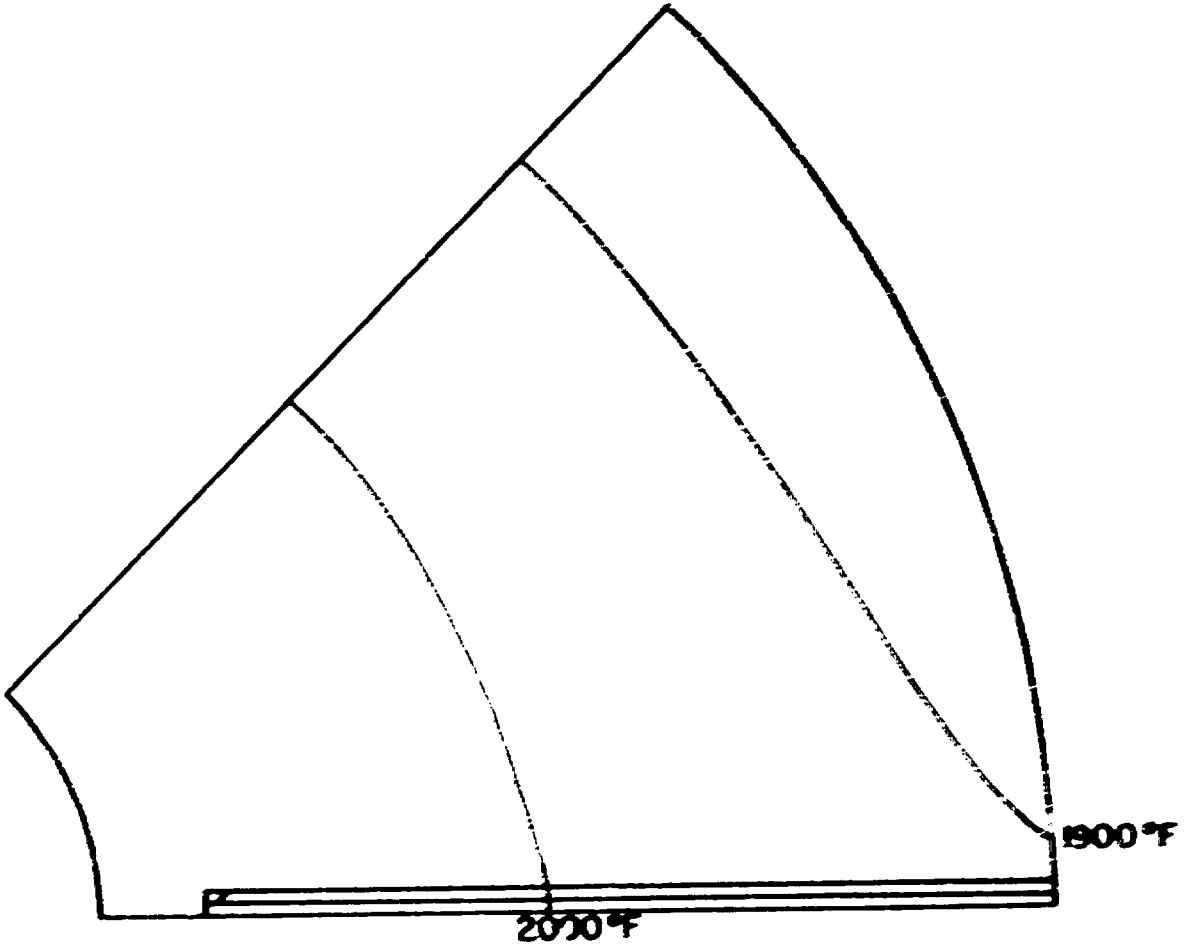

Figure 61. Steady State Temperature Distribution for Constant Thermal Conductivity and Thermocouples 4 mm from the Surface

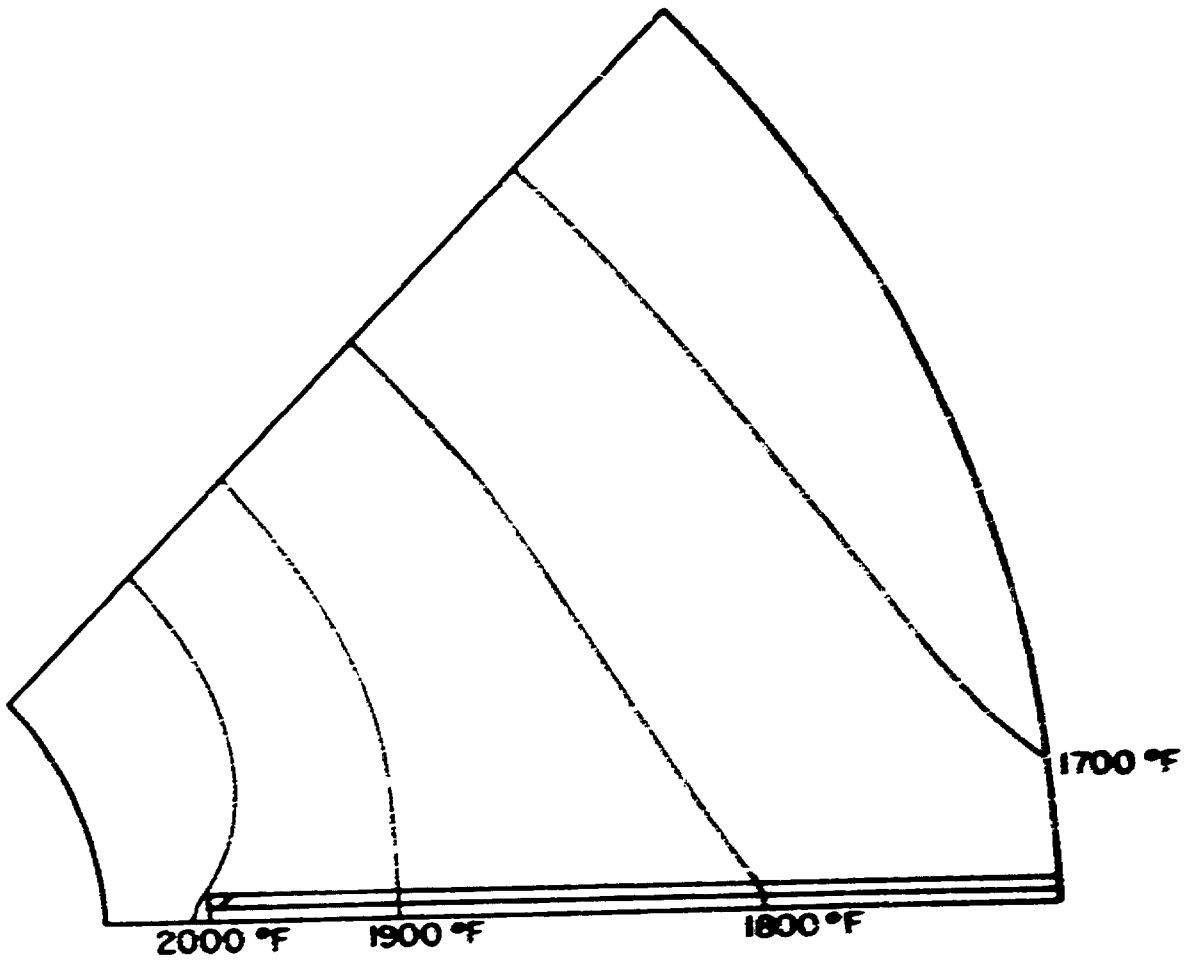

Figure 62. Steady State Temperature Distribution for Variable Thermal Conductivity and Thermocouples 4 mm from the Surface

elements were taken as having unit thickness. This assumption of unit thickness would magnify the actual error produced by the thermocouple thickness.

TABLE 14

Depth	Temperature Solid Wedge	Temperature Wedge with Thermocouple	Temperature Difference	% Error
1 mm	2162.783	2048.450	114.333	5.27
2 mm	2118.149	2020.116	98.033	4.67
3 mm	2077.643	1950.512	127.131	6.12
4 mm	2040.612	1950.820	89.792	4.31

The next step was to construct the rock specimens and measure the temperatures produced by the Kanthal heaters.

From the temperature measurements a one-dimensional analysis is to be made to determine the rock surface temperature as a function of time. This temperature function will then be used in the two-dimensional programs to calculate the temperature distribution within rock materials.

Experimental Results

Figure 63 shows the temperatures of the rock at 1 mm depth for three selected power settings. Figure 64 shows the outside surface temperatures for the same power settings of Figure 63. Figure 65 shows the four thermocouple readings for a maximum power setting.

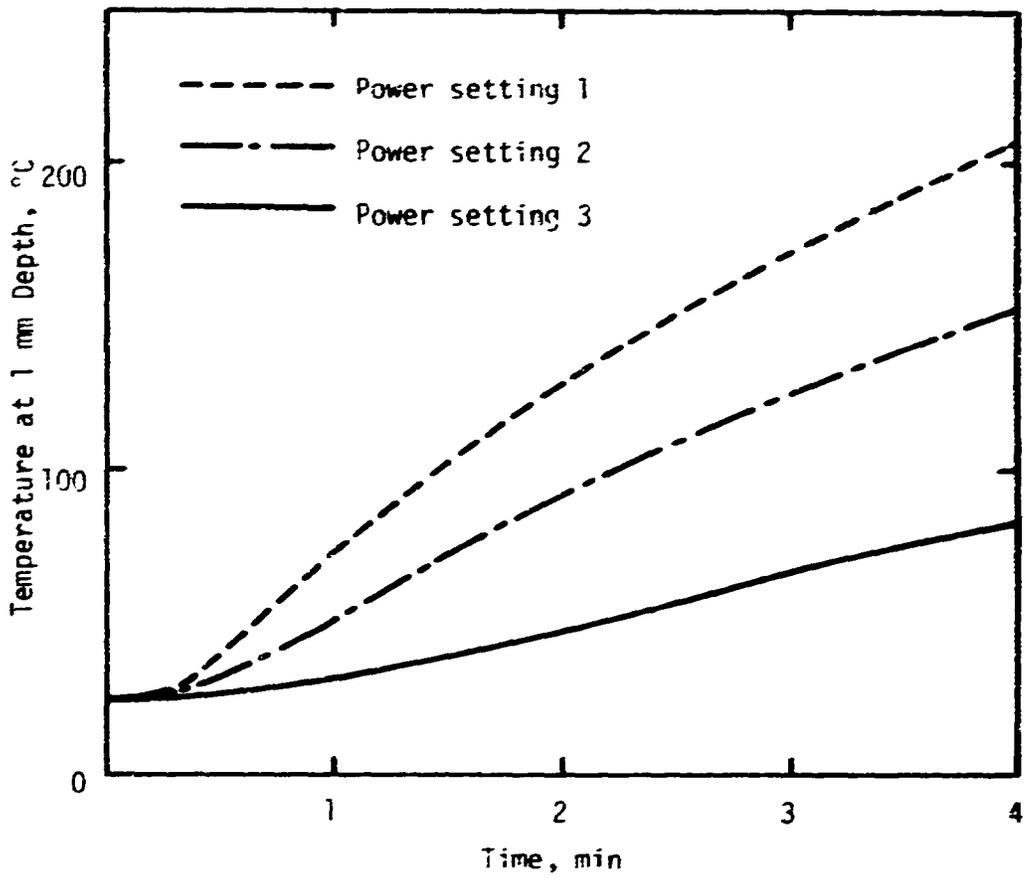

Fig. 63. Temperature Variation with Time at 1 mm from the Inner Surface for a Dresser Basalt Cylinder.

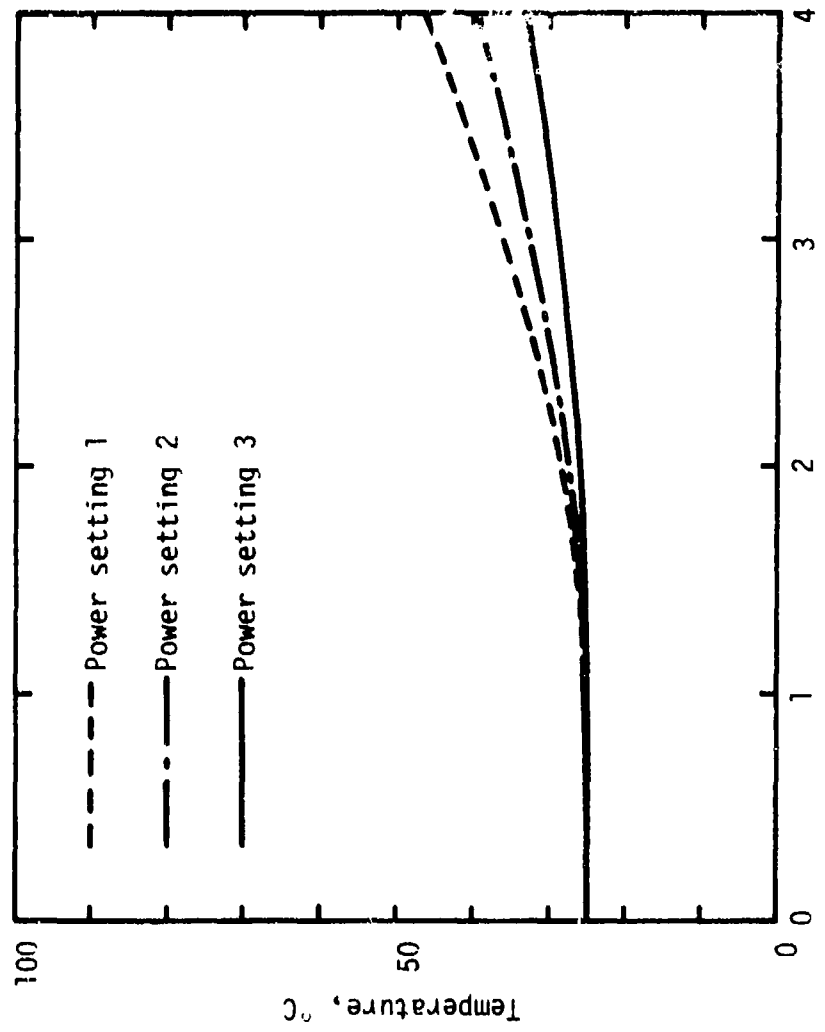

Fig. 64. Outside Surface Temperature Variation with Time for a Dresser Basalt Cylinder.

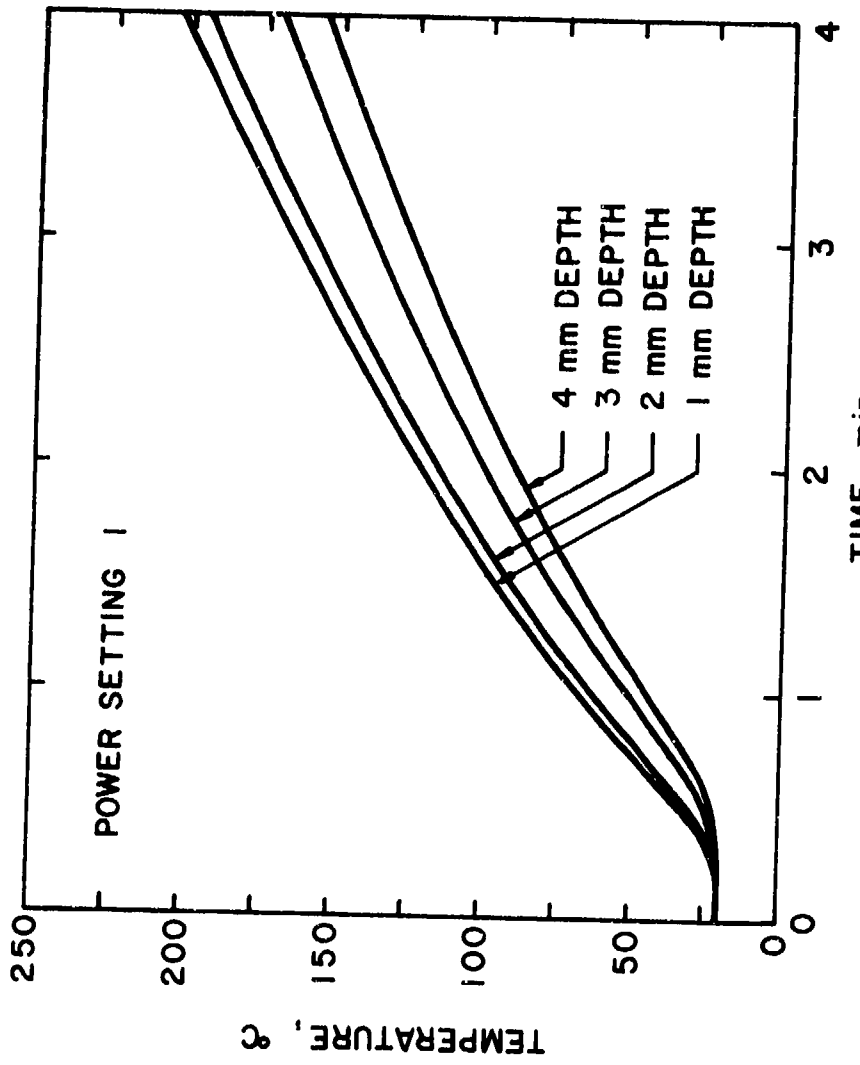

Fig. 65. Temperature Variation with Time for a Dresser Basalt Cylinder.

Chapter X

LABORATORY AND FIELD FRACTURE TESTS

Introduction

Research on thermal fragmentation of hard rock was begun at UMR in 1969 and has been carried out in three phases:

1. Surface heat weakening and chipping.
2. Mechanical slot cutting and thermal kerf removal.
3. Investigation of a thermal round similar in design to an explosive round.

In phase one the surface of blocks of selected igneous and metamorphic rock was subjected to heat from a small flame jet torch causing shallow fractures. The rock was then chipped off with a traversing jackhammer. It was found that while the surface of most of the rocks tested was weakened by heat, rock removal by impact was not enhanced by the heating process.

In phase two slots 1-3/4 inches wide by six inches deep were cut in the surface of three-foot cubes of granite, quartzite and basalt, with six-inch ridges in between the slots. When heat was applied to the bottom of the slots the ridges between were readily fractured off from the rock face.

Phase three is being devoted to the investigation of the feasibility of developing a thermal round which will function in principle in a manner similar to an explosive round. The application of heat at the bottom of deep slots within the rock in phase two demonstrated clearly that the rock is much more effectively fractured if the heat energy is deposited within the rock.

Thermal Stress Fracture of Rock

It is a well established principle of blasting that a cylindrical column of explosive must have one or more free faces to which to break. With stress waves generated by explosives the free face provides a means for spallation to occur and subsequent fracture to the explosive will take place in a properly designed round. Each hole is placed so that it will provide the necessary free faces to which other holes may break.

The process of fracture from thermal inclusions is different in several ways from fracturing by explosives. When a heater is placed in a hole in the rock a thermal stress is generated around the hole. The immediate periphery of the hole is in biaxial compression with a tensile stress beyond. The magnitude of the tensile stress depends upon the properties of the rock, the temperature and the radius of the hole.

The nonstationary state of stress due to a constant temperature suddenly applied to a spherical cavity in an infinite medium was analyzed theoretically by Sternberg (83). The radial displacement of the cavity surface is zero for all time. The temperature drops rapidly with distance away from the cavity surface (Fig.66) and does not penetrate beyond 3 cavity radii for $\tau = 3$ ($\tau = \frac{\kappa t}{a^2}$, t = time, κ = diffusivity and a = cavity radius). Radial displacement increases with time as does the radial stress, which is always compressive. The tangential stress at a given r/a greater than one is compressive, becomes tensile and then compressive again with increase in time. The magnitude of the tensile stress decreases with r/a.

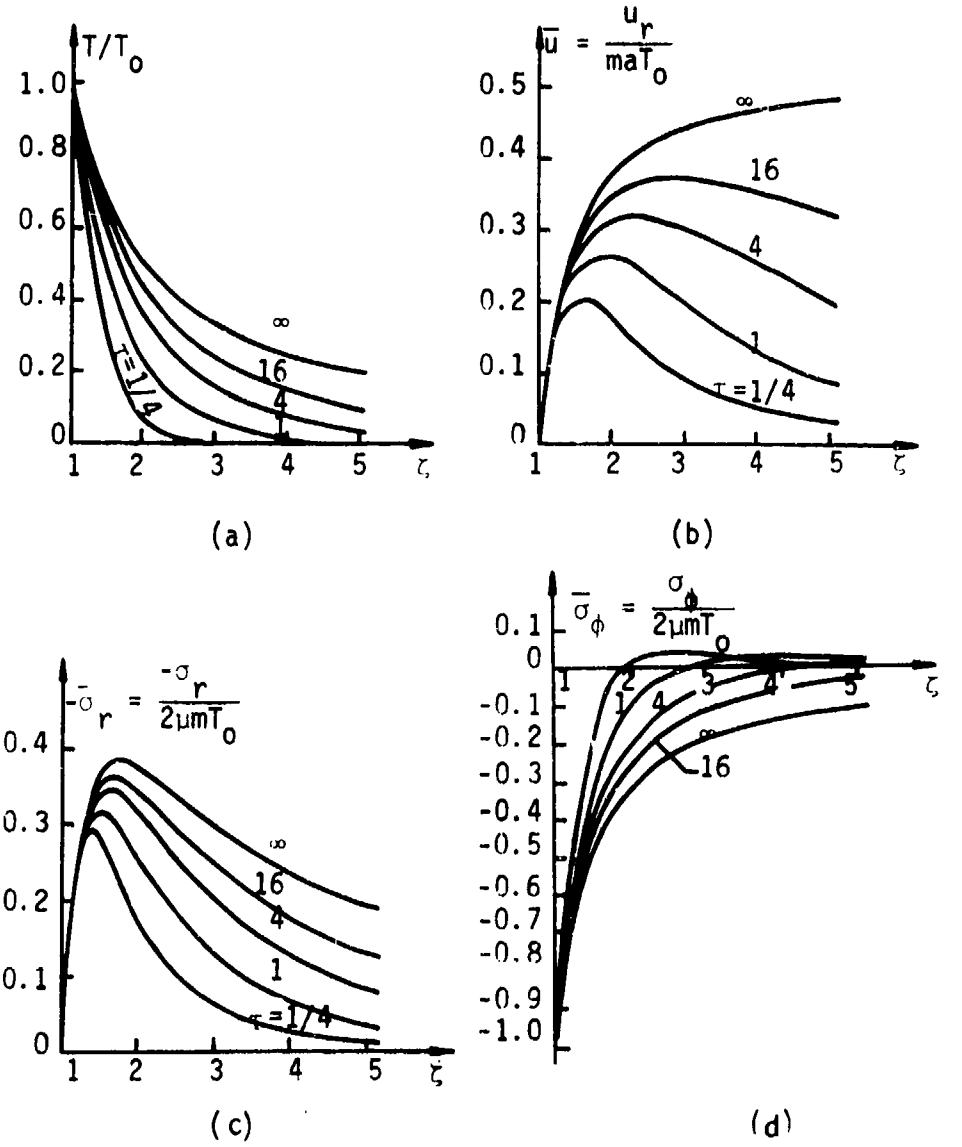

Fig. 66. Temperature Distribution, Displacement, and Thermal Stresses Around a Spherical Cavity in an Infinite Medium ($\zeta = r/a$).

For constant diffusivity, the magnitude of the tangential tensile stresses is largest for small values of r/a, or for large values of the cavity radius, and increases linearly with the cavity temperature.

The curves in Figure 66 may serve as approximate guides to the thermal stress history around the thermal inclusion created by carbon electrodes in a hole in a solid granite face. However, the cavity in granite increases in size with time and some of the rock properties are temperature dependent. Also, the stress pattern is altered by the presence of the drill hole.

The analysis by Sternberg (83) agrees qualitatively with that by Nixon (4), the latter being the (cylindrical) finite element thermal stress analysis for electron beam penetration. That is, the magnitudes of compressive stresses are ten times those of the tensile stresses, and for longer heating times the zone of tension extends considerably beyond the heater zone.

The initiation and propagation of fractures in rock in the configurations used herein due to internal thermal stresses are controlled by two important factors, (1) the magnitude and direction of the tensile stresses, and (2) strain relief due to compressibility of the rock or nearby tractionfree surfaces.

Displacement Relief and Fracture

When a high temperature heat source is placed in a cylindrical or spherical cavity in an infinite (rock) medium thermal stresses are induced in patterns as indicated above (Fig. 66). This may be shown graphically for a given time after a temperature T_0 has been applied to the surface of the cavity. When σ_θ in the tensile zone exceeds the tensile strength of the material a crack normal to the stress direction will form.

However, the distance it will propagate and the amount it will widen depends upon strain displacement relief in body which may permit displacements. In nonporous hard granite it has been found that the rock cannot readily move normal to the crack unless there are three planes or faces of strain relief within critical distances. (In this respect thermal stresses function differently than explosively induced stresses which will create craters with only one free face). With less than minimum displacement relief only hairline fractures are formed, extending into the cavity and a short distance into the rock. However, where free faces are present and multiple heater holes furnish stress fields which reinforce each other, cracks propagate for longer distances and widen to 1/4 inch or more due to the expansion of the rock around the cavities. The blocks of rock formed by the fracture are easily removed. That is, thermal forces have demonstrated a significant amount of follow-through in dislodging the fractured blocks in experimental tests.

Experimental Results - Laboratory

Thirumalai (8) had shown earlier that thermal inclusions generated by dielectric current would readily fracture small blocks of basalt but not quartzite. Thus, a positive method of heating was desired which is independent of the electrical properties of the rock. In the first experiments coiled nichrome wire was wrapped in a spiral on alundum cores and placed in pneumatically drilled holes in three-foot cubes of quartzite and granite. The heaters successfully fractured the rock parallel and perpendicular to the heater holes, but the nichrome wire burned out at sustained temperatures of 600° to 700°C. Kanthal wire resistance heaters were employed at temperatures of 900° to 1200°C. These fractured the rock more readily, but also burned out in heater holes in granite at sustained temperatures of 1000°C. They were, however, employed

successfully to fracture granite in place with ten-inch burden on the holes and with three directions of strain relief.

Coiled Kanthal wire electric resistance heaters one foot long and 1-3/4 inches in diameter will generate from 3.5 to 4.5 kw at temperatures from 900°C to 1200°C. They will successfully fracture a strong granite in place with 10-inch burden and spacing to a depth of 15 inches where three free faces are present. However, there is a little follow-through by radial compression and fractured blocks are sometimes difficult to remove. Also, in spallable rocks such as granite, flakes of minerals spall off from the cavity walls and clog up the heater coils, causing them to burn out after 15 to 20 minutes of use.

The results obtained with coiled wire heaters indicated that higher temperatures might be desirable, and that the heater should be of an economical type that could furnish high temperatures in a hole in rock without breaking down. Refractory metal heaters of a type similar to those used for the LASL melting drill (11) were considered, but the cost was too high.

The initial internal heater tests were made with 30-inch cubes of quartzite and granite. A slot 3/4 inches wide, 12 inches long and 8 inches deep was cut in one face of a cube of quartzite with six 1-1/4 inch diameter heater holes drilled on either side of the slot (Fig. 67). The first tests were made with nichrome coiled wire heaters at a temperature of 650°C and 3 kw power level in one set of holes. The heat flux was about 350 watts per inch of hole. Cracks connecting the holes appeared in about 1-1/2 minutes. Other cracks appeared and grew until one of the heaters burned out in 2-1/2 minutes. Smaller heaters (150 watts/inch) were placed in the second row of holes (Fig. 67).

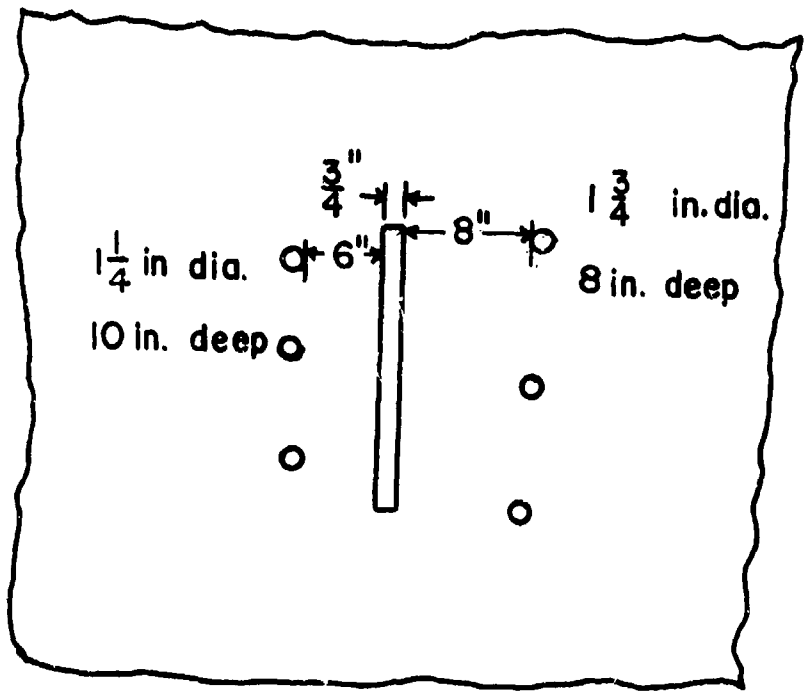

Figure 67. Slot and Hole Pattern

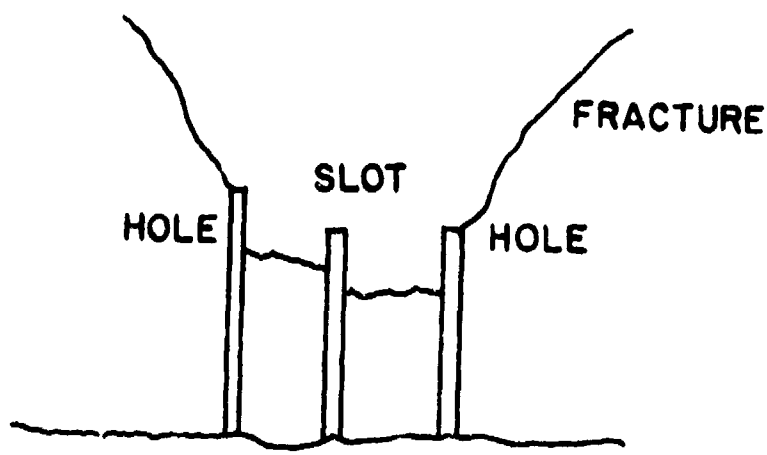

Figure 68. Vertical Fracture Pattern Parallel to Face

Initial fractures appeared in 3 minutes and they continued to widen to 15 minutes. This application of heat resulted in the block being fractured into several large pieces. In the slot area fractures parallel to the face occurred about 4 inches from the bottoms of the drill holes (Fig. 68,69).This type of fracture occurred consistently in eight tests of all of three kinds of rock, i.e., quartzite, granite, and basalt.

Electric arcs with carbon electrodes were suggested as a source of heat and these were tested. Depending upon the size of electrodes and other factors, from 10 kw to 20 kw of power are easily obtainable in a 2-inch drill hole. Temperature of the arc is in the neighborhood of 7,000°C. While carbon electrodes are brittle, with reasonable care they can be used under difficul working conditions.

In an initial test two 1/2-inch electrodes were placed in a 2-1/4 inch diameter hole in a granite block with about 5 to 6 kw power from a 250 amp arc welder. The block broke with a loud noise in 6 minutes, using about 0.6 kwhr, and producing a fracture completely through the block parallel to the heater hole, as well as breaking the top half of the block into three large segments (Fig. 70). The heat developed a hollow, bulb-shaped thermal inclusion about eight inches long and a four inch maximum diameter. The mass of the inclusion was made up of partially fused granite and chemically altered mineral flakes, of 380 cc volume, representing 0.2 percent of the volume of the rock. The time and energy requirements for tests at UMR and those of Thirumalai (8) indicate that the cube root law of energy scaling may apply. Similar tests were conducted on 30-inch blocks of quartzite and basalt with the following results:

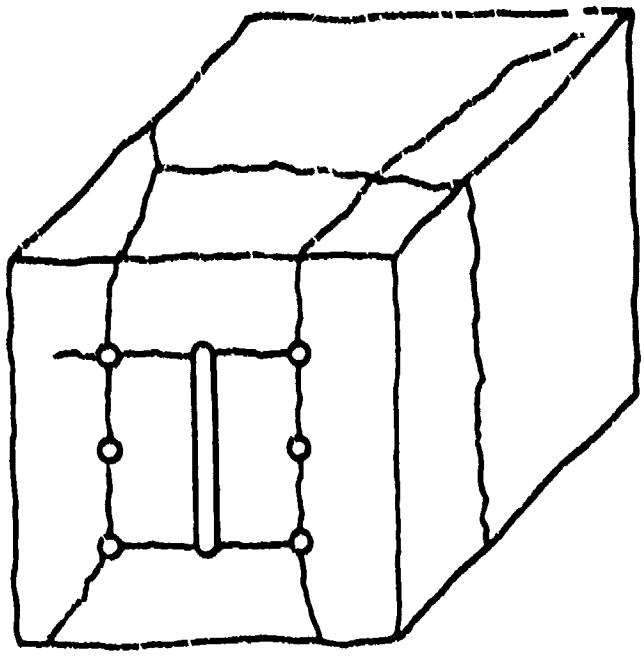

Figure 69. Typical Fracture - Slot and Hole Pattern - Wire Heaters

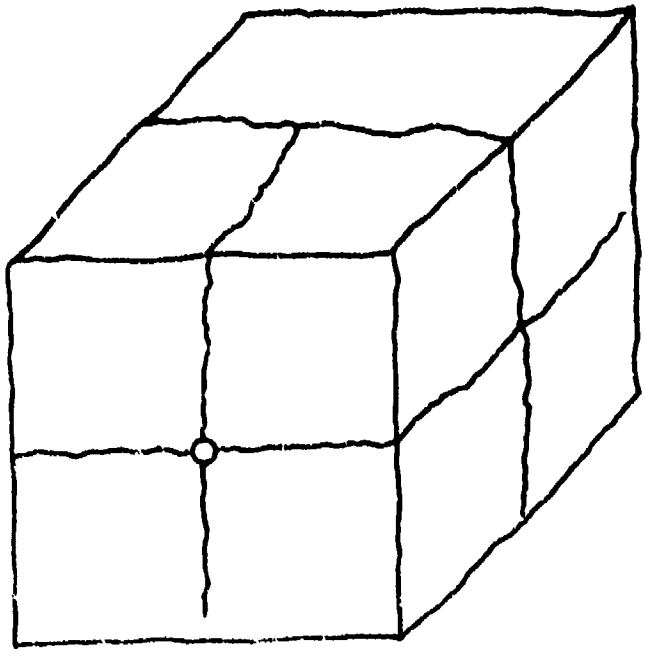

Figure 70. Typical Fracture - Single Hole - Arc Heater

Type of Rock	Block Breakage Dimensions	Power (kw)	Fracture Time
Mo. red granite	24 x 24 x 20	6	9 min
Mo. red granite	24 x 24 x 24	5	6 min
Sioux quartzite	16 x 30 x 30	5	2½ min
Dresser basalt	30 x 30 x 24	6	3 min

The Missouri red granite is less brittle and stronger than the quartzite, which broke easily, probably due to the high coefficient of thermal expansion of quartz and its change from α to β quartz as its temperature is increased. Basalt fractured readily even though it contains little or no free quartz, its lava being very liquid.

Field Tests

All equipment used in the field was made portable and included as of the final tests reported below, a 300 cfm compressor, a 100 kw diesel-driven generator, four 600 ampere dc welders, pneumatic drills, three trucks, a drill post mounted on a truck bumper, high frequency units, carbon arc heaters, and accessory equipment. Because of the improvised nature of the drilling equipment, progress has been slower than that which could be achieved with an automated jumbo, a new compressor, etc.

The results of the internal heating tests on 3-ft cubes of quartzite and granite showed conclusively that in situ conditions of confinement and other mass effects could not be easily simulated in the laboratory. It was therefore planned to conduct full-scale field tests in an abandoned quarry in Missouri red granite located near Graniteville, Missouri. The granite in the old working faces of the quarry has a wide variety of structural features suitable for in place thermal fragmentation tests, varying from solid masses to rock which are heavily

jointed and fractured. The most solid appearing faces were chosen for initial tests. These consisted of the following configurations:

Type 1. A single slot 1-3/4 x 15 in. with three heater holes on either side of the slot (Fig.71), with cylindrical resistance wire heaters.

Type 2. Two mutually perpendicular slots, 2 in. x 6 ft in the rock face with heater holes parallel to the slots (Fig. 72), with cylindrical resistance wire heaters.

Type 3. Three heater holes in line with three free faces (Fig. 73), with carbon arc heaters.

Type 4. Four heater holes in a square pattern (Fig. 74), with carbon arc heaters.

Type 1. Resistance wire heaters at 900 to 1000°C and 4.5 kw energy level were placed in the holes on each side of the slot (Fig.71) for a period of 12 to 18 minutes. Several fractures formed between the heater holes and radially from some of them, but only a few surface fragments could be removed with a pry bar. The rock between the holes and the slot were broken out with some difficulty with a Darda rock splitter, indicating that more displacement relief may be required for easy removal. Also some of the rock partings between the holes in the slot had not been completely removed and these offered some resistance to fracturing and rock removal.

(It was found later in Type 4 tests that the fracturing and rock removal was markedly enhanced when internal pressure was applied with a rock splitter during the heating of the rock. This type of experiment is planned in future work for the cut portion of a thermal round to create additional free faces for displacement relief.)

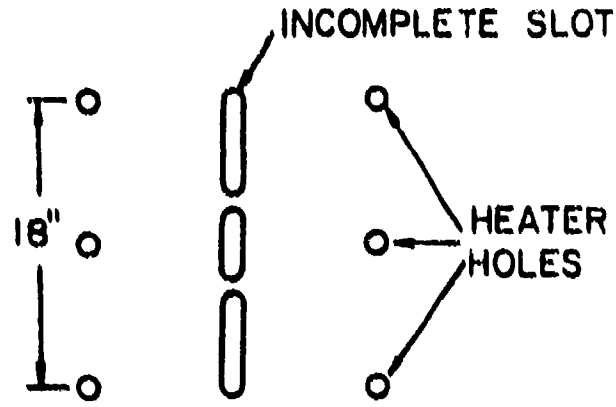

Figure 71. Incomplete Slot with Heater Holes Used in First Field Test

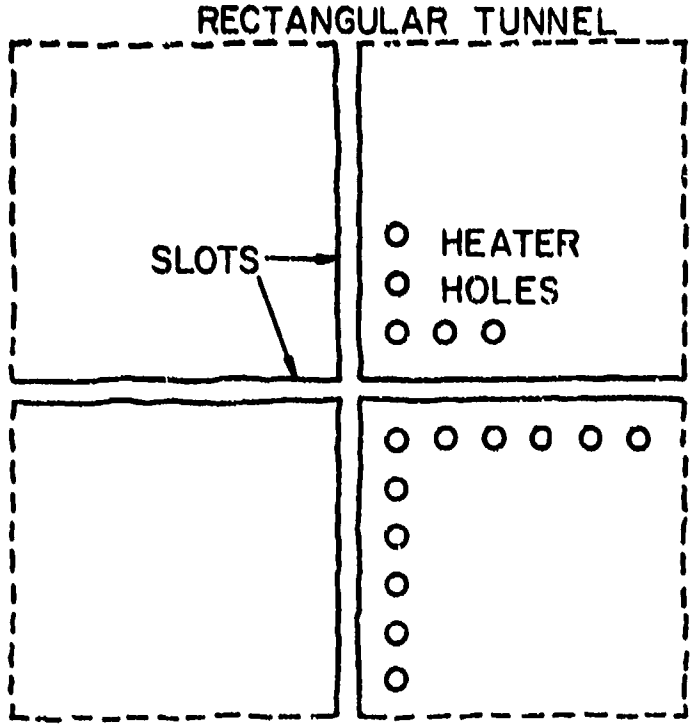

Figure 72. Two Slot Cut with Example Heater Holes for Tunnel Round

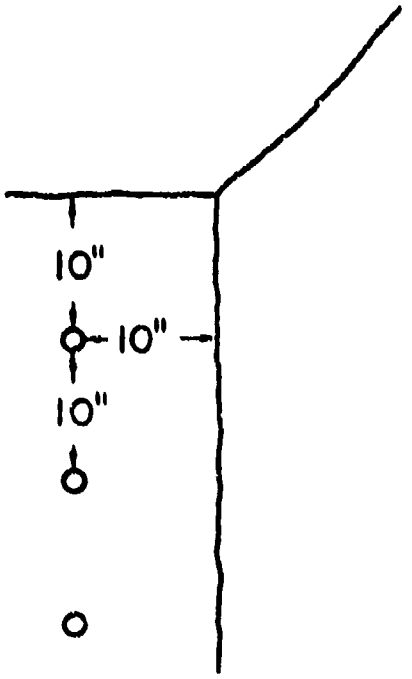

Figure 73. Three Hole Experiment on Cubic Corner

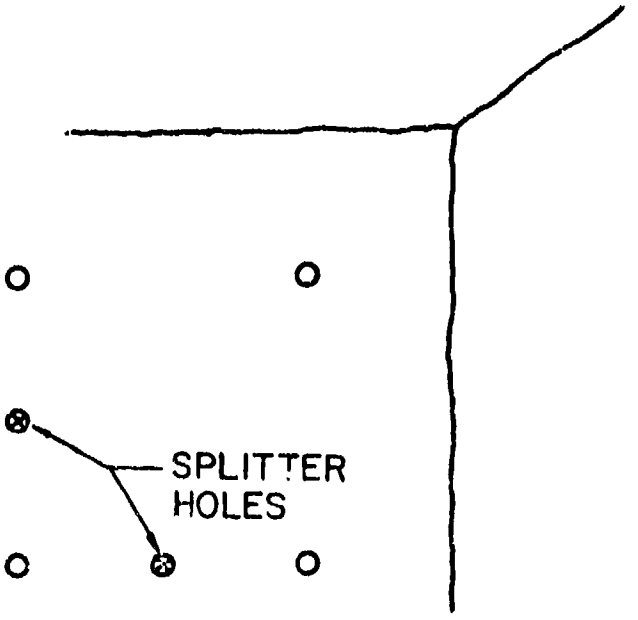

Figure 74. Four Hole Experiment with Two Splitters

Type 2. Two mutually perpendicular slots (Fig.72) 1-3/4 in. wide by 6 ft long by 30 in. deep were cut in a granite face and heater holes 2 in. diameter were drilled parallel to the slots with a burden and spacing of 8 in. to 10 in. With small burden and spacing much of the rock fractured was easily removed with a pry bar, in some cases the fracture process being aided by joints parallel to the rock face. However, the cylindrical resistance heaters failed after about 12 minutes at a load at 4.5 kw.

With the drilling equipment on hand the slots were time consuming to cut and a natural approximately cubic corner of a rock section in the quarry was selected for subsequent tests utilizing carbon arc heaters.

Type 3. In laboratory tests with arc heaters a 250 ampere (7.5 kw) power source (arc welder) was employed. For field work a higher power level was desired, and an ac, three phase, 100 kw generator could be used for three 12 kw heaters. However, difficulties were encountered in maintaining arc stability. Two tests were successfully conducted with three holes in line using ac current, with 12 in. and 14 in. burdens (Fig. 75). Visible fractures appeared in about 4 to 6 minutes, and were widened to about 1/8 in. after the heaters were left on for about 20 minutes. The blocks were easily removed with a pry bar.

The thermal stress fields created around the heated cavities mutually augmented the affects of each other, creating fractures between the holes and a fracture perpendicular to the holes, extending to the second and third faces and into the rock normal to the axes of the holes. The latter fracture aids the formation of new fractures

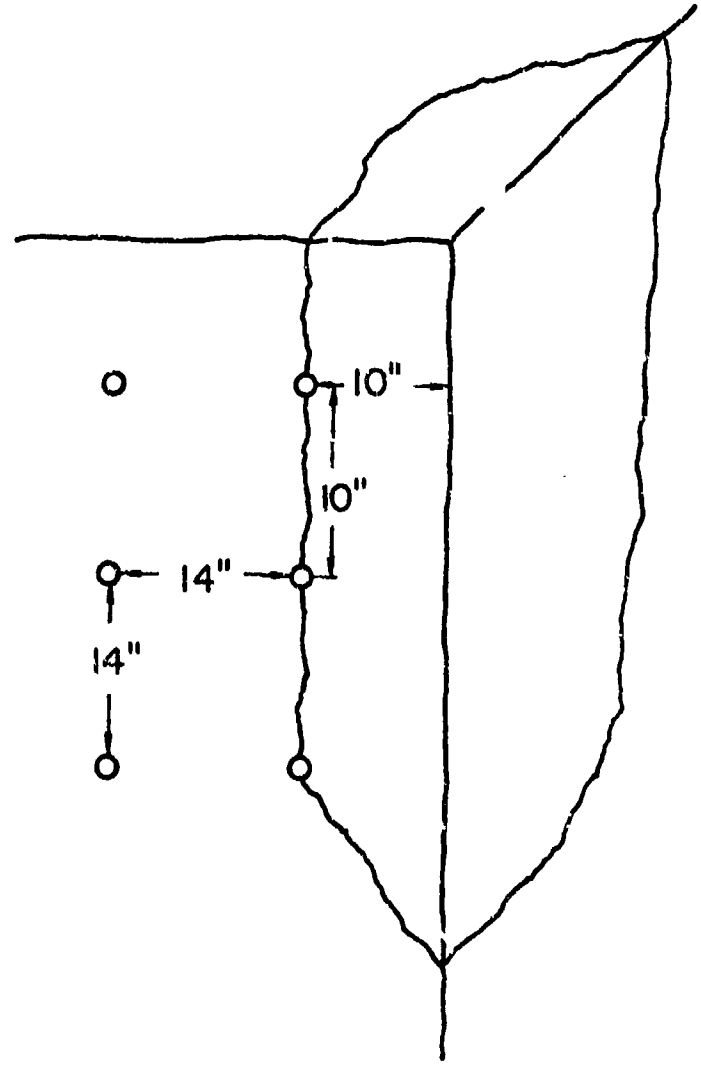

Figure 75. Second Three Hole Experiment with 14 Inch Burden

behind additional blocks of rock which are broken off. This fracture does not form normal to the second free face but curves away from the first face. Also, a set of fractures appear to be formed tangent to the thermal inclusion, furnishing the primary separation surface near the heated cavity.

One test with two heater holes was conducted with 20 kw per hole. No improvement in fracture time was observed although two holes may be less than minimal for effective fracture.

Type 4. Theoretical analyses of the thermal stress distribution caused by multiple cylindrical and spherical thermal inclusions shows that if stress concentrations can be induced in the proper orientation and location, direction and location of the fracture surface created can be controlled. Thus, the stress concentrations around the closed ends of cylindrical holes will result in a plane of fracture if the holes all bottom in the same plane. Likewise, if spherical inclusions lie in the same plane, the stress concentrations will mutually act to create a plane surface of fracture extending between and beyond the heated cavities. The cylindrical holes also serve to concentrate stresses in such a manner as to cause fractures to form parallel to the axes of the holes.

While high temperature gradients in the rock will cause correspondingly large stress gradients, the strain and the displacement induced by thermal expansion accompanying the critical fracture stress levels is relatively small, and fractures may be formed in the rock before they are visible to the naked eye. Hence, in the later tests one or two Darda rock splitters were placed in holes in the rock between the heater holes (1) to aid in fracture initiation, (2) to exploit the fractures formed by the thermal stresses, and (3) to move fractured blocks of rock sufficiently so that they could be removed.

Four 500 amp (continuous duty) welders were obtained as power sources, and holes drilled on a rectangular pattern (Fig. 74). The variables investigated were the burden, hole spacing, depth of hole, and time to fracture. Each heater was operated at an average of 12 kw power level, or the maximum continuous level accommodated by single welders. One experiment was conducted with two heaters in two holes at 800 amps each to ascertain some of the effects of higher power level as noted above.

Test No. 5 (Table 15) was conducted with heaters only. The initial observable fractures appeared in about 4 minutes, and they were widened considerably in 10 minutes total heating time. The block was later removed with a splitter. The next two tests with 18-inch spacing were made with a splitter in one hole only (one splitter was available at the time). Initial fractures appeared in about 3 minutes and subsequent fracturing was materially aided by the single splitter, although in one test the horizontal fracture occurred at the level of the splitter. Vertical fractures occurred parallel to the working face and through the heater holes.

Two subsequent tests with 24-inch spacing were made with two rock splitters. In the first test the arc in No. 4 hole operated only a short time and the block fractured diagonally. The second test in this series functioned in a normal manner, the fracture times being decreased considerably by the mechanical stress induced by the splitters. The results of the test indicate that 24-inch spacing may be approaching the practical limit for a 12 kw power level in each heater. A total of seven experiments was conducted at the second site (Figs. 76 & 77).

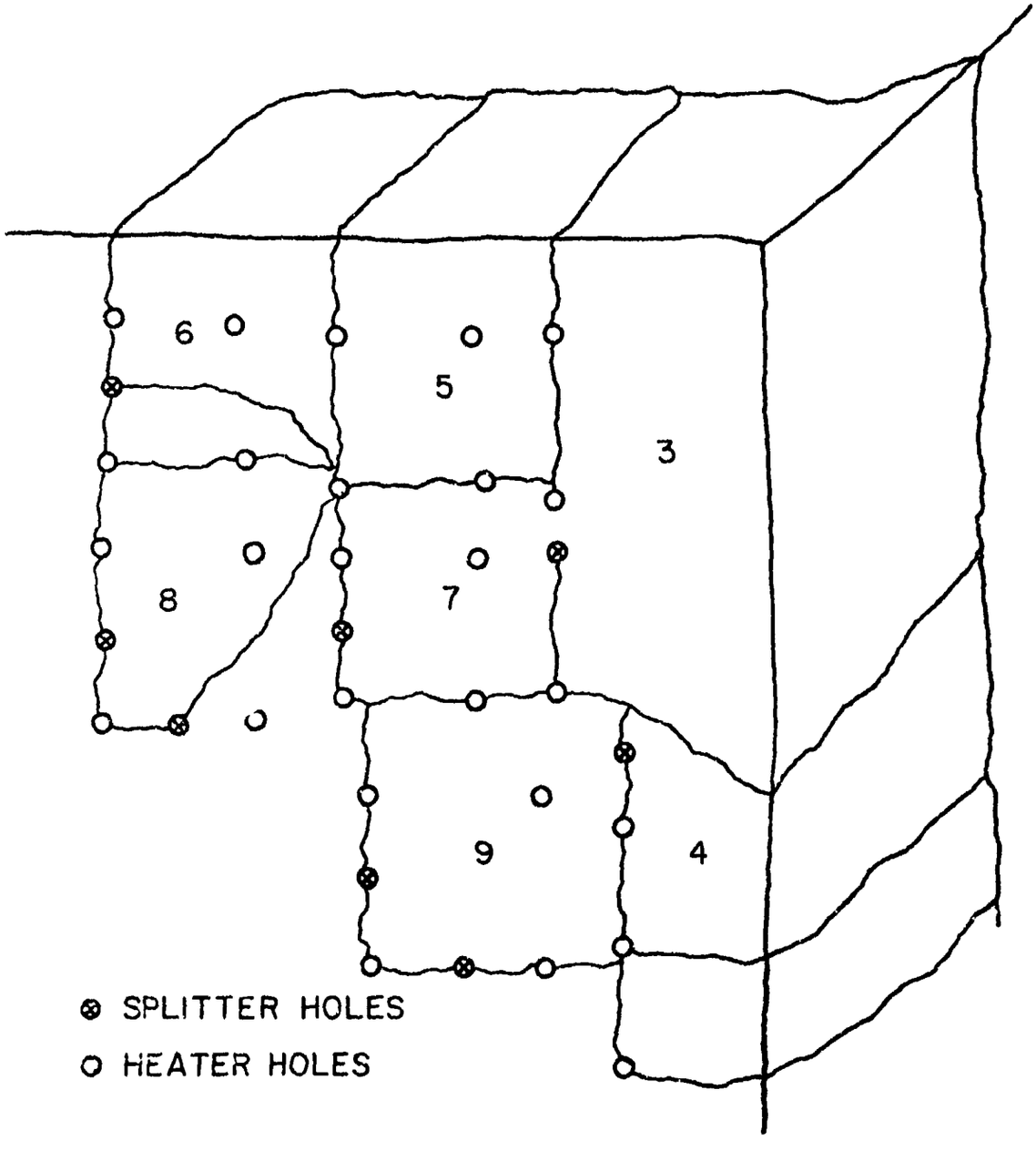

Figure 76. Composite of Experiments Four Through Nine Showing Successful Controlled Block Fracture

Fig. 77. Four electric arc heaters in place with one Darda rock splitter (wrapped in asbestos cloth).

Fig. 78. Drill holes and fracture patterns for heaters and splitters. All blocks were easily fractured and removed.

TABLE 15

Summary of Field Tests

Test No.	Geometry		Depth	Hole spacing	Burden	Power/Hole kw	Time
1	Line	3 holes	16	12	12	8-10	15
2	Line	3 holes	22	4	4	8-10	15
3	Line	3 holes	30	24	24-30	8-10	25
4	Line	(2 holes)	30	18	16	20-25	25
5	Square	4 holes	28	18	10	12	10
6	Square	4 holes*	28	18	10	12	3-f 10+
7	Square	4 holes*	28	18	10	12	4-f 11+
8	Square	4 holes**	32	24	12	12	15++
9	Square	4 holes**	32	24	12	12	10++

* 1 hole 5 min. only

** 1 hole 8 min. only

\+ with one splitter

++ with two splitters

Round Design and Displacement Relief

If one considers a section of a heated cylindrical hole near the corner of a quadrant of a large elastic body, after the heat has been applied for a certain time there is a biaxial compressive stress immediately around the hole which becomes tensile (tangential) with increase in distance from the hole. With increase in time the width of the compressive zone increases as does that of the tensile zone, the magnitude of the latter decreasing with distance of constant hole diameter. If the medium were infinite, radial cracks could form, their orientation depending upon properties and imperfections of the medium. However, if there is one free face within a distance such that the magnitude of the tensile stress is affected by the free surface, a crack will propagate from the hole normal to the free surface, but it will not widen because of the constraining effect of the mass. If two surfaces exist within a critical distance, then two cracks will propagate from the hole normal to the two free surfaces and will continue to open up if there is sufficient displacement relief. One of the objectives of further experimentation is to determine more exactly the value of optimum burden for given rock properties, hole size and energy level.

For three dimensions, an octant of an infinite mass is considered with multiple holes drilled parallel to one face. The problem now becomes one of determining the optimum distance from a free surface (burden), the spacing, and the depth of the holes. The holes act as loci for stress concentration and fracture guides. However, for this mode three planes within critical distances of the thermal inclusion are needed for controlled fracture and most efficient breakage. For breakage of the cut portion of a round in a normal tunnel face where no slots are cut, the same principle applies but only one free face

is present, and cut designs similar to those used in blasting are required. Such cut design is to be investigated in future research.

Thermal Round Operational Concepts

There appear to be several concepts of thermal rounds which will function to break the rock. The primary problem is providing initial displacement relief. The possible "cut" portion of a round may be patterned after explosive tunnel rounds, which use draw, V, pyramid, burn and other types of cuts.

Slot Round

In the first experimental field test at a granite quarry two perpendicular slots 2 inches wide by 30 inches deep were cut in the granite in the center of the tunnel face with a pneumatic (drifter) drill. Such a slot requires about five times as much drilling as an explosive round. At an estimated cost of 30¢/foot of drill hole the total cost of drilling for a 15 by 15 foot tunnel 216 feet of drill hole is required or $64.80/foot of tunnel. Assuming for purposes of illustration that half of the work time is used for drilling at a rate of 24 inches/min, 15 drills would be required for 100 foot/day tunnel advance. The total heat energy for breakage is estimated at a maximum of 2 kwhr per foot length of heater hole (36 holes) to be 72 kwhr. At 3¢/kwhr the energy cost for breakage would be $2.16/foot of tunnel.

The initial heater hole size required is determined largely by the space required for insertion of the heater. The most effective temperature for inducing stresses in the rock is theoretically the highest that can be applied, because higher temperatures result in greater heat flow and sharper stress increases at large distances. Carbon electrodes first create an arc (6,000°C), causing the rock to spall, melt, and change chemical and physical form. After a melt is formed,

however, most of the heat generated which comes from the arc is transferred by several complex processes. The maximum effective temperature in the cavity is the melting temperature of the rock, which is usually lower than 1700°C for silicate rocks. With any type of heater that causes the rock to melt the cavity is being continually enlarged, which is advantageous. That is, the larger the cavity the greater the stresses are at larger distances from the cavity.

A hole spacing of 2 feet, which may be about optimum for 12 kw carbon electrode heaters, is similar to hole spacing required for explosives. Explosive energy equivalent varies from 0.4 to 0.6 kwhr/lb for 40 percent to 75 percent dynamites, with about 1 lb per ft of hole for strong rocks.

While electrical breakage energy requirements, based upon tentative information, are about three times greater for thermal fragmentation than for explosives, electricity costs about 2 to 3¢/kwhr, dynamites at 50¢/lb range from $0.83 to $1.25/kwhr. Most inexpensive ammonium nitrate-fuel explosives are not suitable for breaking hard rocks.

The time required for automated insertion of heaters such as carbon electrodes in a hole is a very small fraction of that required for loading explosives. More important is that the operational characteristics of the proposed system will permit simultaneous drilling, fragmentation and mucking. That is, the operation as planned will be semi-continuous or continuous.

Although for a single slot of 2-foot length it was not possible to obtain effective fracture of rock on the sides of the slot, it may be that a single long slot in the full height of the face will be sufficient to provide displacement relief for breakage.

At the present stage of development the thermal round concept appears to have few of the disadvantages of the other novel concepts, and has promise of overcoming most of the disadvantages of the drill and blast method. While there are several basic and operational problems to be solved, the state-of-the-art is sufficiently well advanced in the areas involved to permit an optimistic prediction of early application.

No radically new types of equipment will be required. Current types of drill assemblies can be adapted for slot and heater hole drilling. Heater elements (carbon electrodes) are currently available at very low cost, and will require only minor improvements and the development of mobile holders. Capital equipment and operation costs appear to be in the same range as drill and blast, but higher rates of advance are indicated.

Important characteristics may be summarized as follows:

Characteristics of Thermal Fragmentation Method of Excavation - Slot Cut

Drilling required:	1 ft of hole/cu ft of rock removed
Drilling energy:	200 to 390 j/cc
Percent of face drilled:	5%
Breakage energy:	0.2 kwhr/cu ft
Rock melted:	maximum of 0.3%
Labor at face:	4 men in 15 x 15 tunnel
Character of muck:	Small fragments to 3 ft cubes
Continuity:	Semicyclic to continuous
Down time:	Minimal
Heat developed:	Negligible
Noise and vibration:	From pneumatic drilling only
Gases created:	Small amounts - easily removed
Environmental problems:	Minimal
Equipment Costs:	Nominal, drills, jumbos, etc., costs for modification and redesign
Services:	Electrical power
	Compressed air, assists ventilation
Tunnel wall stability:	Some slight fracturing of surrounding rock
Equipment required:	Standard drilling equipment - modified
	Mountings for electrodes
	Improved electrodes

Estimated time to prototype: 3 years

Estimated time to full operation: 4-6 years

Cost Analysis

The direct costs for excavation are usually considered under the categories of fixed costs, or those which are constant per foot of advance, and variable costs, which are constant per day charges, and consequently vary with the rate of advance. Examples of fixed costs are power and bit wear, and variable costs are equipment and labor costs. Overhead costs also fall into the last category.

It is not possible to make a simple comparison by category of the direct costs of rock breaking or removal by such methods as tunnel boring machines, drill and blast, and excavation utilizing melting processes, because of differences in the operational characteristics of each. Also, each method has different types of trade-off costs. For example, the smooth walls created by tunnel boring machines may reduce the cost of tunnel support, and the glass liners created by melting may have the same value. One method may require less ventilation than another, or incur higher muck removal costs.

Hence, a complete comparison of methods would need to include cost factors in all categories which are affected by the overall operation.

Costs for Drilling and Rock Breaking. In a study of excavation costs in the NE Corridor by Harza Engineering Company in 1968 (84) rock breaking costs were given for four general types of rock:

X. Rocks assumed to be mineable with boring machines with relative drillability factors between 5 and 7, average unconfined compressive strength 4000 to 32,000 psi.

Y. Same as X with higher average compressive strengths, 18,000 to 20,000 psi, 65 percent of rock type is mineable with boring machines. Relative drillability factor of 1 to 4.

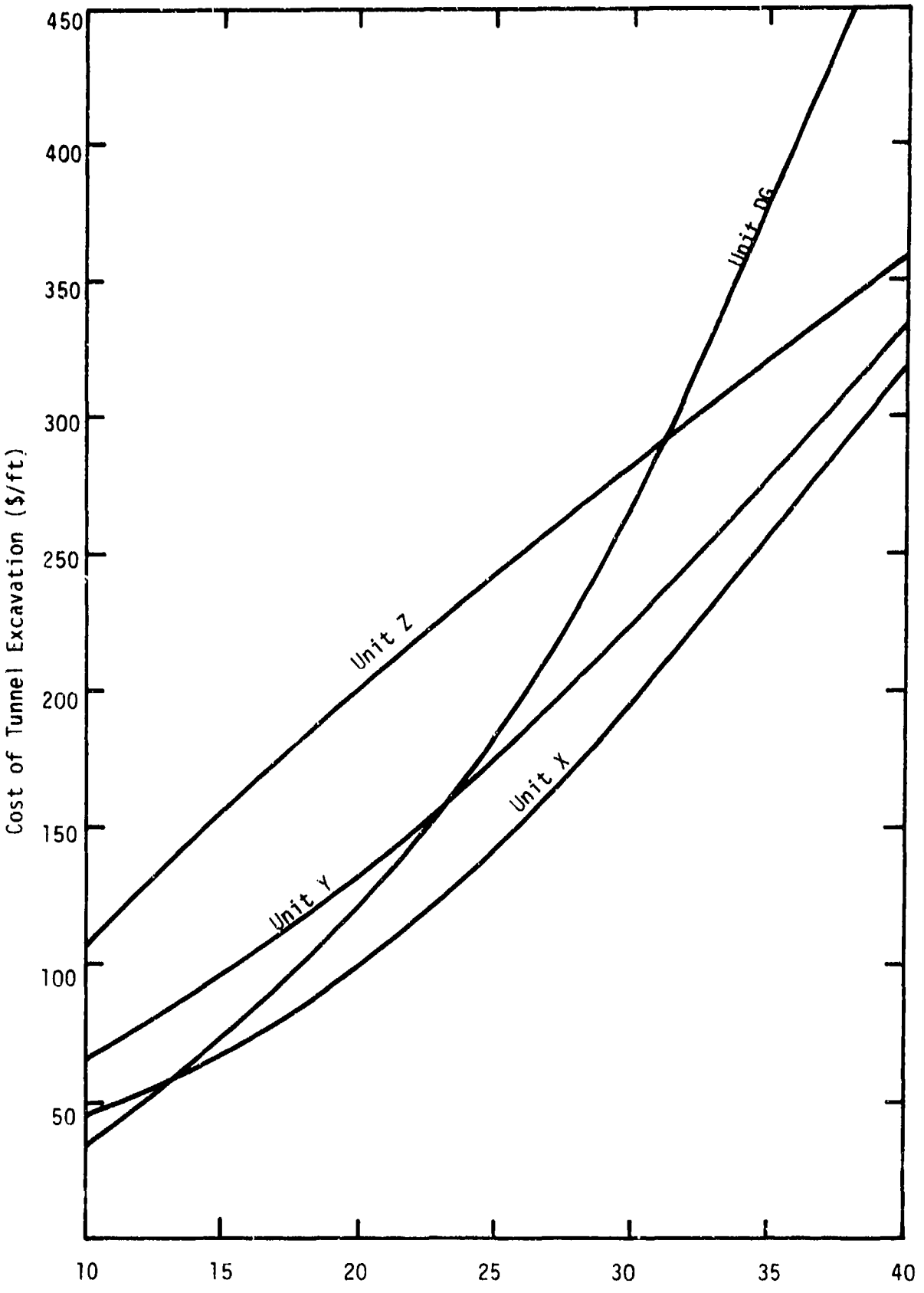

Fig. 79. Tunnel Excavation Costs

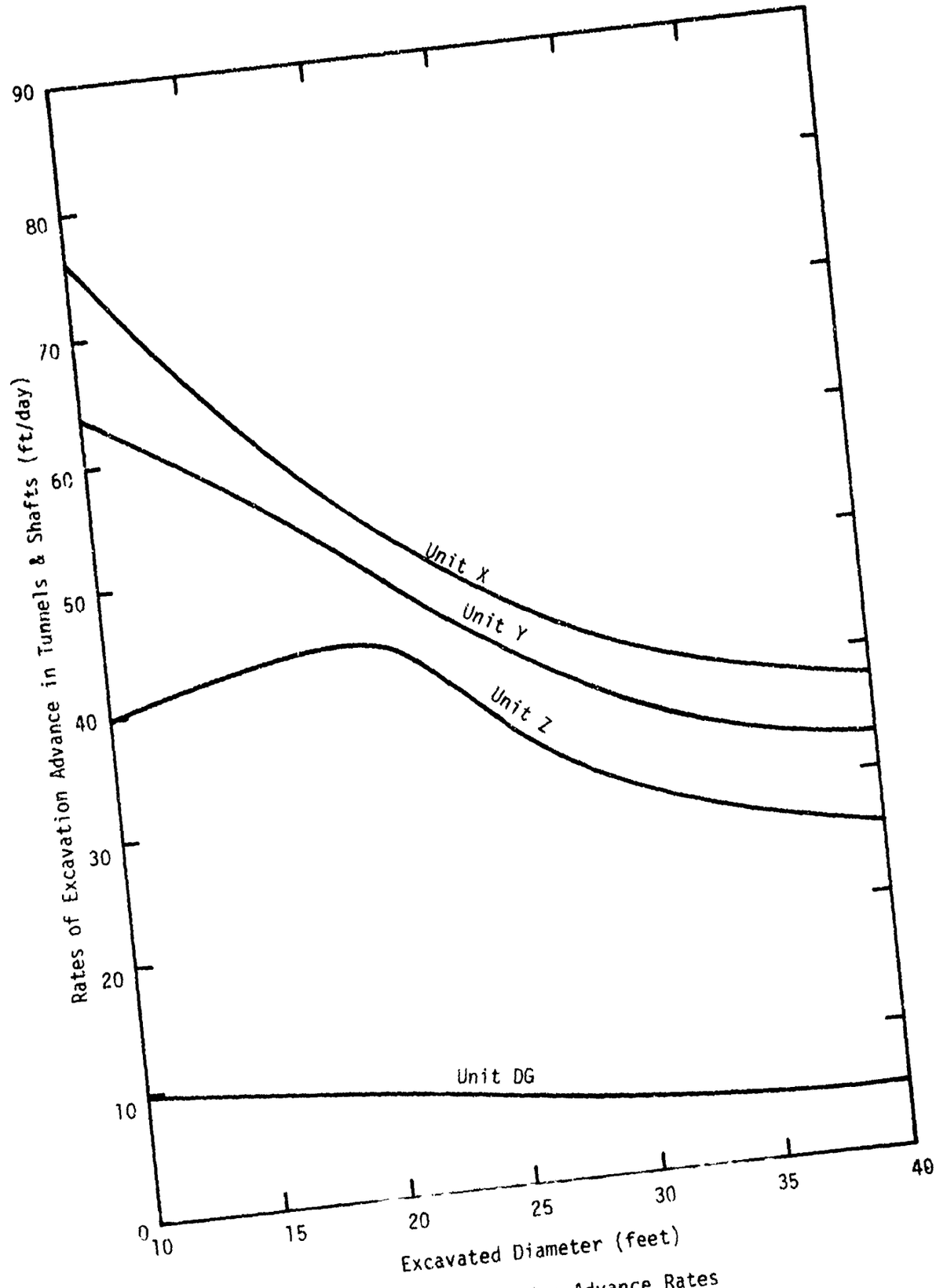

Fig. 80. Excavation Advance Rates

Z. Rocks of somewhat the same strength as Y, but requiring conventional drill and blast methods.

D.G. Difficult ground associated with faults, gouge, susceptible to squeezing.

The representative direct rock breaking costs were categorized as follows by percentage distribution

Unit	X	Y	Z	DG
Labor	33	39	50	30
Equipment	62	54	38	65
Materials	5	7	12	5

It is notable that labor costs are the highest for drill and blast (Z) partly due to the cyclic nature of this method. It is notable also that costs per foot increase almost linearly with the excavated diameter (Fig. 79).

Because of the high labor costs of drill and blast, novel methods of breaking hard rock have a considerable margin of capital which can be expended for additional energy and equipment if the method is automated and has other requisite cost advantages similar to boring machines. Thus, for a tunnel driven by a thermal fragmentation method, possible trade-off for increased drilling costs will be labor reduction, reduction in cost of breakage energy, higher rate of advance, and other factors yet to be defined.

In analyses of pneumatic drilling costs it has been found that the factors of greatest cost are for labor, equipment, and maintenance (85). Amortization or rental charges per foot for equipment are less for two or three shift operation.

For a single 2" pneumatic drill the costs are approximately as follows:

	Per hr		
Compressor	$ 3.75	Bit Cost	$25.00
Drill	4.25	Life	2,000 ft
Labor (2 men)	7.00	Reconditioning	$15.00
Fuel (4 gal)	0.60	Rod cost/ft	$ 0.03
2" carbide bit & rod	3.00		
	$18.60		

Rate of drilling in hard granite (overall) 60 ft/hr

Cost/ft = $0.35

A method of excavation employing thermal fragmentation may be semicyclic or continuous. One procedure would permit simultaneous drilling of heater holes and slots, or another the cutting of a slot first and simultaneous drilling of heater holes and fragmentation. The latter would probably require dry drilling. Also, after the rock is fractured, rock removal is accomplished by rock splitter or impact tool. Direct costs may be estimated as follows:

Example: 10 x 10 tunnel

Hole spacing: 2 ft centers

Depth of round: 2 ft

Number of heater holes: 36 - 2-1/4" - 72 ft total

Slots: 2 - 2" x 2' x 10' 240 ft of 2" diam hole

Advance: 16 ft/shift = 576+
1920
2496 ft of hole

Equipment Costs:	Cost/hr	Total/hr	3 Shifts
10 small drifter drills 150 cfm	3.50 ea.	35.00	11.67
4 large drifter drills 400 cfm	4.75 ea.	19.00	6.33
1 compressor 3000 cfm	4.50/drill	63.00	21.00
Jumbo	5.00	5.00	1.66
Fuel (compressor 5 gal/drill	10.50	10.50	10.50
Rods	0.40	5.60	5.60
Bits .40/drill	0.40	5.60	5.60
Maintenance & Misc.	0.50	2.00	2.00
Labor (3 men)	15.00	15.00	15.00
		160.70	79.36
Cost per ft of hole		0.50	0.25
Drilling costs/ft of tunnel	$40.00		

Drilling costs would be reduced for other types of cuts under investigation. Electrical energy costs are given under Thermal Round Concepts.

Other factors which are critical in the design of a thermal round are the hole placement with respect to geologic structure, effect of water in small and large amounts, and the most effective type of strain relief that can be obtained [illegible].

From fracture phenomena observed to date the investigators feel that heater holes can be placed advantageously in relation to existing cracks. Fractures parallel to a heater hole relieves the stresses locally but are exploited by the expansion of the rock around the cavity. In granites the joint systems are seldom orthogonal and may present problems in obtaining the most effective use of stress fields.

Thus, the effects of hole placement and direction with respect to natural joint patterns in the rock will be investigated with the objective in mind of utilizing the joints in aiding the thermal fracture process.

The overall effects of moisture on heaters, heat coupling, and related factors are not known. However, for small amounts of water, few problems are expected. Where large amounts of water are present, loss of heat for water vaporization will be minor unless water is flowing into a heater hole. On the other hand, it may be necessary to protect high temperature portions of the heaters, refractory metals or carbon electrodes, from sudden cooling and consequent fracture due to thermal shock.

To date, crossed slots in the working face appear to be one effective means for providing displacement relief for rock fracture. Arrangements of heater and splitter holes similar to those in a V-cut, a pyramid cut, or a burn-cut utilized in explosive round offer real promise. These configurations are being analyzed and investigated experimentally.

Rate of Advance

Observations of pneumatic drilling operations as an integral part of a fragmentation system indicate that for an optimum number of drills in a tunnel heading, the rate of advance will be determined by the absolute and overall rate of drilling. For a larger number of drills, the rate of advance will be determined by a balance of the number of drills and heaters which can be efficiently and economically used in a heading of a given size and shape.

The overall rate of drilling is fixed by the absolute rate of drilling adjusted for the time required to position the jumbo, the drills, and for delays, i.e., for effective drilling time. A further adjustment must be made for the time required for drilling and breaking the cut portion of a round. Thus, a drilling time factor, the percent of the total working time at the face during which the drill is actually operating, will govern the rate of advance.

In the current experiments in Missouri red granite a 2-3/4 inch diameter hole is drilled for heater holes and 1-3/4 inch diameter hole for splitters. The absolute rate of drilling is

2-3/4 inch: 10 in./min

1-3/4 inch: 20 in./min

The following example calculations can be made for seven and nine drills per heading in a 20 ft diameter tunnel:

Tunnel size:	20 ft diam	20 ft diam
Heater hole spacing:	2.5	5.0
No. of heater holes:	81	65
No. of splitter holes:	40	34
No. of drills large:	9	7
small:	3	2

Max. rate of adv. ft/day:	150	150
75% d.t.f.:	113	113
50% d.t.f.:	75	75
No. of heaters:	8	8

With a heater hole spacing of 2.5 ft ideally 3 x 3 x 2 ft block would be broken. For maximum advance at 2 ft/round, this would require 1.8 blocks per minute. With four sets of four heaters each, and a fracture time of three minutes per block, and simultaneous heating of two or more blocks, the required advance rate would be achieved. With three or four heat sets operating simultaneously, the power level would be approximately 150 kw at 12.5 kw per heater. Rates at 75% or 50% drill time factor appear to be readily attainable.

With automated jumbos and manual splitter and heater placement, and efficient muck removal, a high drilling time factor can be obtained. It can be further improved if holes normal to the face can be drilled for more than one round from one drill setup.

It is estimated that drill time factors will vary from about 50 to 75 percent, which would give a rate of advance varying from 75 to 113 ft/day in 20 ft diameter tunnels for 2.5 and 3 ft spacing. Th'. is 1.5 to 2.8 times the rate of advance in similar hard rocks which require drill and blast methods, as reported by Harza (Fig. 80).

Chapter XI

SUMMARY AND CONCLUSIONS

Temperature and Stress Analysis

A close correlation between the theoretically predicted and the experimentally observed fracture patterns and the fracture length-fracture time relationships indicate that the conclusions drawn regarding the influence of various process parameters using the two two-dimensional plane models can be applied fairly accurately to a three-dimensional configuration. Also, for rock types with characteristics similar to Dresser basalt, the approximate fracture completion time corresponding to any given fracture length can be approximated from the data for a single test using the power relationship $t_f^* = L^{*2.7}$ between the dimensionless fracture length.

For a given geometry, the predicted fracture time is only a small fraction of the time necessary to reach a steady-state temperature distribution. The temperature field at the time of the fracture is thus highly localized, and the major portion of the fractured volume experiences only a small increase in temperature. The fracture-inducing stresses in this region are, therefore, entirely due to the load vector resulting from the thermal constraint. Since the severity of thermal constraint depends on the relative volumes of the cold and the hot zones, the fracture time is significantly influenced by both the hole spacing and the melt-free depth.

For very small melt-free depths, the fracture is characterized by mainly a compressive failure according to the McClintock-Walsh modified Griffith criterion. This fracture mode is naturally undesirable as the compressive strength of hard rocks is many times greater than their tensile strength.

While the McClintock-Walsh compressive failure zone remains relatively unchanged in the region of the high temperature gradients, the compressive stress components in the cold zone decrease steadily with an increase in the melt-free depth. With further increase in the melt-free depth, a condition is reached when the major principal stress components become tensile. Thus, with a continuous increase in the melt-free depth, the McClintock-Walsh fracture zone in the cold region transforms first into a partial Griffith compression zone and finally into the Griffith tension zone. The effectiveness of this transformation is evident from the drastic reduction in the fracture time as the fracture now results from the tensile failure.

The melt-free depth associated with the completion of the transformation of the compressive fracture into the tensile fracture mode is approximately equal to half the fracture length, that is, half the difference between the hole spacing and the hole diameter. Any further increase in this parameter has only a slight effect on the fracture time.

Another significant effect of the melt-free depth involves the location of the parallel fracture (subsurface fracture parallel to the working face). The optimum location of this fracture requires the crack initiation to occur very close to the hole base and the crack propagation in a plane approximately parallel to the hole base. From the slot model analysis, to obtain such a location, it is necessary that the thermal inclusions should be concentrated at the very base of the holes (requiring only a small melt depth) while the melt-free depth should, at least, be equal to half the fracture length.

The hole model analysis is performed using a plane stress assumption. The actual three-dimensional fragmentation configuration, however,

involves a condition somewhere between the plane stress (shallow holes heated along their entire lengths) and the plane strain (deep holes heated along their entire lengths) formulations. Also, this analysis does not involve the melt-free depth parameter which as shown from the slot model studies can be used advantageously to transform the mode of failure from compressive to tensile and thereby to greatly reduce the fracture time. Thus, it is natural to expect a predominantly compressive failure in the case of the hole models, the results of which, in view of the above considerations, are obviously representative of the upper bound of the theoretical solution.

The results of the plane analysis indicate that since the fracture initiates in the vicinity of the point of transition from the melt condition to the convection condition (along the hole depth), only small melt depths should be used. Also, in order to optimize the location of the parallel fracture and the fracture time, the melt-free depth should, at least, be equal to half the difference between the hole spacing and the hole diameter. Although any further increase in the melt-free depth shows an insignificant influence on the location and time of the parallel fracture, it will mean that the heat source will have a greater burden against which to open cracks between the holes. The optimum depth therefore seems to be one associated with a melt-free depth equal to approximately half the difference between the hole spacing and the hole diameter.

Both the slot and the hole model analyses indicate the hole spacing to be the most influential parameter governing the fracture time. The effects of the changes in the hole diameter, on the other hand, are

only secondary in nature, and can be taken into account by adjusting the hole spacing such that the fracture length remains unchanged. Thus, the effects of the hole spacing and the hole diameter can be expressed in terms of a single variable, the fracture length.

In practice, the hole diameter will be determined mainly from heater size considerations, and since the optimum hole depth is expressed in terms of the fracture length, the thermal fragmentation configuration can be optimized by a proper choice of the single parameter, the hole spacing.

While the power relationship, $t_f^* \propto L^{*2.7}$ between the dimensionless fracture time and the dimensionless fracture length (for Dresser basalt) implies faster fragmentation for smaller spacings, it is important to note that smaller spacing also means higher drilling costs as well as smaller rock volume that can be removed through each cycle of operation. The choice of an optimum spacing, therefore, will also involve factors such as the drilling rate, the cost of heating and drilling, the muck removal capacity and the overall efficiency of the actual excavation machine.

Thus, while the analysis presented here is not sufficient to enable one to optimally choose the process parameters, it serves two very useful purposes. First, it reduces the optimal choice of various process parameters to the choice of a single parameter, the hole spacing, and also provides a relationship between the fracture time and the hole spacing. Secondly, since this investigation considers fractures due entirely to the effects of thermal inclusions, the results presented here can be used with advantage to approximately determine the effectiveness of the mechanical loading to be incorporated in designing an excavation prototype.

Field Experimentation and Analysis

An investigation of the technical and economic feasibility of thermal-mechanical fragmentation of hard rock is being carried out in the field to advance the research toward an early proof of concept. Research has advanced through phases of surface heating and chipping, deep slot cutting and kerf removal, to hole drilling and insertion of heaters inside the rock. Coiled wire heaters successfully fractured granite blocks, but carbon arcs were more effective.

Carbon arc heaters are inexpensive, consisting of two carbon rods secured to asbestos board. These furnish efficient heat sources up to a 12 kw level for 5/8 in. diameter carbon rods. Problems encountered with the arc heaters include arc stability, electrode erosion, restarting arcs in a solidified melt, and brittleness of the carbon. All of these difficulties appear to be amenable to correction with proper heater design and application of arc engineering techniques.

Blocks of rock can be readily fractured along orthogonal planes if three directions of displacement relief are provided. That is, four thermal inclusions generate a fracture plane at depth and parallel to the working face as well as longitudinal fractures between the drill holes, forming rectangular blocks of rock. The temperature field creates intense stresses, but little displacement without prolonged heating. Hence, Darda rock splitters are employed to enhance and exploit the early thermal fractures, and to remove the blocks, which are often keyed in place. This type of fracturing lends itself to the design of a thermal round, similar to a blasting round, with heat employed instead of explosives. As with a blasting round a critical factor is

the design and proper functioning of the cut portion of the round in such a manner that adequate displacement relief is provided for subsequent fracture and removal of blocks of rock from the remainder of the working face.

Several types of cuts will be investigated in future research such as pyramid, V, draw, simulated burn cuts, as well as a breakage process employing a continuous spiral drill and fracture process.

Preliminary economic studies indicate that costs of excavation should be approximately the same as for conventional drill and blast methods, and that projected rates of advance will be two to three times as great. Much of the drilling equipment required can be obtained by minor modifications of available items. About the same amount of drilling, or slightly more, may be required as for drill and blast procedures. Considerable heater development may be required for a type of element needed for continuous use underground. Breakage energy costs are about three times as great as for explosives, but electrical energy costs are only one-third those of explosives. Mobile, multiple purpose jumbos will be required for mounting drills, heaters, and rock splitters.

A different type of mucking system may be required for handling and removal of large blocks of rock. Shields will be needed at the face so that drilling and breaking can be carried on simultaneously.

To date experimentation and analysis indicate that this method of fragmentation of both hard and soft rock for tunneling and other types of excavation is both technically and economically feasible.

REFERENCES

1. Maurer, W. C., Novel Drilling Techniques, Pergamon Press, London, 1968.

2. Carstens, J.P., "Thermal Fracture of Rock - A Review of Experimental Results," 1st No. Am. Rapid Excav. and Tunneling Conf., June 1972.

3. Thirumalai, K., "Rock Fragmentation by Creating a Thermal Inclusion with Dielectric Heating," Bur. of Mines RI 7424, 1970.

4. Nixon, D.R., and Schumacker, B.W., "Use of an Electron Beam Gun for Hard Rock Excavation," Westinghouse Electric Corp., Repts. R71-35, R71-32, 1971.

5. Zar, J., "The Use of a Laser for ARPA Military Geophysics Program (Rock Mechanics and Rapid Excavation) AVCO." Semi-annual Tech. Rept. Bur. of Mines Cont. No. H-210039, December 1971.

6. Carstens, J.P., and Brown, C.O., "Rock Cutting by Laser," SPE Paper 3529, October 1971.

7. Carstens, J.P., et al, "Heat Assisted Tunnel Boring Machines," UARL Rept. No. J-970802-12, September 1970.

8. Thirumalai, K., and Chueng, J.B., "A Study of a New Concept of Thermal Hard Rock Crushing," 14th Symp. on Rock Mechanics, June 1972.

9. Clark, G.B., et al, "Combined Thermal Weakening and Mechanical Disintegration of Hard Rock," U. of Mo. RMERC, Annual Rept., July 1972.

10. Robinson, E.S., et al, "A Preliminary Study of the Nuclear Subterrene," Rept. LA-4547, LASL, 1971.

11. Ionarc Gets USBM Aid for Tunneling Research E & MJ, July 1972.

12. Clark, G.B., "Internal Reports on Research Contract No. USDI-H-0220068," Bur. of Mines (ARPA), 1972.

13. Sarapu, E., "Electrical Fragmentation of Magnetic Iron Ores," AIME Preprint 69-AO-52, 1969.

14. Thirumalai, K., "Potential of Internal Heating Method Rock Fragmentation," 12th Symp. on Rock Mechanics, U. of Mo., Rolla, Mo., 1970.

15. Thirumalai, K., Private communication referencing research in 1969.

16. Neudecker, J.W., "Fifty Foot Hole Melted by Two-inch Diameter Subterrene," Memo S-37, February 18, 1972.

17. Armstrong, D.E., et al, "Rock Melting as a Drilling Technique," LASL Rept. LA-3243, March 1965.

18. Krupka, M.C., "Thermodynamic Stability Considerations in the MO-BN-C System's Application to Prototype Subterrene Penetrators," LASL Rept. LA-4959-MS, May 1972.

19. Krupka, M.C., "Internal Reaction Phenomena in Prototype Subterrene Radiant Heater Penetrators." LASL Rept. LA-5094-MS, November 1972.

20. Johannsen, A., "A Descriptive Petrography of the Igneous Rocks," Vol. II, Univ. of Chgo., 1939.

21. Huang, W.T., Petrology, McGraw-Hill, New York, 1962.

22. Eitel, W., Silicate Science, Vols. 1-5, Academic Press, 1965.

23. Clark, S.P., "Handbook of Physical Constants," GSA Memoir 97, 1966.

24. Skinner, B.J., Thermal Expansion, Sec. 6," Handbook of Physical Constants," GSA Memoir 97, 1966.

25. Geller, L.B., et al, "Jet Piercing Research Project," MBIR 62-27, Dept. of M & T Surveys, Canada, 1962.

26. Kracek, F.C., and Clark, S.P., "Melting and Transformation Points in Oxide and Silicate Systems at Low Pressure," Handbook of Physical Constants, GSA Memoir 97, 1966.

27. Rawson, H., Inorganic Glass-Forming Systems, Academic Press, 1967.

28. McMaster, R.C., and Hecox, W., "Drilling Oil Wells with Electric Arcs," Drilling Research Inc., Pt. IV, Collected Reports, 1949.

29. Cooper, D.E., et al, "Summary Report of Study of Electric Arcs for Oil Well Drilling," Drilling Research Inc., Battelle, Min. Inst., December 1950.

30. Somerville, J.M., The Electric Arc, Wiley, 1959.

31. Wood, F.W., and Beale, R.A., "Studies of High Current Metallic Arcs", Bur. of Mines Bull. 625, 1965, p. 35.

32. Hurlbut, C.S., Jr., "Dana's Manual of Mineralogy, 18th Ed.," Wiley, 1971.

33. Clark, G.B., et al, "Rock Properties Related to Rapid Excavation," Office of High Speed Ground Transportation, Washington, D.C., Rept. 3-0143, March, 1969.

34. Obert, L., Windes, S.L., and Duvall, W.J., "Standardized Tests for Determining the Physical Properties of Mine Rocks," U.S. Bur. Mines RI 3891, August 1946.

35. Jaeger, J.C., and Cook, N.G.W., "Fundamentals of Rock Mechanics," Methuen & Co., Ltd., 1969.

36. Robertson, E.C., "Experimental Study of the Strength of Rocks," Bull. Geol. Soc. Am., Vol. 66, Oct. 1955, pp. 1275-1315.

37. Nishihara, M., "Stress-Strain Relation of Rocks," Doshisha Engineering Review, Vol. 8, No. 2, August 1957.

38. Walsh, J.B., "The Effect of Cracks on the Compressibility of Rocks," Jl. Geophys. Res., Vol. 70, No. 2, January 1965.

39. Walsh, J.B., "The Effect of Cracks on the Uniaxial Elastic Compression of Rocks," Jl. Geophys. Res., Vol. 70, No. 3, January 1965.

40. Walsh, J.B., "The Effect of Cracks in Rocks on Poisson's Ratio," Jl. Geophys. Res., Vol. 70, No. 20, October 1965.

41. Griggs, D.T., et al, "Deformation of Rocks at 500° to 800°C," Rock Deformation (a symposium), Geol. Soc. Am. Memoir 79, 1960, pp. 39-104.

42. Brace, W.F., "Some New Measurements of Linear Compressibility of Rocks," Jl. Geophys. Res., Vol. 70, 1965, pp. 391-398.

43. Carstens, J.P., et al, "Feasibility of Flame-Jet Tunneling," United Aircraft Research Laboratories, Rept. PB 1781988, May 1968.

44. Moavezadeh, F., et al, "Laser Assisted Rock Fracture," PB 174245, January 1967.

45. Moavenzadeh, F., et al, "Thin Disc Technique for Analyzing Rock Fractures Induced by Laser Irradiation," PB 179-205, May 1968.

46. Moavenzadeh, F., et al, "Rock Fracture Research," MIT Rept. R66-56, PB 173-638, November 1966.

47. Thirumalai, K., "The Process of Thermal Spalling Behavior in Rocks - An Exploratory Study," Rock Mechanics-Theory and Practice, ed. W.H. Somerton, Proc. 11th Symp. Rock Mech., 1970, pp. 705-727.

48. Birch, F., and Clark, H., "Thermal Conductivity of Rocks and Its Dependence Upon Temperature and Composition - Part I," Am. Jl. Sci., Vol. 238, No. 8, Aug. 1940, pp. 529-558.

49. Lindroth, D.P., and Krawza, W.G., "Heat Content and Specific Heat of Six Rock Types at Temperatures to 1000°C," Bu. Mines RI 7503, April 1971.

50. Birch, F., "Elasticity of Igneous Rocks at High Temperatures and Pressures," Bull. Geol. Soc. Am., Vol. 54, 1943, pp. 263-286.

51. Baidiuk, "Mechanical Properties of Rocks at High Temperatures and Pressures," Consultant Bureau, New York, 1967.

52. Wingquist, C.F., "Elastic Moduli of Rock at Elevated Temperatures," Bur. Mines. RI 7269, 1969.

53. Mirkovich, V.V., "Experimental Study Relating Thermal Conductivity to Thermal Piercing of Rocks," Intl. Jl. Rock Mech. Min. Sci., Vol. 5, May 1964, pp. 205-218.

54. Norton, F.H., "A General Theory of Spalling," Jl. Am. Cer. Soc., Vol. 9, 1920, pp. 29-39.

55. Preston, F.W., "Theory of Spalling," Jl. Am. Cer. Soc., Vol. 16, No. 3, 1933, pp. 131-133.

56. Gray, W.E., "Surface Spalling by Thermal Stresses in Rocks," Proc. Rock Mech. Symp., Univ. of Toronto, Mines Branch, Ottawa, 1965, pp. 85-106.

57. Griffith, A.A., "The Theory of Rupture," Proc. 1st Intl. Congress Appl. Mech., Delft, 1924, pp. 55-63.

58. Sack, R.A., "Extension of Griffith's Theory of Rupture to Three Dimensions," Proc. Phys. Soc., 58, 1946, pp. 729-736.

59. Brace, W.F., "Brittle Fracture of Rocks," Proc. Intl. Conf., ed. W.R. Judd, American Elsevier Publishing Co., June 1963.

60. Bieniawski, Z.T., "Mechanism of Brittle Fracture of Rock, Part II - Experimental Studies," Intl. Jl. Rock Mech. Min. Sci., Vol. 4, 1967, pp. 407-423.

61. McClintock, F.A., and Walsh, J.B., "Friction on Griffith Cracks under Pressure," Proc. 4th U.S. Cong. Appl. Mech., Berkeley, 1962; ASME, New York, 1963, pp. 1015-1021.

62. Bieniawski, Z.T., "Mechanism of Rock Failure Under Compression," Report of the South African Council of Scientific and Industrial Research, No. MEG459, June 1966.

63. Hoek, E., and Bieniawski, Z.T., "Brittle Fracture Propagation in Rock under Compression," Intl. Jl. Fracture Mech., Vol. 1, No. 3, 1965, pp. 139-155.

64. Marovelli, R.L., and Veith, K.F., "Thermal Conductivity of Rock-Measurement by Transient Line Source Method," Bur. Mines RI 6604, 1965.

65. Marovelli, R.L., et al, "Thermal Fragmentation of Rock," Trans. Soc. Min. Engrs., No. 265, March 1966, pp. 1-5.

66. Marovelli, R.L., and Chen, T.S., "Analysis of Stresses in a Rock Disc Subjected to Peripheral Thermal Shock," Bur. Mines RI 6823, 1966.

67. Manson, S.S., and Smith, R.W., "Theory of Thermal Shock Resistance of Brittle Materials Based on Weibull's Statistical Theory of Strength," Jl. Am. Cer. Soc., Vol. 38, No. 1, 1955, pp. 18-27.

68. Lauriello, P.J.J., "Thermal Fracturing of Hard Crystalline Rocks," Ph.D. Dissertation, Rutgers University, October 1971.

69. Carslaw, H.S., and Jaeger, J.C., "Conduction of Heat in Solids," 2nd ed., Oxford Univ. Press, London, 1959.

70. Baumeister, T., and Marks, L.S., "Standard Handbook for Mechanical Engineers," 7th Ed., McGraw-Hill Co., New York, 1967.

71. Boley, B.A., and Weiner, J.H., "Theory of Thermal Stresses," John Wiley & Sons, Inc., 1960.

72. Paone, J., and Bruce, W.E., "Drillability Studies; Diamond Drilling," Bur. Mines RI 6324, 1963.

73. Ozisik, M.N., "Boundary Value Problems of Heat Conduction," International Textbook Company, 1968.

74. Luikov, A.V., "Methods of Solving the Nonlinear Equations of Unsteady-state Heat Conduction," Heat Transfer-Soviet Research, Vol. 3, No. 3 May-June 1971, pp. 1-51.

75. Crank, J., "The Mathematics of Diffusion," Oxford Univ. Press, London, 1956.

76. Bio, M.A., "Variational Principles in Heat Transfer," Oxford Univ. Press, London, 1970.

77. Goodman, T.R., "Application of Integral Methods to Transient Nonlinear Heat Transfer," Advances in Heat Transfer, Vol. 1, Academic Press, New York, 1964.

78. Mikhlin, S.G., "Variational Methods in Mathematical Physics," The Macmillan Company, New York, 1964.

79. Zienkiewicz, O.C., "The Finite Element Method in Structural and Continuum Mechanics," McGraw-Hill Publishing Company, 1967.

80. Wilson, E.L., and Nickell, R.E., "Application of the Finite Element Method to Heat Conduction Analysis," Nuclear Engineering and Design, Vol. 4, pp. 276-286, 1966.

81. Jones, R.N., and Crose, J.G., "SAAS II-Finite Element Stress Analysis of Axisymmetric Solids with Orthotropic, Temperature Dependent Material Properties," Aerospace Corporation, California, 1968.

82. Patel, M.R., "Rock Fragmentation by Subsurface Thermal Inclusions - A Finite Element Study," Ph.D. Dissertation, Univ. of Missouri-Rolla, 1973.

83. Sternberg, E., "Transient Thermal Stresses in an Infinite Medium with Spherical Cavity," Proc. Kon, Akad. Wetensch., B, 1957.

84. Harza, R.D., "A Computer Program for Estimating Costs of Hard Rock Tunneling," 2 Vols., Final Rept., May 1970.

85. Phillips, E.H., and Kunan, A.F., "Percussion Drilling", Chapt. 6.2, Surface Mining, AIME, 1968.